



An-Najah National University
Faculty of Graduate Studies

**THE SYNTHESIS OF CHITOSAN
DERIVATIVES AS A VERSATILE TOOL IN
SUSTAINABLE AGRICULTURE**

By

Renad Jalal Yahya Hamed

Supervisor

Prof. Shehdah Jodeh

**This Dissertation is Submitted in Partial Fulfillment of the Requirements for the Degree of
PhD of Chemistry, Faculty of Graduate Studies, An-Najah National University,
Nablus - Palestine.**

2023

THE SYNTHESIS OF CHITOSAN DERIVATIVES AS A VERSATILE TOOL IN SUSTAINABLE AGRICULTURE

By

Renad Jalal Yahya Hamed

This Thesis was Defended Successfully on 13/8/2022 and approved by

Prof. Shehdah Jodeh
Supervisor

Shehdah Jodeh
Signature

Prof. Ibrahim Kayali
External Examiner

Ibrahim Kayali
Signature

Prof. Ahed Zyoud
Internal Examiner

Ahed Zyoud
Signature

Prof. Mohammed Al-Nuri
Internal Examiner

Mohammed Al-Nuri
Signature



An-Najah National University
Faculty of Graduate Studies

**THE SYNTHESIS OF CHITOSAN
DERIVATIVES AS A VERSATILE TOOL IN
SUSTAINABLE AGRICULTURE**

By

Renad Jalal Yahya Hamed

Supervisor

Prof. Shehdah Jodeh

In accordance with An-Najah National University Deans Council Regulations for the award of Doctor of Philosophy, the following papers have been published after their extraction from the dissertation:

Visible light-driven ZnO nanoparticles/carbon nanodots hybrid for broad-spectrum antimicrobial activity

Dedication

I dedicate this thesis to my loving family, whose unwavering support and encouragement have guided me throughout this challenging journey.

I want to dedicate this thesis to the exceptional academic teachers who have shaped my intellectual growth and academic journey. Your passion for knowledge, dedication to teaching, and unwavering commitment to our education have left an indelible mark on my life.

Lastly, I would like to express my heartfelt appreciation to all the participants who generously dedicated their time and shared their insights, making this research possible. Your contributions have added depth and significance to the findings of this thesis.

This thesis is dedicated to all those who have believed in me, supported me, and inspired me to reach beyond my limits. Your love, encouragement, and unwavering faith have been my constant motivation. I am forever grateful for your presence in my life.

Acknowledgment

First and foremost, I want to express my deepest gratitude to Allah, The most merciful and the most gracious, for granting me strength, guidance, and blessing throughout this arduous journey.

I would like to extend my heartfelt appreciation to my supervisor Prof. Shehdeh Jodeh, for his invaluable guidance, expertise, mentorship, and support in this journey insights have shaped my academic background and my research and enriched my understanding of the subject matter. Your contributions have been invaluable, and your involvement in this endeavor has broadened my perspectives.

I also sincerely appreciate Prof. Raed Alkowni for his unwavering support, guidance, and mentorship in shaping my academic skills in this research, and sharing your insights has added depth and significance to my research and my academic life journey.

I'm also profoundly grateful to Dr. Shadi Sawalha and Dr. Mohyeddin Assali; thank you for your tireless efforts in imparting wisdom, challenging my thinking, and nurturing my intellectual curiosity.

I'm also thankful for Eng. Hazem Kittani and Dr. Subhi Samhan from the Palestinian Water Authority (PWA) for their continuous support and for sharing insights have added depth to my research throughout this academic journey.

I'm also very dedicated to MEDRC center /Oman and its workers for their support, fellowship, and internship that really add value to my research work and its implementation.

I'm also thankful to Forschungszentrum Julich for hosting such a successful research trip and to all academic professors and Doctors (Prof. Roland Bol, Dr. Nina Sbier, and others) for their advice and support.

Lastly, I would like to thank all the teachers, professors, and scholars whose work and teachings have shaped my academic journey. Furthermore, I pray that my work serves as a source of benefit and contributes to advancing knowledge in the future.

Declaration

I, the undersigned, declare that I submitted the thesis entitled:

THE SYNTHESIS OF CHITOSAN DERIVATIVES AS A VERSATILE TOOL IN SUSTAINABLE AGRICULTURE

I declare that the work provided in this thesis, unless otherwise referenced, is the researcher's own work, and has not been submitted elsewhere for any other degree or qualification.

Student's Name: _____ Renad Hamed _____

Signature: _____ *Renad Hamed* _____

Date: _____ 2023-8-13 _____

List of Content

Dedication.....	IV
Acknowledgment.....	V
Declaration.....	VI
List of Content.....	VII
List of Tables.....	XII
List of Figures.....	XIII
Abstract.....	XVII
Chapter One: Introduction.....	1
1.1 Preface.....	1
1.2 Literature Review.....	4
1.3 Introduction of Nano bio-fertilizer.....	5
1.3.1 Polymeric Nanoparticles.....	5
1.3.1.1 Natural Polymer.....	5
1.3.1.1.1 Chitosan.....	6
1.3.1.1.2 Alginate.....	7
1.3.2 Humic Acid as Cross-linker Bridging.....	8
1.3.3 PGPR and Their Role.....	9
1.3.4 Nano capsules Synthesis Route.....	10
1.3.4.1 Ionotropic Gelation of Calcium–Alginate Complexation.....	10
1.3.4.2 Polyelectrolyte Complexation Chitosan –Alginate Complexation.....	12
1.3.5 Active Nutrient Entrapment Method.....	14
1.4 Chitosan and its Derivatives As Antimicrobial Agents.....	14
1.4.1 Chitosan –ZnO.....	15
1.4.2 Chitosan –CNDs.....	16
1.4.3 Chitosan –Hybrid.....	17

1.5 Chitosan based Amino Acids as PGPRs and Plant Bio-stimulant.....	18
1.5.1 Chitosan Functionalized with Amino Acid	18
1.5.2 1- Amino Cyclopropane 1- Carboxylic acid (ACC) Amino Acid.....	19
1.5.3 L- Valine Amino Acid.....	19
1.5.4 L-Tryptophan Amino Acid.....	20
1.5.5 L- Lysine Amino Acid	20
1.6 Recent Research Related to Nano bio-fertilizer	21
1.7 Recent Research Related to Chitosan Derivatives as Antimicrobial Agents for Agricultural Application.....	23
1.9 Recent Research of Chitosan Functionalized Amino Acid as a Plant Bio- stimulant.....	25
1.10 Scope of the Research.....	27
Chapter Two: Experimental Part	32
2.1 Materials and Methods.....	32
2.2 Preliminary Study for Synthesis of Nano-bio fertilizer Capsules.....	33
2.2.1 Stock Solutions Preparation.....	34
2.2.1.1 Chitosan Nano particle Solution (0.05 % w/v).....	34
2.2.1.2 Alginate Nanoparticle Solution (0.06 % w/v)	34
2.2.1.3 Humic Nanoparticle Solution (1 % w/v)	34
2.2.1.4 Selecting and Culturing PGPR (Pseudomonas fluorescense (PL 5.4)).....	35
2.2.2 Iontropic Gelation of Nano capsules and Polyelectrolyte Complexation	35
2.2.3 Homogenization, Purification, and Lyophilization Of Nano bio-fertilizer Capsules.....	36
2.2.4 Encapsulation Efficiency of Nano bio-fertilizer	37
2.2.5 Controlled Release of Active Nutrients from Nano bio-fertilizer.....	37
2.2.6 Water Retention Behavior of Soil with and without Formulated Nano bio- fertilizer.....	38

2.2.7 Particle Size and Zeta Potential Analysis	39
2.2.8 Thermogravimetric Analysis	39
2.2.9 Enumeration of <i>P. fluorescens</i> in the Nano capsules	39
2.3 Synthesizing and Characterizing Chitosan-based Nanocomposites (Chitosan-based Photocatalyst Materials) and Testing In Vitro Antimicrobial Agents.....	40
2.3.1 Synthesis of Chitosan.ZnO	40
2.3.2 Synthesis of Chitosan. CNDs	40
2.3.3 Synthesis of Chitosan. Hybrid (ZnO /CND)	41
2.3.4 Antimicrobial Activity	42
2.3.4.1 Microbial Strains.....	42
2.3.4.2 Preparation of Antimicrobial Stock Solution.....	42
2.3.4.3 Preparation of Microbial Suspension.....	43
2.3.4.4 Agar Disk Diffusion Test Zone Inhibition Test.....	43
2.3.4.5 Determination of Minimum Inhibitory Concentration (MIC)	44
2.3.4.6 Determination of Microbial Colonies Forming Unit Reduction (CFU)	44
2.3.4.7 Glutathione Deficiency Test	44
2.3.4.8 Time- Kill Kinetics	45
2.4 Chitosan-based Composites (Chitosan-based Amino Acids Materials) are Active Plant Bio-stimulants with in Vitro Agricultural Applications.....	45
2.4.1 Synthesis of ACC(1- amino cyclopropane -1- carboxylic acid).....	45
2.4.1.1 Synthesis of spiro [2,5].5,7- dioxo-6,6- dimethyl octane-4,8-dione	46
2.4.1.2 Synthesis of hydrazinocarbonyl cyclopropane-1-carboxylic acid	46
2.4.1.3 Synthesis of amino cyclo propane-1- carboxylic acid (ACC)	47
2.4.2 Synthesis of Chitosan –ACC	48
2.4.2.1 Synthesis of N- phthaloyl chitosan	48
2.4.2.2 Synthesis of 6- <i>O</i> -toyl-N-phthaloyl chitosan	49

2.4.2.3 Synthesis of N-phthaloyl chitosan ACC	50
2.4.2.4 Reduction of N- phthaloyl of chitosan ACC mild de-protection.....	51
2.4.3 Synthesis of Chitosan-based –Amino acids	52
2.4.3.1 Synthesis of N-Boc chitosan.....	52
2.4.3.2 Synthesis of 6- O- Tosyl-N-Boc chitosan.....	53
2.4.3.3 Synthesis of 6- O- Valine-N-Boc chitosan	54
2.4.3.4 Synthesis of 6- O- Tryptophan-N-Boc chitosan	55
2.4.3.5 De-protection of 6- O- Valine chitosan	56
2.4.3.6 De-protection of 6- O- Tryptophan chitosan	57
2.4.3.7 Synthesis of 6- O- Valine chitosan N- Lysine	58
2.4.3.8 Synthesis of 6- O- Tryptophan chitosan N- Lysine	59
2.4.4 Kaiser Test.....	60
2.4.5 Plant Cultivation and Growth Condition.....	61
2.4.5.1 Sample Data Collected.....	62
2.4.5.1 Measurement of Plant Photosynthesis with PAM Fluorometry	62
Chapter Three: Results and Discussion	64
3.1 Nano bio-fertilizer Capsules	64
3.1.1 Synthesis and Characterization of Nano capsules	64
3.1.2 Surface Structure and Morphology Analysis	69
3.1.3 FT-IR Spectral Analysis	71
3.1.4 Thermogravimetric Analysis.....	73
3.1.5 Water Retention Behavior of Nano capsules in Soil.....	75
3.1.6 Nano bio-fertilizer Release Studies	76
3.2 Synthesis and Characterization of Chitosan-based Photocatalytic Composites	81
3.2.1 Atomic Force Microscope Analysis	84
3.2.2 X-Ray Diffraction	86

3.2.3 FT-IR Spectra	88
3.2.4 Optical Properties of Synthesized Materials.....	90
3.2.5 Antimicrobial activity.....	93
3.2.6 Time killing	101
3.2.7 Glutathione Deficiency Test.....	103
3.3 Characterization and Chemical Modification of Chitosan as Plant bio-stimulant..	106
3.3.1 Application of chitosan-ACC to enhance the growth of fluorescence pseudomonas bacterial strain	111
3.3.2 Agronomic Parameters	112
3.3.3 Physiological Parameters	118
Chapter Four: Discussions and Conclusions	121
List of Abbreviations	125
References.....	126
Appendices.....	139
الملخص.....	ب

List of Tables

Table 1: Hexagonal lattice constants and Bragg's spacing of ZnO and Hybrid	87
Table 2: Size comparisons of inhibition zone for /ZnO, CNDs, and Hybrid for different bacterial and fungal strains under sunlight and dark modes	93
Table 3: Size comparisons of inhibition zone for Chitosan, Chitosan/ZnO, Chitosan/CNDs, and Chitosan/Hybrid for different bacterial and fungal strains under sunlight and dark modes	95
Table 4: Minimum inhibition concentration of microbial growth (MIC) values ($\mu\text{g/ml}$) of ZnO, CNDs, and Hybrid under sunlight and dark modes.....	97
Table 5: Minimum inhibition concentration of microbial growth (MIC) values ($\mu\text{g/ml}$) of Chitosan, Chitosan/ZnO, Chitosan/CNDs, and Chitosan/Hybrid under sunlight and dark modes.....	98
Table 6: Kill Time kinetic of ZnO, CNDs, and Hybrid for different bacterial and fungal strains under sunlight and dark modes	102
Table 7: Kill Time kinetic of Ch.ZnO, Ch.CNDs, and Ch.Hybrid for different bacterial and fungal strains under sunlight and dark modes	103
Table 8: Effect of amino acids treatments on the root and shoot length system for (A) shoot length (cm) after 15 days, (B) shoot length (cm) after 30 days, (C) Measurements of root length (cm) after 30 days (D) diameter (E) number of internodes	113
Table 9: Effect of amino acids treatments on the growth system for (A) wet mass (g), (B) dry mass (g), (C) moisture content for Barely Plant trails after 30 days	117
Table 10: Photocatalytic activity measurement for treated trials	118

List of Figures

Figure 1: Chitosan polymer structure	6
Figure 2: Alginate polymer structure.....	8
Figure 3: Ionotropic gelation of calcium–alginate complexation.....	12
Figure 4: Polyelectrolyte complexation chitosan –alginate complexation	13
Figure 5: (a) Suggested (Ch./Alg.HA.NPK.PGPR) nano capsules interaction, (b) Suggested (Ch. /Alg. NPK.PGPR) nano capsules interaction.....	65
Figure 6: a. (a)Surface of (Ch. Alg.NPK.PGPRs) Nano capsule,(b) inside the matrix of nanocapsule with the appearance of entrapped NPK and PGPRs. b. (a) Surface appearance of (Ch. Alg. HA.NPK. PGPRs),(b) inside the matrix of nanocapsule with the appearance of entrapped NPK and PGPRs, (c) Network of cross-linking inside the nanocapsule with embedded entrapped materials	70
Figure 7: TGA analysis for (Ch. Alg. NPK) and (Ch. Alg. HA.NPK) nanocapsules....	73
Figure 8: Water Retention of Formulated (Ch.Alg.NPK.PGPRs) and (Ch. Alg. HA.NPK.PGPRs) nano capsules	75
Figure 9: (a) Nitrogen Cumulative Release (%) profile for synthesized nanocapsules,(b) Phosphorous Cumulative Release (%) profile for synthesized nanocapsules,(c) Potassium Cumulative Release (%) profile for synthesized nanocapsules.....	78
Figure 10: (a).: (a) The Ch. ZnO white forming film,(b) The structural interaction of Ch.ZnO (b). : (a) The Ch.CNDs pale yellowish film,(b) The structural interaction of Ch.CNDs. (c)(a).: CNDs and ZnO-CNDs hybrid preparation summary. (c)(b): (a) The Ch.Hybrid yellowish film,(b) The structural Chitosan/ Hybrid(ZnO-CNDs) Interaction.....	82

List of Appendices

Appendix A: FT-IR of synthesized Ch- Amino acids compounds.....	139
Appendix B: Nano Biofertilizer.....	146
Figure S.1: The appearance of prepared nanocapsules solutions	146
Figure S.2: The DLS (particle size) measurements of synthesized Nano capsules	146
Figure S.3: FT_IR of Chitosan ,Alginate, Humic acid, (Ch.Alg.NPK), (Ch.Alg.HA. NPK)	147
Table S.1: Water retention percentage for (Ch.Alg.NPK) and (Ch. Alg. HA. NPK) Nanocapsules	149
Table S.2: Release behavior of active nutrient Nitrogen for (Ch.Alg.NPK) and (Ch. Alg. HA. NPK) Nanocapsules	150
Table S.3: Release behavior of active nutrient Phosphorous for (Ch.Alg.NPK) and (Ch. Alg. HA. NPK) Nanocapsules	150
Table S.4: Release behavior of active nutrient Potassium for (Ch.Alg.NPK) and (Ch. Alg. HA. NPK) Nanocapsules	151
Figure S.4: Nitrogen Kinetic release of (Ch.Alg.HA. NPK) and (Ch.Alg.NPK) Nanocapsules	151
Figure S.5: Phosphorous Kinetic release of (Ch.Alg.HA. NPK) and (Ch.Alg.NPK) Nanocapsules.....	152
Figure S.6: Potassium Kinetic release of (Ch.Alg.HA. NPK) and (Ch.Alg.NPK) Nanocapsules	152
Appendix C: Chitosan-based photocatalyst.....	153
Figure S.1.a: (a) AFM image of CNDs particles, (b) CNDs size distribution histogram (c) AFM image of ZnO nanoparticles, (d) ZnO size distribution histogram,(e) AFM image of ZnO-CNDs hybrid, (f) Hybrid size distribution histogram	153
Figure S.1: XRD patterns for CNDs, ZnO, and Hybrid (ZnO/CNDs)	153
Figure S.2: (a) AFM image of Ch.ZnO, (b) AFM image of Ch.CNDs,(c) AFM image of Ch.Hybrid (ZnO-CNDs)	154

Figure S.3: X-Ray Diffraction of ZnO, CNDs, Hybrid (ZnO/CNDs)	155
Figure S.4: FT-IR spectra of Chitosan, ZnO, CNDs, Ch.Hybrid (ZnO/CNDs)	155
Figure S.5: FT_IR of Ch.ZnO, Ch.CNDs	156
Figure S.6: Raman Spectra of CNDs and Hybrid (CNDs/ZnO).....	157
Figure S.7: (a) UV-Vis absorption spectra of CNDs, ZnO, and Hybrid (ZnO/CNDs), (b) Band gaps of ZnO and Hybrid (ZnO/CNDs), (c) UV Vis absorption of Ch.CNDs, Ch.ZnO, and Ch. Hybrid	157
Figure S.8: Loss of Glutathione (%) for synthesized samples in dark mode.....	158
Figure S.9: Loss of Glutathione (%) for synthesized samples in sunlight mode.....	158
Table S.2: Number of CFU reductions for ZnO, CNDs, and Hybrid for different bacterial and fungal strains under sunlight and dark modes before and after treatment	159
Table S.3: Number of CFU reductions for Chitosan, Chitosan/ZnO, Chitosan/CNDs, and Chitosan/Hybrid for different bacterial and fungal strains under sunlight and dark modes before and after treatment.....	159
Table S.4: Percentage of CFU reduction for ZnO, CNDs, and Hybrid for different bacterial and fungal strains under sunlight and dark modes	160
Table S.5: Percentage of CFU reduction for Chitosan, Chitosan/ZnO, Chitosan/CNDs, and Chitosan/Hybrid for different bacterial and fungal strains under sunlight and dark modes	160
Table S.6: Log of CFU reduction for ZnO, CNDs, and Hybrid for different bacterial and fungal strains under sunlight and dark modes.....	161
Table S.7: Log of CFU reduction for Chitosan, Chitosan/ZnO, Chitosan/CNDs, and Chitosan/Hybrid for different bacterial and fungal strains under sunlight and dark modes	162
Appendix D: Chitosan based Amino Acid as PGPRs and Plant biostimulants	163
Table S1: Calculated amine groups obtained from Kaiser test for N-protected compound using two N-protection approaches.....	163

Figure S1: In vitro test of Petri-plate of testing of bacterial growth of (a)chitosan, (b)ACC, (c) chitosan-ACC	163
Appendix E: Certificate of approval to publish the research	164

The Synthesis of Chitosan Derivatives as a Versatile Tool in Sustainable Agriculture

By

Renad Jalal Yahya Hamed

Supervisor

Prof. Shehdeh Jodeh

Abstract

Agro-fertilizers and pesticide chemicals are identified as primary agricultural and environmental pollutants. Chitosan polymer has attracted interest in agriculture and plant sciences applications; therefore, in this current research, considerable scientific contributions are ongoing to improve the formulation and functionalization of chitosan polymer.

This research focuses on the utilization of chitosan in the synthesis of innovative nano bio-fertilizer capsules, aiming to deliver active agro nutrients, namely Nitrogen, Phosphorous, and Potassium ions (NPK), along with beneficial plant growth-promoting rhizobacteria (PGPRs) microorganisms. These entrapped components are coated using innovative cross-linking of chitosan and alginate with humic acid through ionic gelation and polyelectrolyte complexation technique. The morphological and structural characteristics of the formulated nano capsules are investigated using DLS, FT-IR, SEM, and TGA. The entrapped materials' encapsulation capability, water retention behavior, and release kinetics are also determined. The findings provide insights into implementing nano bio-fertilizers to deliver agro-nutrients, efficiently contributing to agricultural productivity and sustainability.

On the other hand, the functionalization of chitosan with photocatalyst materials has emerged as a promising approach to developing bio pesticides. This research focuses on the functionalization of chitosan with three different photocatalyst materials: ZnO, carbon nano dots (CNDs), and a hybrid of (CNDs/ZnO), and their potential role as active antimicrobial agents against a broad spectrum of bacterial and fungal strains under dark and sunlight conditions. Functionalized chitosan photocatalyst materials' resulting morphological, structural, and optical properties were examined using FT-IR,

AFM, XRD, RAMAN, and UV-Vis instruments. The findings provide insight into the ability to utilize these synthesized as bio-pesticides for agriculture purposes.

Finally, the potential of functionalizing chitosan with amino acids as PGPRs and plant bio-stimulant products was also determined. A PGPR precursor named 1- amino cyclopropane-1- carboxylic acid (ACC) was synthesized and functionalized with chitosan. Also, different amino acids (L- Valine, L- Tryptophan, and L- Lysine) functionalized chitosan were synthesized using new approaches. The structural characteristics were also determined using FT-IR and NMR instruments. The plant agronomic and physiological parameters associated with these materials were examined. The findings provide insight into using these bio-stimulant products in agricultural applications.

Keywords: Nano bio-fertilizer, Nano capsules, cross-linking, hetero-photocatalyst composite, plant bio-stimulant.

Chapter One

Introduction

1.1 Preface

The agricultural sector is a primary source of increasing chemical pollutants via the excessive use of synthetic chemical fertilizers and pesticides, where agrochemical fertilizers are used to promote crop production and soil remediation, and agropesticides are used to manage pathogenic microorganisms to ensure crop health and productivity. Many issues have been reported concerning the problems of excessive and uncontrolled utilization of these agrochemical fertilizers and pesticides, causing harmful pollutants that lead to climate change issues, soil acidification, the decline of soil fertility, nutrient degradation, groundwater pollution, loss of biodiversity, and high energy consumption in the manufacturing process. These chemical pollutants also remain in the environment for generations and can disrupt the hormonal systems of humans and wildlife. Synthetic toxic farms, agrochemical fertilizers, and pesticides are examples of the excessive use of synthetic nitrous oxide (N_2O) or ammonium nitrate (NH_4NO_3) chemical pollutants. Natural denitrification microorganisms reduce the excess of nitrous oxide in the soil to gaseous products, which are then released into the atmosphere, causing significant global warming issues. [1]

Additionally, the biological nitrogen fixation in the soil is affected by the high nitrogen, causing the symbiotic natural microbes to be diminished. Furthermore, nitrifying microorganisms utilize the excess ammonium compounds in the soil and produce more nitrate. This high excess nitrate is also utilized by denitrifying microorganism bacterial strains to produce more nitrous oxide (N_2O), which leaches into fresh, drinkable groundwater resources and leads to more serious water pollution issues and other environmental harms.[2]

The indiscriminate use of synthetic agrochemical fertilizers and pesticides can ultimately cause these environmental issues. Therefore, it has become urgent to develop new alternative agro-based natural techniques and materials to reduce the enormous consumption of agrochemical products.[3] This alternative strategy shall also effectively support plants' innate immunity and bio-stimulate crop production. Great efforts have been made to replace synthetic agrochemical fertilizers with sustainable,

eco-friendly natural agrochemical fertilizers and natural agro pesticides, where over the last decade, researchers have shifted towards implementing new nano-enabled agrochemical products based on formulating nano-fertilizer and bio-fertilizer materials, as well on synthesizing natural or synthesized compounds based on formulating eco-friendly materials with different precursor approaches, which acts as antimicrobial agents or plant bio-stimulant or even both of these roles for various agronomical practices.[4, 5]

Nano-enabled agrochemicals are classified as nanotechnology techniques in the natural agrochemical field. Nano-enabled agrochemical fertilizers can be divided into macro-, micro-nano, and nano-particulate, based on active nutrients supplied to the plants. Recently, most of these nano-enabled agrochemicals based on nanoparticle formulation can hold the key to developing plant growth within a controlled release of active ingredients and site-specific delivery, with integrated antimicrobial and antioxidant ingredient management.[6] Nano-enabled agrochemicals can also minimize the toxicity of environmental contamination and excessive use of conventional agrochemical fertilizers and pesticides and minimize volatilization, leaching, and run-off agrochemicals to water resources. Moreover, its nano-delivery system can enhance the agrochemical uptake and improve soil and plant stability and solubility, offering a considerable advantage in supporting agriculture and production. [7]

Bio- and nano-fertilizers are the main classes of nano-enabled agrochemical fertilizers. These bio- and nano-fertilizer materials mainly apply natural biodegradable, bioavailability, and bio-compatibility polymers in their formulation with nano scale dimensions ranging from 10 to 1000 nm, depending upon the various green preparation precursors method for preparation, nano sphere, or nano capsule to be obtained, and bioactive agro ingredients or inoculant microorganisms are dissolved, encapsulated, entrapped, or chemically or physically bound to prepared matrix.[8] The encapsulation mechanism of active agrochemical ingredients or microorganisms inoculants can be described as enclosing required particles from solids, droplets of liquids, gases, or inoculant beneficial microorganisms into an inert polymeric shell, which isolates and protects it from the external environment's stress and deteriorative reactions and regulates the release and diffusion of incorporated compounds in a controlled and gradual manner at the nano scale with a rate required for a specified treatment to meet

the plants' needs, offering significant agriculture and environmental advantages.[9] Thus, these new nano formulation materials make them ideal as emerging alternative conventional synthetic chemical fertilizers for retaining safe, reliable, clean, non-toxic, low-cost, and eco-friendly, with sustained-release nanoparticles in a controlled process that are highly efficient for plant fertilization and regulation, and help us eliminate environmental contamination and eutrophication.[10]

A variety of natural polymers have been used in nano-enabled agrochemical fertilizers to entrap hydrophilic, hydrophilic substances, or inoculant microorganisms, including proteins, polysaccharides, synthetic and natural polymers, lipids, dendrimers, and peptides. Naturally occurring biopolymers such as chitosan, alginate, starch, and cellulose are considered predominant polysaccharides utilized in agriculture manufacturing for entrapments active bio ingredients and formation of either nano-fertilizer or bio-fertilizers.[11]

Chitosan is considered the most studied biopolymer and has received remarkable attention over recent decades due to its biocompatibility, biodegradability, bioactivity, and non-toxicity. Chitosan is also the most abundant biopolymer after cellulose with distinct properties of bio-adhesion, adsorption enhancer, coating, anti-inflammatory, antimicrobial, antifungal, and antiviral. Furthermore, chitosan consists of many hydroxyl and amino groups along its polymeric chain, making it suitable for ease of chemical modification and functionality. Several function groups can functionalize chitosan. [12] Functionalization can be addition, coupling, grafting, cross-linking, and other synthetic routes in preparing nanoparticles, suspensions, composites, antimicrobial materials, functionalized materials, or (nano) hybrids, where the functionalization of chitosan with other materials can enhance and advance its features for diverse eco-friendly agriculture purposes and applications.[7, 13]

Besides that, as a standard polymer, chitosan can act as a potent biocidal agent against pathogenic microbes. Incorporating chitosan with other active agents exhibited good potential as a sustainable alternative antimicrobial rather than conventional antimicrobial pesticides. Recently, there has been a growing interest in using heterogeneous photocatalyst materials to develop efficient and greener antimicrobial materials.[14, 15] These heterogeneous photocatalyst materials-based chitosan have

stabilized and immobilized nanocomposite materials. This leads to an efficient heterogeneous photocatalyst promoter in this approach, indicating that their antimicrobial activity can be significantly improved. They have shown promising results in different fields due to their unique physical and chemical properties, such as structural features, biocompatibility, biodegradability, and low toxicity. These heterogeneous photocatalyst materials based on chitosan include a wide range of photocatalytic materials such as semiconductor materials such as metal, metal oxides, carbon-based materials, and hybrid materials consisting of metal oxide with carbon-based nanoparticles with efficient antimicrobial activity.[16, 17]

On the other hand, chitosan is gaining attention as an eco-friendly matrix as one of the most suitable carrier matrices for agro-nutrient components in plant harvesting and productivity. [18-21] Nonetheless, new developments are always essential for new sustainable environmental solutions, where chitosan can play an important role in functionality, yield, and efficiency. Various studies have introduced amino acids to polysaccharide matrices by setting diverse reaction pathways. Amino acids are extracted natural materials that have attained extensive research interests in these divergent fields of plant science. They consist of natural plant elements such as nitrogen and carbon.[21] These elements stimulate plant growth in bio-stimulants, seed germination, flower formation, photosynthesis, and vegetative growth. Besides, Amino acids enhance the growth of specific beneficial bacteria known as plant growth-promoting bacteria (PGPR). These bacteria are critical in enhancing plants to overcome biotic and abiotic stress conditions.[22]

1.2 Literature Review

The following literature review will demonstrate a brief of nano fertilizer and bio-fertilizer-based chitosan related to this research work as nano enables- agrochemical delivery system, presenting bio polymeric nanoparticles, the relevant nanoparticle delivery systems synthesis and preparation techniques, encapsulation process of active materials at the nano scale, as well brief microbial inoculants of plant growth promoting rhizobacteria (PGPR) as beneficial microorganisms for various agrichemical practices.[23]

After that, the review will briefly present chitosan derivatives and their potential uses in sustainable agriculture. Photocatalytic functionalized as antimicrobial agents, amino acids functionalized chitosan as plant bio-stimulants and soil restoration.

1.3 Introduction of Nano bio-fertilizer

1.3.1 Polymeric Nanoparticles

Natural polysaccharide nanoparticles are synthesized in this research to obtain nano spheres or nano capsules as nano-bio-fertilizer materials. The aim of designing a nano bio-fertilizer at the nanoparticle scale is to control particle size, type, and amount of active encapsulated properties and release it in a controlled manner with its permeability profile. Nano bio- fertilizer capsules represent a vesicular system where active NPK nutrients and PGPR can be encapsulated, entrapped, chemically bound, or absorbed by a polymeric matrix.[24, 25] These polymeric matrices shall have mucoadhesive properties and hydrophobic surface characteristics. The advantages of these synthesized nano capsules in this research include their biocompatibility and biodegradability, ability to sustain control release of entrapped material via pH media, small particle size with maximized payload capacity, cheaply fabricated technique with large quantity, high surface characteristics to volume ratio. However, past researchers have some drawbacks related to the fast burst release of their synthesized nano capsules with limitation of types of entrapped materials and only focused either on encapsulating active nutrients or beneficial microorganisms; therefore, this research will justify these types of nano capsules by bridging them with humic acid to give more rigidity of formulated nanoparticles also merging the active nutrient with beneficial microorganisms to have a nano bio-fertilizer with dual effect and with more stable and storage.[26, 27]

1.3.1.1 Natural Polymer

Natural polymers are widely used in agriculture applications due to their fascinating properties and their stability, safety, biocompatibility, biodegradability, high availability in nature, varying chemical composition and electro potential, flexibility, hydrophobicity, and low cost in manufacturing. Also, its unique physical properties like solubility, melting, and ability to phase change are the main advantages of encapsulation applications. These natural polymers included proteins, lipids, and ionic

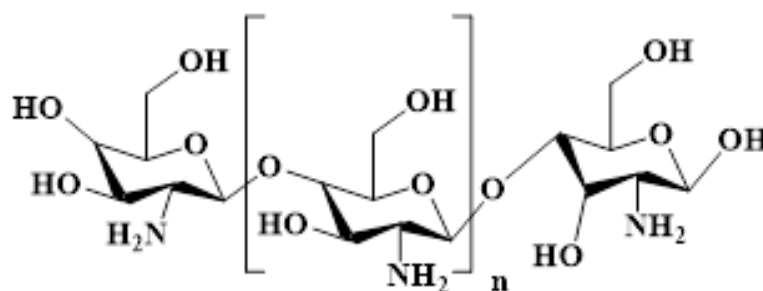
polysaccharides. Specifically, polymers such as albumin, gelatin, pectin, starch, chitin, chitosan, and alginic acid, which can control particle size as pH, the polarity of the solvent, altering temperature, and concentration of the solution is changed due to several free end groups being existence for ionic bonding or electrostatic interaction and particle formation. [28]

1.3.1.1.1 Chitosan

Chitosan is a natural bioavailability, biodegradable, and biocompatible polysaccharide polymer. It is derived from chitin products found as primary components in the exoskeletons of crustaceans, insects, fish scales, and fungi cell walls. Chitosan is composed of linear beta-(1-4)- linked monosaccharides structure as present in **Figure 1**, which consists of varying amounts of (β 1 \rightarrow 4) N- acetyl- 2- amino-2-deoxy-D- glucose and 2- amino-2-deoxy- D- glucose linkages, with most reactive groups sites found in the primary amino group(C2) and primary and secondary hydroxyl groups (C6, C3). The number of D-g, glucosamine, and N- acetyl-D-glucosamine residues in the chitosan polymer varies, and its charge density depends on the varying degrees of deacetylation. The acetylation degree ranged from 60-95 % and the pH of the media. Usually, its average molecular weight depends on its viscosity, ranging from 50,000- 190,000 Daltons, which affects its solubility and reactivity.[29-31]

Figure 1

Chitosan polymer structure



Chitosan oligomers are known for their solubility over a wide pH range, from acidic to essential solutions, and they undergo various chemical reactions with other compounds through their active hydroxyl and amino groups, including carboxylation, acylation, hydroxylation, alkylation, and esterification. These unique chemical reactions introduce new functional groups into the chitosan matrix, affecting and changing its crystal

structure and consequently increasing the solubility. These properties make it very useful in various types of implemented applications in multiple fields like drug carrying, food packaging, wound treatment, chelating agents, sensors, pharmaceutical and biomaterial, water treatment, and agriculture sectors; therefore, researchers have concentrated over the last decades on utilizing various types of chitosan derivatives and advancing its physicochemical and biological properties related to concern purposes. [32]

Chitosan and its derivatives are widely used in the nanotechnology discipline. Mostly, chitosan-based nano capsules are a predominant application in this field that emphasizes utilizing chitosan in nano capsules formulation through various techniques.[33] These chitosan-based nano capsules are considered the unique main target for their absorption rate, including active substances, high carrying capacity to ensure delivery of targeted trapped materials with a controlled release, and so on.

Additionally, chitosan and its derivatives possess anti-insecticidal, antimicrobial, bio-stimulators, and soil remediation, considered a vital issue active polymer effective for different agricultural purposes.[34]

1.3.1.1.2 Alginate

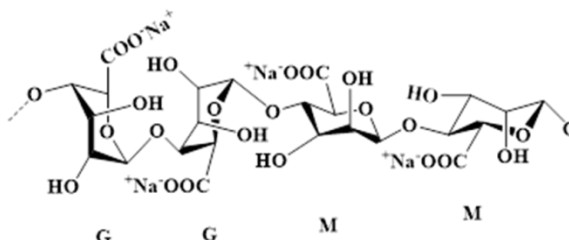
Sodium Alginate naturally occurs as an anionic polysaccharide typically found in brown seaweed; it uniquely forms water-insoluble gels as ionic-mediated gels through ionic gelation. Its gel is considered mild, biodegradable, biocompatible, and non-toxic, with the primary function of entrapping and merging active molecules and sustaining their release. The molecular weight of alginate salts can vary widely between 50,000-100,000,000 Daltons.[35]

Alginate structure consists of a linear unbranched copolymer of D- mannuronic acid (M) and L- guluronic acid (G). The two monomers 1,4 are linked by glycosidic bonds, generating homopolymeric M or G blocks and heteropolymeric MG blocks, as presented in Figure 2. The arrangement of these blocks strongly affects this biopolymer's functional properties. The existence of carboxyl groups gives its polyanion character, where alginate maintains a negative charge under acidic conditions; thus, it

enhances the electrostatic interaction with other cationic polymers or elements as well as forming micro or nano capsules or hydrogel networks.[35]

Figure 2

Alginate polymer structure



Alginate gels have been vastly used to encapsulate different bioactive materials and microbial inoculants for various industrial and agricultural application, even though it has some drawbacks related to their low viscosity, porosity, fast release of trapped active materials, and lack of physical and mechanical stability. As a result, researchers advanced its formulation with different coating membranes, as synthetic and natural polymers are used to increase its efficiency and overcome the mentioned drawbacks. Chitosan biopolymer is one of these coating cation membranes utilized in this fashion; it is also suggested in the formulation of nano bio-fertilizer in this research scope.[33]

1.3.2 Humic Acid as Cross-linker Bridging

Humic acid is a complex organic substance derived from the decay of plant and animal matter in the soil, and it contains different functional groups whose quantities depend on extraction and production methods. Mainly, functional groups in humic acid compounds are attributed to carboxylic acid and phenol groups. These functional groups can be deprotonated, giving different chemical reactions many capabilities. Humic acid has gained significant attention in agriculture in recent years due to its unique properties and versatile agriculture purposes, such as the ability of these compounds to improve plant growth and nutrition, complexation, and pollutant remediation. [36]

Moreover, its application as a cross-linker in nano capsules enables the encapsulation and sustained release of active nutrients. Also, humic acid has been shown to be a suitable matrix for plant growth-promoting rhizobacteria (PGPR); different studies revealed that humic acid not only enhances the survival and growth of these beneficial

microorganisms but also improves their colonization and bio control capabilities without any contaminations. These findings highlight the multifunctional role of humic acid proposed in this research as both cross-linkers for synthesized nanoparticles in nano capsules and a beneficial matrix for encapsulating the PGPR with bio control capabilities.[37]

1.3.3 PGPR and Their Role

Plant Growth-Promoting Rhizobacteria (PGPR) are a diverse group of beneficial microorganisms found naturally and able to enhance plant tolerance and growth under different environmental conditions for sustainable agricultural purposes. These beneficial bacteria exert their positive impact on plant growth through multiple mechanisms. Firstly, PGPR engages in nitrogen fixation, enabling plants to access nitrogen compounds and reduce the need for synthetic agrochemical fertilizers. Secondly, the ability of PGPR to enhance the availability of mineral phosphate in the soil for plants reduces the need for synthetic agrochemical fertilizers. Thirdly, some of these PGPR can synthesize growth-promoting hormones such as auxin (indoleacetic acid), gibberellic acid, abscisic acid, and cytokinins, which stimulate plant growth and tolerate it under biotic and abiotic conditions. Fourthly, PGPR possesses the ability to produce a particular type of enzyme called 1- amino cyclopropane -1- carboxylate (ACC) deaminase, where this enzyme can lower the plant stress by decreasing the ethylene stress hormones levels in the plant's roots, thereby confederated resistance to drought and oxidative stress, and the increasing ability of nutrient and water uptake.[38]

Additionally, PGPR exhibits antagonistic activities against different phytopathogenic microbes with the production of certain antibiotics in the plants' rhizospheres, enhancing its disease resistance. All these diverse PGPR beneficial mechanisms offer promising prospects for sustainable bio-fertilizer materials. Thus, encapsulated PGPR-based bio-fertilizers exhibited prolonged viability, increased efficacy in promoting plant growth with fixation of natural nitrogen compound, and reduced consumption of chemical pollutant compounds of conventional formulations.[38, 39]

For example, Fluorescent *Pseudomonas* belongs to PGPR, which plays a significant role in the biological control of pathogens, plant growth promotion, and induced disease resistance. These mechanisms induce resistance and plant-promoting growth under biotic and abiotic stress conditions.[39]

Encapsulation of plant-promoting rhizobacteria has emerged widely in agriculture applications, where encapsulation techniques provide a surrounding protective structure for PGPR microorganisms and control its release with the required functionality. This encapsulation approach, referred to as bio-fertilizer, offers several advantages, including reducing the unlimited consumption of synthetic agrochemical products, enhanced stability and viability of encapsulated microorganisms by improved shelf-life, and protection from depletion against environmental stresses. Encapsulated PGPR-based bio-fertilizers exhibited prolonged viability and increased efficacy in promoting plant growth. It is worth noting that the success of encapsulated PGPR heavily relies on formulation, storage, and application methods. Nevertheless, the implemented encapsulated PGPR as bio-fertilizer still had some main constraints related to their short shelf life and uncontrolled releases; therefore, there is a real need for improving the formulation of these bio-fertilizers and to have a new bio-fertilizer more effective and have long –term stability.[40]

1.3.4 Nano capsules Synthesis Route

1.3.4.1 Ionotropic Gelation of Calcium–Alginate Complexation

The ionotropic gelation (IG) technique is based on forming nanospheres, offering a versatile approach in different fields, mainly agriculture. In this research synthesis method, the ionic gelation is based on the ability of used polyelectrolytes to interact in the presence of counter ions of other polymers. This leads to the formation of spherical particles with controlled size, high loading capacity, and sustained release profile, which also can undergo precipitation. [41]

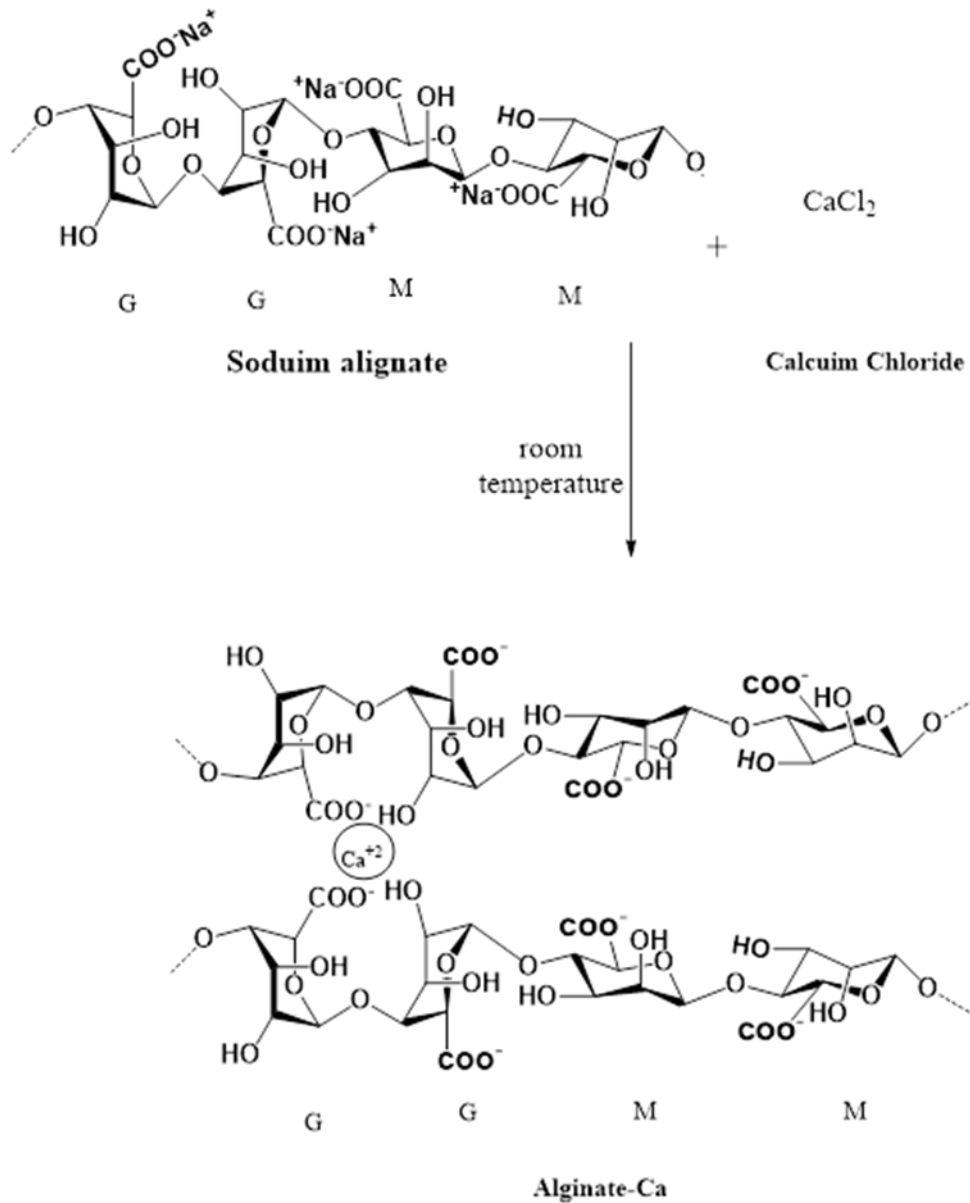
Alginate polysaccharides are dissolved in a suitable acidic solution to form ionic solutions; then, the anionic solution is cross-linked with calcium chloride as a counterion, forming a hydrogel. There are two synthesis methods: internal and external. The cross-linking cation is incorporated within the polymeric solution in the internal method. Meanwhile, the cross-linking cation is positioned externally in the external

method, resulting in nanoparticles with efficient matrix strength and slower active release. Ideally, the calcium–alginate hydrogel core will be bounded by a membrane containing the active nutrient either by absorption or chemical interaction, where the poly-guluronate units of alginate moiety form a chelated structure with the calcium cation, forming spherical structures. [42]

Calcium cation is also used for optimal encapsulation efficiency with high mechanical strength. Calcium ions act as cross-linkers that distribute with an unequal affinity for the mannuronic unit (M) and guluronic unit (G) of polymeric alginate structure and interact with G blocks of alginate due to structurally chelation stires resulting in a meshwork egg box network pre-gels structure form as shown in Figure 3. Further addition of calcium cations with pursue interaction with unreacted poly guluronate units of alginate forming a stacked calcium-alginate complex in a planar two-dimensional manner; this is called the dimerize process of alginate chains with each other through the stacking of (G) groups, ending with a hydrogel network. Literature shows the importance of The ionotropic gelation step for enabling ionic interaction in the polyelectrolyte complexation step and improving active nutrient encapsulation efficiency and bioavailability.[42]

Figure 3

Ionotropic gelation of calcium–alginate complexation



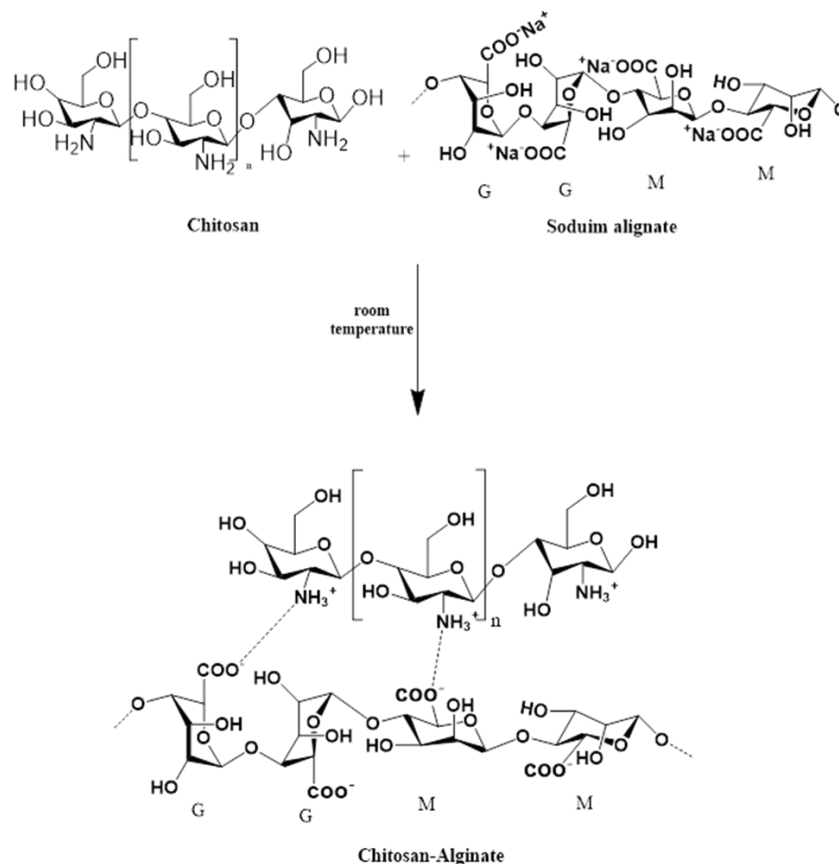
1.3.4.2 Polyelectrolyte Complexation Chitosan –Alginate Complexation

The polyelectrolyte complexation (PEC) technique followed the ionic gelation method, which is based on the addition of a polyvalent cations polysaccharide into the formatted hydrogel solution, where the cations diffuse into the coated polymeric drops with strong electrostatic interactions between oppositely charged polyelectrolytes forming polyelectrolyte complexation (PEC) with nano spheres as shown in Figure 4. Likewise, in this research work, the chitosan dissolves in an acidic solution with a specific adjusted pH value range since a low pH value affects the alginate to be shrunk; also, the

high pH value range affects both chitosan and alginate solubility's; therefore, the pH value shall be considered in the preparation. Mechanistically, the electrostatic interaction between the chitosan and alginate based on ionically cross-linked between amine groups (NH_3^+) of chitosan with carboxyl groups (COO^-) of alginate in adjusted acidic pH ranges, fabricating chitosan – alginate nanoparticles entrapped of active nutrient and PGPRs. [43]

Figure 4

Polyelectrolyte complexation chitosan –alginate complexation



The chitosan function coats the calcium–alginate forming pre-gel, decreases the porosity of alginate beads, and adds mechanical strength to the nanoparticles, while alginate's function is to entrap the materials inside its matrix. The process of PEC of chitosan dropping into the alginate solution leads to more stable nanoparticles through Brownian motion or the thermal motion of suspended particles with a decreased leakage of encapsulated material with a controlled release performance. Even though these biopolymers are great candidates for creating an encapsulation system to be a nano-bio-

fertilizer, this encapsulation type still has some drawbacks regarding low mechanical strength and fast burst release of their synthesized nano capsules with limitations of entrapped materials. Therefore, the cross-linking of chitosan-alginate nano capsules will be encountered in this research work using humic acid as a cross-linker and suitable matrix media for preserving PGPR microorganisms. The cross-linker can enhance the stability of formulated nano capsules with high encapsulation efficiency, mechanical strength, and prolonged nutrient release.[44]

1.3.5 Active Nutrient Entrapment Method

The method of trapping active nutrient and PGPR strains within or throughout calcium-alginate and humic acid matrixes was described in this research. In this research, encapsulation has been implemented with semi-permeable membranes to attain the controlled prolonged release of encapsulated molecules. Two physical methods are usually achieved by loading entrapped or embedded molecules into the matrix or absorbing them onto the surface: absorption or incorporation, where incorporation means loading active materials at the time of nanoparticle production technique, while absorption is loading active molecules after the formation of nanoparticles. The incorporation method is better than the absorption method in controlling the release of entrapped molecules; also, the incorporation method allows for maximum loading of dissolving hydrophobic materials in miscible organic solvents, according to Ford and others[45] and Li and others.[46] This resulted in the Tyndall effect, with a biopolymer membrane layer controlling the diffusion out of the entrapped materials and protecting them from environmental impacts.

1.4 Chitosan and its Derivatives As Antimicrobial Agents

The increasing prevalence of microbial infections and antibiotic resistance in the agriculture sector has made the development of novel natural, non-toxic antimicrobial agents a critical area of recent research. Recently, there has been a growing interest in using heterogeneous photocatalyst materials to develop efficient and greener antimicrobial materials. These heterogeneous photocatalyst materials include natural or artificial polymers such as chitosan, alginate, polyvinyl alcohol, and polypropylene, in combination with different photocatalyst materials, leading to an efficient heterogeneous photocatalyst promoter in this approach. Among these, chitosan-based

nanocomposites are preferably used as robust metrics for different nanocomposite materials. They have shown promising results in different fields due to their unique physical and chemical properties, such as structural features, biocompatibility, biodegradability, and low toxicity.[47]

1.4.1 Chitosan –ZnO

Zinc oxide nanoparticles are considered one of the most attractive semiconductors metal oxide nanostructures due to the unique direct immense band gap of (3.37 eV) with an excitation binding energy of (60 meV). The large band gap of ZnO of semiconductors gives it superior features, such as high breakdown voltage, high stability, and extensive electric field conditions. This conductivity and properties are thought to be the existence of nonstoichiometric defects in the ZnO crystal lattice structure. Moreover, ZnO nanoparticles have been explored in many antimicrobial applications since they are bio-safe and biocompatible polar semiconductor materials, as their synthesis depends on the ease of preparation methods with green, non-toxic, and low-cost precursors. Mainly, its antimicrobial mechanism relies on the illumination of visible light irradiation to excite electrons with sufficient energy compared to its band gap value, which releases its Zn cation and produces reactive oxygen species (ROS) formation.[48, 49]

Additionally, ZnO in heterogeneous photocatalysis has been recently applied as an antimicrobial agent for different industrial applications due to its high chemical stability, significant photocatalytic properties, suitable band gap, and ease of production with outstanding environmental resistance ability. Despite the mentioned advantages, ZnO nanoparticles still exhibit some drawbacks, such as a low photocatalytic activity because of the high recombination rate of charge carriers, low photon utilization efficiency, narrow spectrum range, and direct absorption only in the visible light region. Therefore, ZnO nanoparticles required more treatment to improve their photocatalytic activity efficiency and other properties through combination with other materials, semiconductors, or nanomaterials.[49]

There are diverse methods for combining ZnO nanoparticles with other materials, semiconductor catalysts, and biopolymers to address the main photocatalytic activity challenges. The usage of stable materials in the photocatalyst structure with the

availability of large surface area has dramatically increased since they showed a wide range of economic advantages of stability and photocatalytic efficiency.

Recent studies have highlighted the potential of chitosan-based photocatalytic materials, indicating their antimicrobial activity can be significantly improved. These include a wide range of photocatalytic materials such as semiconductor materials such as metal, metal oxides, carbon-based materials, and/or hybrid materials consisting of metal oxide with carbon-based nanoparticles. Incorporating chitosan with metal oxide, notably TiO_2 , ZnO , and Fe_2O_3 , is commonly employed as photocatalytic film materials. Among these, chitosan- ZnO has emerged as exceptional and versatile as an antimicrobial photocatalyst film material due to its unique optical, electrical, and mechanical properties compared to other semiconductor metal oxide materials. Also, these photocatalytic material films were carried in various domains, including antimicrobial, solar energy, sensor, and UV protection films.[50]

The interaction mechanism of chitosan with ZnO nanoparticles occurred through chelation, coordination of amine groups in chitosan matrix, co-precipitation with ZnO nanoparticles exchange, or electrostatic interaction with protonated amine groups. However, the application of these hetero-photocatalyst materials has some constraints related to their dispersion and limited photocatalytic activity, which must be addressed in the modification through physical or chemical methods to alter its physicochemical properties and overcome the limitation of a particular photocatalyst. Some efficient methods have been recently improved in combining these photocatalytic-based chitosan materials with an inorganic filler such as calcium phosphate cement, silica, or organic materials such as carbon nanomaterials, nanostructure materials to sustain the role of heterogeneous photocatalytic applications.

1.4.2 Chitosan –CNDs

Carbon Nano Dots (CNDs) or Carbon Quantum Dots (CQDs) are new categories of carbon nano-allotropes produced from several raw and waste organic materials. CNDs usually have a particle size of less than 10 nm, and their surface consists of diverse functional groups such as sulfur, nitrogen, and oxygen groups according to synthesis and raw materials used. These CNDs have significant optical fluorescent properties, which gain broad excitation wavelength in the UV-visible region. These unique

photocatalytic properties make them good candidates for various agriculture applications, mainly as antimicrobial agents. Nevertheless, these CNDs suffer from fast biodegradation either in their implementation or formulation, thus limiting their implementation. For that cause, CNDs have been incorporated with other materials, such as semiconductors and biopolymer materials, to enhance their stability and photocatalytic properties. [51]

On the other hand, incorporating chitosan with carbon-based materials, particularly carbon nanoparticles such as carbon allotropes, graphene oxide, and carbon nano dots (CND) materials, has been demonstrated to amplify its optical properties performance by increasing the available surface area. This amalgamation has enormous potential to be an active material as an antimicrobial agent. Specifically, chitosan-CND possesses an array of advantages over traditional chitosan-carbon-based materials. This is attributed to the exceptional tunable fluorescence, luminescent properties, and chemical inertness of CNDs, making them more efficacious in photocatalyst fields. Indeed, carbon nanoparticle sizes are typically less than 10 nm with diverse functional groups on their surface, such as amino, carboxyl, and hydroxyl groups, in different portions based on their synthesis routes and used precursors. Hence, it eases their incorporation with chitosan matrices through covalent or non-covalent interactions and provides further scopes for surface passivation and photoluminescence properties. [52]

1.4.3 Chitosan –Hybrid

Carbon nanostructure and ZnO nanoparticles can combine to form hybrid nanocomposites with exceptional photocatalytic properties, which achieve better performance and further extend their possible practical applications. CNDs can easily be incorporated with such ZnO metal oxides and effectively increase light absorption of metal oxide / CNDs nanocomposites in Uv-visible light region, leading to massive photocurrents production with favorable conduction band and electrochemical activity. [53]

CNDs have been characterized by their significant photocatalytic properties, photo-induced electron transfer activity, and up-convection behaviors. Therefore, combining CNDs with ZnO to form a hybrid nanocomposite can alter and increase the photocatalytic properties that can be efficient in many application fields. The

advantages of this combination come with a modification of ZnO photocatalytic properties in the charge transfer mechanism from fluorescent CNDs to ZnO nanoparticles, causing an increment in charge separation and altering the band gap.[53]

Thenceforwards, newly developed hybrid nanocomposites of metal oxide and carbon nanostructure materials have shown great potential as ideal candidates for various applications, such as solar cells, semiconductor-based industries, energy conversion, chemical sensing, water disinfection, and environmental remediation. Mainly, the hybridization of carbon nano dots conjugated with zinc oxide nanocomposites has shown an outstanding antimicrobial performance in different studies due to its unique photoluminescence properties resulting from newly synergistic photocatalytic effects. Incorporating chitosan with hybrid nanocomposites leads to a heterogeneous photocatalyst film that has been shown to enhance its efficiency in many usages. Several studies have explored the synthesis of these heterogeneous photocatalyst films and their implementation, including Yang et al. on the Synthesis of CND-MnO₂-based glutathione sensor[54], Wang et al. on the Synthesis of CND-MnO₂-based N-acetyl-L-cysteine sensor[55]. The results demonstrate that functionalizing chitosan with hybrid materials can improve their photocatalytic properties and performance. Furthermore, these heterogeneous photocatalyst materials show promise as efficient and sustainable solutions for various applications, with the potential to overcome the limitations of conventional hybrid materials or even individual materials.

1.5 Chitosan based Amino Acids as PGPRs and Plant Bio-stimulant

1.5.1 Chitosan Functionalized with Amino Acid

The utilization of naturally derived products, including fertilizers and pesticides, has garnered notable attention within contemporary research. Among these, amino acids have emerged as particularly intriguing natural materials, commanding substantial interest across various domains of plant science. Comprising inherent constituents of plants, such as nitrogen and carbon, amino acids play a pivotal role in diverse processes, encompassing bio-stimulation, seed germination, floral morphogenesis, photosynthesis, and vegetative expansion. Additionally, amino acids can foster the proliferation of specific beneficial bacteria known as Plant Growth-Promoting Rhizobacteria (PGPR). These microorganisms are vital in fortifying plants against biotic and abiotic stressors.

Incorporating amino acids into fertilizers aligns harmoniously with their status as essential or non-essential significance compounds, further accentuating their role in advancing agricultural practices.

1.5.2 1- Amino Cyclopropane 1- Carboxylic acid (ACC) Amino Acid

1- Amino cyclopropane 1- carboxylic acid (ACC), a non-proteinogenic amino acid, was discovered as an immediate precursor of ethylene hormone in plants. Ethylene hormone can regulate the plant growth and its responses to abiotic and biotic stresses, in part by complex interactions with phytohormones exerted by plants under occurred conditions, where reduction of ACC could inhibit the bio production of ethylene and alleviate the inhibitory effects of ethylene on plant growth. Also, the conjugation of ACC with other materials has played a role in regulating the level of ethylene hormone biosynthesis and, therefore, can be utilized by plants to control the level of ethylene production. [56, 57]

Some PGPR strains revealed a high activity of ACC deaminase, where this kind of PGPR is called ACC deaminase-producing bacteria, such as *Azospirillum*, *Chromobacterium*, *Azotobacter*, *Bacillus*, and others. These PGPR bacteria can hydrolyze ACC to α - ketobutrate and ammonia to utilize them as a carbon and nitrogen source. In addition to regulating the ethylene hormone level, the ACC compound can facilitate the growth of PGPR strains. [39, 56, 58]

Recent studies focus on studying the effect of ACC deaminase exerted by different types of PGPR strains and its role in promoting plant growth under biotic and abiotic stress conditions; others handled the conjugation of ACC with other compounds and tested their effects in different application fields. As a small amino acid compound, ACC has a high water solubility; therefore, in this research, ACC will be functionalized with chitosan biopolymer to decrease its biodegradability in the soil and promote PGPR strains' growth.[56-58]

1.5.3 L- Valine Amino Acid

L-valine is one of these amino acids essential in promoting plants' root growth and improving their photosynthetic rate. This amino acid consists of α - amino group, α - carboxylic acid group, and a side chain isopropyl group, making it a non-polar

aliphatic amino acid. Numerous studies have highlighted the importance of L-valine in various physiological processes of plants, including protein synthesis, nitrogen fixation, and stress response mechanisms. For example, the impact of L-valine supplementation on rice plants' growth and stress tolerance significantly improved the plant's biomass, photosynthetic, and antioxidant defense system. Also, other studies revealed the involvement of L-valine in regulating plant immune responses and its role in nitrogen metabolism and nutrient uptake.[59-61]

L-valine can promote plant growth, nutrient intake, and immune responses. Conjugated amino acids with other biopolymers can play a role and enhance their stability for long-term effects.

1.5.4 L-Tryptophan Amino Acid

L- Tryptophan contains α - amino group, α - carboxylic acid group, and a side chain of indole as polar and aromatic beta carbon as non-polar.

L- Tryptophan is an essential precursor molecule to the plant growth hormone indole acetic acid (IAA), produced by 80 % of bacteria from the rhizosphere. L- Tryptophan is considered an efficient physiological precursor of IAA in microbial biosynthesis of auxins and higher plants. Auxin is an essential plant hormone in cell elongation, root formation, and plant growth. So, as L-tryptophan exists in the soil, it can enhance these microbes to produce significant quantities of auxins and positively influence plant growth and development. Besides that, L-tryptophan contributed to activating plant defense pathways, leading to resistance against various pathogens. L-tryptophan shows diverse importance in plant physiological processes and significantly enhances plant growth and resilience.[62]

1.5.5 L- Lysine Amino Acid

L-lysine contains α - amino group, α - carboxylic acid group, and a side chain of lysyl ((CH₂)₄ NH₂) with actual charges. L-lysine plays a crucial role in the growth and development of plants; it serves as a building block for proteins and is involved in various metabolic pathways. Several studies have highlighted the importance of L-lysine in enhancing plant tolerance to abiotic stress and stimulating its growth. Also, L-lysine participated in synthesizing osmoprotectants and antioxidants, thereby

mitigating the harmful effect of stress-induced oxidative damage. Furthermore, studies investigated the impact of L-lysine on plant nutrient uptake and photosynthesis efficiency, which observed that L-lysine improved the absorption of essential nutrients, such as nitrogen and phosphorus, leading to enhanced plant growth, chlorophyll content, and photosynthesis performance, indicating the positive impact of L-lysine on plant physiological processes.[63]

In this nexus, a controlled release of quantized amino acid in a sustained manner can be regulated throughout formulation as amino acid-containing polysaccharides or referred to as amino biomaterial. These biomaterials possess unique chemical, physical, and biological properties, and their monosaccharide building blocks give them diversity and complexity. The amino acid group containing polysaccharide derivatives can commonly be found in different applications, from wastewater to biomedical uses. Various pathways were presented for the introduction of amino acids with biomaterial moieties. On a technical scale, different pathways are implemented to prepare polysaccharide amino acids to be tested as fertilizers and steer profound with a sustainably long-lasting effect on plant growth.

1.6 Recent Research Related to Nano bio-fertilizer

Many efforts have been encountered in formulating nanoparticles as either nano-fertilizers or bio-fertilizers for altering environmental risks. These nano–and bio-fertilizers have many classifications regarding their synthesis and formulation techniques. Nano capsules are the most abundant methods for encapsulating active agro-nutrient materials or microorganisms' inoculants. Also, these nano-capsules mainly consist of chitosan–alginate polymer matrices due to their unique physical and chemical characteristics. Some of these nano capsules have been recently modified and cross-linked with other polymers to advance their mechanical strengths and sustain their steady-state release. Still, until now, no research has handled the formulating nano bio-fertilizer cross-linked with humic acid material.

Different studies have emerged on the importance of cross-linking of chitosan–alginate nano capsules to increase efficiency in controlling the release of trapped active agro-nutrients.

A study by Dhiman et al. explored the chitosan-alginate nano capsules in their review for encapsulating NPK active nutrients. The nano encapsulation method was found to have advanced the stability and mechanical strength of the formulated nano capsules, facilitating its controlled released mechanism with a prolonged release.[64]

A study by Mesias et al. investigated the encapsulation of NPK in chitosan alginate no capsules cross-linked with calcium chloride and citric acid. The results revealed that the cross-linked effectively protected NPK from fast leaching, volatilization, and degradation, improving its release. The results show high encapsulation efficiency and sustained nutrient release, improving their uptake within plants' rhizosphere and interactions. These studies highlight the potential cross-linked benefits of chitosan-alginate nano capsules for encapsulating NPK active agro nutrient at the nano scale, offering controlled release and sustained nutrient management in agriculture practices. [65]

In a study for bio-fertilizers, Mohsin et al. demonstrated in the review that the application of polysaccharide in the encapsulation of beneficial microorganisms enhanced the survival rate and controlled the release of PGPR microorganisms, promoting their colonization in the rhizosphere and stimulated plant growth. These findings highlight the potential of chitosan-alginate nanocapsules cross-linked with other materials as efficient delivery systems for NPK and PGPRs microorganisms, offering sustainable agriculture strategies. [66]

In this regard, the novelty of this research work will investigate the controlled release property of the cross-linked active agro-nutrients NPK and beneficial microorganisms PGPRs (*Pseudomonas fluorescens*) formed from the cross-linking of the chitosan /alginate using humic acid encapsulating NPK fertilizer hereby referred to as nano bio-fertilizer (Ch. Alg./HA / NPK/PGPRs). Moreover, this study determined the effect of the varying amounts of cross-linker (humic acid as the cross-linker) and polymer blend (Ch./Alg.) ratio on the particle size and encapsulation efficiency. It also determined the controlled release behavior in vitro.

1.7 Recent Research Related to Chitosan Derivatives as Antimicrobial Agents for Agricultural Application

Previous researchers have proved the antimicrobial efficiency of hybrid composites composed of ZnO nanoparticles with different types of CNDs, where CNDs can enhance the ZnO photocatalytic activity in the visible region and, thus, its antimicrobial activity.

A study by Gao et al. synthesized a hybrid composite, where the CNDs were extracted from glucose material and tested its antimicrobial activity against specific types of bacterial strains (*E.coli*, *S. aureus*) with a minimal inhibitory concentration (6-8 mg/ml). [67]

Hojaghan et al. in their research they extracted CNDs from soya chunks and used them in forming the ZnO/CNDs nanocomposites and showed that the presence of CNDs in combination with ZnO nanoparticles reduced the inhibitory effect of ZnO alone, and there was no effect on tested bacterial strains (*S.aureus*, *MRSA*, *E. faecalis*, *Vancomycin-Resistant Enterococcus faecalis*, *klebsiella pneumonia*, *E.coli*, *Shigella dysenteriae*, *Proteus vulgaris*, *Pseudomonas aeruginosa*). [68]

Khan et al. focus on synthesized hybrid nanocomposite from graphene materials with nano-enhanced conjugate of Ag-doped ZnO nanorods and evaluating its antimicrobial efficiency under UV-photo-irradiation. The results showed that light irradiation enhances the reactive oxygen radical species production, affecting the inhibitory effect of hybrid nanocomposites to reduce the tested microbial colonies (*E. coli* and *S. aureus*) with a minimum inhibitory concentration of 10-20 µg/ml. It is noticeable that the antimicrobial activity of different synthesized nanocomposites mainly depends on the CNDs source and hybrid reaction approaches. Thus, forming hybrids can vary in their antimicrobial activity. [69]

On the other hand, recent studies have highlighted the potential of chitosan-based photocatalytic materials, indicating that their antimicrobial activity can be significantly improved by increasing their stability. These include a wide range of photocatalytic materials such as semiconductor materials such as metal, metal oxides, carbon-based materials, and/or hybrid materials consisting of metal oxide with carbon-based

nanoparticles. Incorporating chitosan with metal oxide, notably TiO_2 , ZnO , and Fe_2O_3 , is commonly employed as photocatalytic film materials. Among these, chitosan- ZnO has emerged as exceptional and versatile as an antimicrobial photocatalyst film material due to its unique optical, electrical, and mechanical properties compared to other semiconductor metal oxide materials. Also, these photocatalytic material films were carried in various domains, including solar energy, sensor, and UV protection films. [70-72]

On the other hand, incorporating chitosan with carbon-based materials, particularly carbon nanoparticles such as carbon allotropes, graphene oxide, and carbon nano dots (CND) materials, has been demonstrated to amplify its optical properties performance by increasing the available surface area. This amalgamation has enormous potential to be an active material as an antimicrobial agent. Specifically, chitosan-CND possesses an array of advantages over traditional chitosan-carbon-based materials. This is attributed to the exceptional tunable fluorescence, luminescent properties, and chemical inertness of CNDs, making them more efficacious in photocatalyst fields. Indeed, carbon nanoparticle sizes are typically less than 10 nm with diverse functional groups on their surface, such as amino, carboxyl, and hydroxyl groups, in different portions based on their synthesis routes and used precursors. Hence, it eases their incorporation with chitosan matrices through covalent or non-covalent interactions and provides further scopes for surface passivation and photoluminescence properties.[73, 74]

This research proposes a novel approach for synthesizing newly heterogeneous photocatalyst films of chitosan/ ZnO , chitosan/CND, and chitosan/ Hybrid (ZnO/CND). CNDs were synthesized from solid olive waste (OSW) through a combination of top-down and bottom-up routes. ZnO nanoparticles were prepared using the precipitation process, and the sol-gel method achieved the conjugation of CND with ZnO nanoparticles, forming hybrid materials. After that, each prepared material was incorporated with chitosan according to physical and chemical synthesis routes, obtaining photocatalytic film materials. This work's novelty relies on utilizing the mentioned prepared materials and their incorporation with chitosan metrics, which has yet to be reported. The morphological characteristics of these materials were examined to identify their structural morphology and photocatalytic effect, revealing the successful fabrication of such photocatalytic functionalized chitosan polymer.

Additionally, photocatalytic functionalized chitosan materials' antimicrobial activity was evaluated against a broad spectrum of various bacterial and fungal strains. The study monitored zone inhibition, minimum inhibition concentration (MIC), and colony formation reductions under dark and sunlight. Also, the photocatalytic mechanism was explored through a glutathione deficiency test for both modes, examining whether reactive oxygen species control the antimicrobial activity and impart their antimicrobial photoluminescence properties. Moreover, the killing time parameter was determined to find the optimal duration for maximum antimicrobial activity, with its potential agriculture application of such hetero photocatalytic composites as natural pesticides rather than considering the solid olive waste product as a troublesome environmental waste.

1.9 Recent Research of Chitosan Functionalized Amino Acid as a Plant Bio-stimulant

Various studies have introduced amino acids to polysaccharide matrices by setting diverse reaction pathways, e.g., converting inulin with dextran and lysine with glycine mediated with diclohexylcarbodiimide. McCormick and Dawsey also have introduced another alternative pathway to cationic polysaccharide ester in the presence of pyridine; throughout the conversion of the biopolymer dissolved in N- methyl-2- pyrrolidone/ LiCl with p- toluenesulfonic acid chloride to yield the 4-[N-methyl amino] butyrate hydrochloride. This final approach was successfully applied to other lactams, and dextroen chitosan was a reference for these reactions.[75, 76]

Suk-Heung conducted another study to study the effect of simulation of γ - aminobutyric acid synthesis and its activity in brown rice by chitosan and amino acid- complexes(glutamic acid) germination solution in combination with calcium/calmodulin on plant growth and yield. This study investigated the effect of chitosan and amino acid complexed fertilizers on tomato growth and yield. Chitosan was used to offer a large surface area for more amino acids to be functionalized and to increase the absorption of amino acids by the plants, promoting plant agronomic and physiological parameters. [77]

A study by Zhai et al. focused on utilizing chitosan-based amino acid complex in enhanced nutrient uptake and growth of tomato plants; this research aimed to investigate the effect of chitosan-based amino acid on enhancing plant growth and nutrient uptake. The results indicate that chitosan increases the surface area for nutrient absorption, improving root development, enhanced nutrient uptake efficiency, and increased plant growth.[78]

A critical review by Rafiee et al. reviewed applied amino acids as plant bio stimulants and highlighted their application's effect on the morphological and phytochemical properties of medical plants either in vivo or in vitro conditions. The review discussed the research that focuses on improving nitrogen use efficiency in lettuce production by utilizing an amino acid mixture, where amino acid played a crucial role in increasing the surface area of the root system, which facilitated the absorption of nutrients and resulted in enhanced nitrogen uptake efficiency and bio stimulate the growth performance of plants.[79]

Mainly, these previous studies focus on reactions of chitosan at the C₂-NH₂ or C₆-OH position with amino acids, leading to various products with selective application. If the incorporation of amino acid occurred onto C₂-NH₂ of the chitosan backbone, it would not be conducive to further amino group modification. Any substitution at C₆-OH will be less adequate than it is. Therefore, blocking the amine group was taken, where a usual C₂-NH₂ is blocked with a phthalic anhydride group, giving the N-Phthaloyl group. The C₆-OH position was then converted to a p-toluene sulfonic acid ester to ease the nucleophilic displacement reaction, yielding terminal amino acid derivatives while preserving the C₂-NH₂ group. Such an approach can significantly expand the application of such a derivative for another substitution on the C₂-NH₂ group.

Even though N-phthaloyl chitosan is still the standard method for amine blocking, it is considered a versatile approach for C₆-OH tosylation. The N-phthaloyl group's unblocking process usually occurs using a hydrazine compound. However, this approach can affect the amino acid structure, where there is an acute chance of a reaction of the carboxylic acid with a hydrazine compound, giving unfavorable side products. Moreover, such a sequence reaction is inefficient as an excess amount of organic solvents as reaction medium and for precipitation of the product is consumed,

with more times required to complete the reactions. That is why the preparation methods established up to now suffer from some main drawbacks, and it becomes necessary to develop new pathways for the synthesis of functionalized chitosan in an efficient manner.[80]

Concerning the extraordinary properties and application of amino acid-functionalized chitosan, in this present research, a novel efficient preparation method for amino acid-functionalized chitosan using a new C₂-NH₂ blocking method with (di-tert-butyl-dicarbonate) as BOC component, subsequently followed with the conversion of C₆-OH chitosan to p-toluene sulfonic acid esters (tosyl chitosan), and then substitution with an amino acid with a nucleophilic substitution pathway.

After that, chitosan was unblocked using a few millimeters of Tri-fluoro acetic acid, and another amino acid addition reaction occurred at the C₂-NH₂ position, with a green chemistry approach and efficient reaction time. This potential pathway with two different amino acids functionalized chitosan can be suitable for controlling its release with efficient attenuation results. Moreover, the effect of these synthesized chitosan derivatives composites will be investigated as plant bio stimulants in enhancing plant growth and nutrient uptake.

1.10 Scope of the Research

Organic farming is up-to-date, such as natural organic fertilizer and pesticide compounds, nano fertilizer and nano pesticides systems, and bio-fertilizer systems. These viable recent agriculture systems deliver fresh and natural farm products by using modern scientific and technical progress for developing agriculture activities to alleviate environmental pollution. Several natural and synthetic polysaccharide polymers have recently gained remarkable attention in this research field.

Some innovative methodologies are being searched to introduce new natural organic materials functionalized polymers formulation as alternative compounds to conventional fertilizer and pesticides; also, other methodologies concentrate on synthesized smart nano-based polymers as nano carriers and nano sensors for innovative delivery and release of active nutrients and pesticides in a sustained, controlled process,

aiming to improve crop production with reducing the various hazardous impacts of these substances.

Currently, chitosan polymer has attracted the interest of research groups from several areas of agriculture and plant sciences application; therefore, considerable scientific contributions are ongoing to improve the formulation and functionalization of chitosan polymer and its implementation in this field.

In this research, three main objectives will be conducted, which are:

1. Synthesis of nano bio-fertilizer capsules by encapsulating active nutrient NPK and beneficial microorganisms (*P. Fluorescence*) through cross-linking of chitosan/alginate nano capsules with humic acid molecule.
2. Bio-pesticide materials are synthesized from chitosan-photocatalytic composites to be used as antimicrobial agents for agricultural purposes.
3. Plant and PGPRs bio stimulant materials are synthesized using amino acid-functionalized chitosan materials for agricultural applications.

The first main objective of synthesizing nano bio fertilizer capsules is based on coating active nutrient NPK and beneficial microorganisms (*P. Fluorescence*) cross-linking chitosan/alginate nano capsules with humic acid molecules. These formulated novel nano capsules will control the release behavior of active NPK nutrients and beneficial microorganisms with higher bioavailability; this general objective was attained by addressing the following specific objectives :

1. Determine the optimal polysaccharide and material concentrations of chitosan/alginate nano capsules and the cross-linker humic acid to achieve the best encapsulation efficiency within optimized particle size and stable surface charge.
2. Characterize the structural, morphological, and thermal stability of the cross-linker of the formulated cross-linked nano capsules (chitosan/alginate) and compare with a controlled trial without cross-linking.
3. Investigate the water retention capability parameter in vitro for synthesized cross-linked nano capsules to depict it as a sustainable solution for water shortage issues .

4. Investigate the active NPK fertilizer release behavior property in vitro of the synthesized nano capsules under specific stress solution conditions within 30 days.
5. Determine the kinetic release behavior of the active NPK fertilizer of synthesized nano capsules and the predominant release module.
6. Investigate the controlled release property of (*P. Fluorescne*) microorganism inoculants in vitro and their stability in synthesized nano capsules within six months.

The second main objective of synthesis of antimicrobial agents as bio-pesticide materials of chitosan-based hetero photocatalytic composites will be conducted with the novel synthesis of chitosan /ZnO nanoparticles (Ch. ZnO), chitosan/CNDs (Ch.CNDs), and chitosan /Hybrid (CNDs/ZnO) nanocomposites (Ch. Hybrid). The Hybrid nanocomposites will be synthesized from a combination of CNDs particles (source olive solid waste) and ZnO nanoparticles, then incorporated in the chitosan polymer matrix. This general objective was also attained by addressing the following specific objectives

1. Characterize the structural and morphological characteristics of synthesized photocatalytic materials ZnO nanoparticles, CNDs, and Hybrid (CNDs/ZnO) nanocomposite.
2. Characterize the structural and morphological characteristics of synthesized photocatalytic materials Ch.ZnO nanoparticles, Ch.CNDs, and Ch.Hybrid (CNDs/ZnO) nanocomposite.
3. Investigating the optical properties parameter of synthesized photocatalytic materials ZnO nanoparticle, CNDs, and Hybrid (CNDs/ZnO) nanocomposite was explored.
4. Investigate the optical properties parameter of synthesized photocatalytic materials Ch.ZnO, Ch.CNDs, and Ch.Hybrid (CNDs/ZnO) was explored .
5. Determine the antimicrobial activity effect of synthetic photocatalytic materials ZnO nanoparticles, CNDs, and Hybrid (CNDs/ZnO) nanocomposite was evaluated against a broad spectrum of various bacterial and fungal strains. The study monitored zone inhibition, minimum inhibition concentration (MIC), and colony formation reductions under dark and sunlight modes.

6. Determine the antimicrobial activity effect of synthetic photocatalytic materials (Ch. ZnO, Ch.CNDs, and Ch. Hybrid (CNDs/ZnO) was evaluated against a broad spectrum of various bacterial and fungal strains. The study monitored zone inhibition, minimum inhibition concentration (MIC), and colony formation reductions under dark and sunlight modes.
7. Determine the killing time parameter of synthetic photocatalytic materials ZnO, CNDs, and Hybrid (CNDs/ZnO) was determined to find the optimal duration for maximum antimicrobial activity.
8. Determine the killing time parameter of these synthetic photocatalytic materials Ch. ZnO, Ch.CNDs, and Ch. Hybrid (CNDs/ZnO) was determined to find the optimal duration for maximum antimicrobial activity.
9. The photocatalytic mechanism of synthetic photocatalytic materials ZnO, CNDs, and Hybrid (CNDs/ZnO) was explored through a glutathione deficiency test for both modes, examining whether reactive oxygen species control the antimicrobial activity and impart their antimicrobial photoluminescence properties .
10. Investigate the photocatalytic mechanism of synthetic photocatalytic materials Ch.ZnO, Ch.CNDs, and Ch. Hybrid (CNDs/ZnO) was explored through a glutathione deficiency test for both modes, examining whether reactive oxygen species control the antimicrobial activity and impart their antimicrobial photoluminescence properties .

The Third main objective is the synthesis of plant bio stimulant materials of dual amino acid functionalized chitosan materials, where this general object is classified into two main categories, as follows:

- Synthesis of plant biochemical precursor 1-aminocyclopropane-1- carboxylic acid (ACC), then functionalized with chitosan polymer. The functionalization process of chitosan was conducted according to predominant N-phthaloyl blocking and C₆-O-tosylation procedure for substituting targeted groups. The aim of this synthesized ACC functionalized chitosan is to study the hypothesis of amendments of these compounds as a promoter for PGPRs strains (*P. Fluorescne*) strains growth, and thus induce soil fertility with reshaping the structure of soil microbiome and alleviate the negative impacts of salinity issues in agriculture aspects.

- The functionality of chitosan with one or two amino acids of the following (L-valine, L-Tryptophan, L- Lysine) to be (Ch. L-valine, Ch. L-tryptophan, L-valine Ch. L- lysine, and L- tryptophan Ch. L- lysine compounds. The synthesis approach was achieved using a new novel synthesis approach of N- N-blocking of chitosan by BOC components; this sub-general objective was also attained by addressing the following specific objectives:
 1. Investigate the two synthetic routes of both illustrated compounds, and the Kaiser test evaluated the efficiency of each synthetic route.
 2. Determine the chemical properties of each synthesized product.
 3. Determine the role of synthesized products as plant bio stimulants on Barely plant growth by measuring selected agronomic and physiological parameters.

Chapter Two

Experimental Part

This chapter focuses on methodologies used on chitosan-based nano capsules and composite synthesis and characterizes which are graded into three main distinct categories as follows: First, synthesis and characterized of chitosan/alginate cross-linked with humic acid nano capsules for entrapped active NPK macronutrient and beneficial bacteria *P.fluorescence* as PGPR strain. These nano bio-fertilizer capsules were optimized for the smallest particle size with maximum encapsulation efficiency and monitoring its Release in a controlled manner. Second, synthesizing and characterizing chitosan-based nanocomposites (chitosan-based photocatalyst materials) and testing in vitro antimicrobial agents. Third, the synthesis and characterize of chitosan-based composites (chitosan-based amino acids materials) as active plant bio-stimulants with in vitro agricultural application.

2.1 Materials and Methods

All used reagents and chemicals were purchased from Sigma Aldrich and used in the research paper without further purification. Distilled water was used for synthesis and antimicrobial procedures.

Fourier Transform Infrared (FT-IR) spectra were acquired in the 4000- 500 cm^{-1} range with 64 scans, each 8 cm^{-1} resolution by Thermo Scientific Nicolet IS5 equipped with an ATR sampling device. The Malvern Zeta Sizer NanoSizer instrument was used to analyze particle size and zeta potential of prepared nanoparticles with Malvern and zeta sizer software at (Forschungszentrum Jülich). The Scanning Electron Microscope (SEM) photograph was obtained by Zeiss Sigma 500 SEM JEOL 7400 E Scanning Electron Microscopy, and the samples were gold-plated at(Forschungszentrum Jülich). The thermal stability for prepared nanocapsules was measured using a Thermo Gravimetric Analyzer (TGA) (Lenovo V520, China) coupled with an MS- Thermostat GSD3220 (Pfeiffer Vacuum) and measured with Pt crucible in nitrogen gas flow (20 ml/min) with a heating rate of 5°C in the range 25 -900 °C. The program was managed by the STAR software v 10.00 (Mettler Toledo). The potassium and phosphorous ions were analyzed using a Thermo I CAP 7000 series ICP spectrometer, and the nitrogen ions were analyzed using a Continuous Flow Analysis(CFU) alliance instrument at(

Forschungszentrum Jülich). UV-Vis absorption spectra were recorded using Beckman Coulter DU 800 Spectrophotometer between 200 and 800 nm. Nano surf core Atomic Force (AFM) Microscope was used to examine particle sizes and morphologies, AFM images were analyzed by Gwyddion software, and AFM samples were prepared by drop-casting of diluted solution on well-cleaned mica substrates. X-ray diffraction spectroscopy was performed by XRD-7000 model diffract meter using $\text{CuK}\alpha$ radiation ($\lambda = 1.5406 \text{ \AA}$) operating at 40 kV/30mA with the step size of 0.02° . The photosynthesis of plant trails was analyzed using Pulse Amplitude Modulated Fluorometry (PAM) (LUCAM, Fluor Cam Version 15.1.0). Nuclear Magnetic Resonance (NMR) Spectroscopy Bruker 500 MHz- Avance III at the Chemistry Department of Jordan.

2.2 Preliminary Study for Synthesis of Nano-bio fertilizer Capsules

The synthesis approach to obtaining the final nano bio fertilizer capsules was based on preliminary and observational stability studies. All these tests were conducted at varying chitosan, alginate, humic acid, and NPK concentrations until the best base model was identified and determined. The optimized parameters of proper pH value, homogenization time, needle gauge size, equilibration time, stirring time, and calcium chloride concentration were also set to obtain the smallest particle size and highest encapsulation efficiency. The observational stability of nanoparticles was taken as transparency, precipitation, and aggregation of these formulated nano capsules. Figure S1 in Appendix B. The Best stable nanoparticle solution with homogenous nano capsules was recorded as the translucent solution with the best transparency observation. Meanwhile, the solutions with opaque, transparent, precipitation, or aggregation solutions and the formulated nanoparticles that had settled down to the bottom of the sample solution immediately or overnight were considered unstable solutions with poor nanoparticle stability. All optimized parameters for the synthesis process with the best particle size and encapsulation efficiency were consolidated and extrapolated into the final nano bio-fertilizer formulation.

2.2.1 Stock Solutions Preparation

The following stock solutions were prepared according to the previously mentioned protocols with some modifications.

2.2.1.1 Chitosan Nano particle Solution (0.05 % w/v)

0.1 g of chitosan material was added to 150 ml of distilled deionized water in a 200 ml volumetric flask and stirred for 30 min. Then, 1 ml of glacial acetic acid was added and allowed to stir for 6 h. After that, the chitosan solution was filtered using vacuum filtration, and its volume was adjusted to 200 ml with the addition of water. Moreover, its pH value was adjusted to 4.6 by adding 6-11 drops of 5 N NaOH to obtain a final chitosan nanoparticle stock solution.

2.2.1.2 Alginate Nanoparticle Solution (0.06 % w/v)

0.15 g of sodium alginate was added to 200 ml of distilled deionized water in a 250 ml volumetric flask and stirred for 4 hours until fully dissolved. Then, the alginate solution was filtered using vacuum filtration using a qualitative filter paper with 10 μm particle retention. After that, 1.25 ml of Tween 20 was added to the solution and stirred for another 2 h until the solution appeared homogenous. Finally, its volume was adjusted to 250 ml by adding water, and pH was adjusted to 4.9 by adding 5-9 drops of 0.5 N HCL to obtain a final alginate nanoparticle stock solution.

2.2.1.3 Humic Nanoparticle Solution (1 % w/v)

Humic acid was extracted from peat soil by alkaline extraction method [81]. 20 g of air-dried sieved homogenized peat soil was mixed in a beaker provided with a four-blade 45 pitched blade stirrer having a diameter of 0.4 m with 100 ml of 0.1 M $\text{Ca}(\text{OH})_2$ and 100 ml of 0.1M NaOH at rotation speed 300 r.p.m for 5 h at ambient room temperature. Then, it was centrifuged at 10000 rpm for 30 min. The obtained supernatant was acidified with 6 M HCL till a pH adjusted to be one and left overnight. After that, the formed humic acid fraction was filtered using a sintered glass funnel and dried in an oven at 80°C, resulting in a solid dark humic acid product. Finally, a stock humic acid solution (1 % w/v) was prepared by dissolving obtained humic acid in distilled water and filtered using a qualitative filter paper with 10 μm particle retention, then stored in

the dark till further use. The obtained humic acid was characterized and compared to the humic content data from the International Humic Substances Society.

2.2.1.4 Selecting and Culturing PGPR (*Pseudomonas fluorescence* (PL 5.4))

Pseudomonas fluorescence (PL 5.4) bacteria strains were cultured in Tryptic Soy Broth (TSB) media and incubated at 30°C for 48 h. After growth, these bacterial strains were striated by depletion on Trypticase Soy Agar plates and incubated at 30 °C for 48 h.

For nano bio-fertilizer capsule preparation, precisely 50 ml of *P. Fluorescence* bacterial culture was centrifuged at 3000 r.p.m for 10 min. The cells were harvested by centrifugation and washed with 0.85 % NaCl (w/v) saline solution, then 10 mg of trehalose sugar was added to enhance the stability of the PGPR bacterial strain without contamination and carried to a shaker for 72 hours. The last cell is obtained as a log growth phase with a 4×10^8 CFU/ml cell density. Then, it was preserved for the preparation of nano capsules.

2.2.2 Ionotropic Gelation of Nano capsules and Polyelectrolyte Complexation

The ionotropic gelation step includes 1 g of each NH_4Cl , KCl , $\text{Ca} (\text{H}_2\text{PO}_4)_2$ as a source of N, P, and K fertilizers were dissolved into the previously 250 ml pH adjusted (4.9) sodium alginate stock solution and stirred for 2 hours at ambient room temperature. After that, 15 ml of 0.2 % (w/v) calcium chloride solution was added dropwise with an adapted burette syringe through a 20-gauze needle into sodium alginate solution to form pre-gel). Subsequently, the pre-gel was stirred for 90 min under mild agitation and sonicated for three cycles of 5 min. Its temperature was raised to 70 °C, and the 15 ml of 1 % (w/v) humic acid was added as a cross-linked and as immobilization of bacterial strains and allowed to stir at 500 rpm for 2 h. After that, the pre-gel mixture was allowed to cool at room temperature, around 25° C, and previously prepared bacterial cell pellets were transferred to the pre-gel mixture, mixed thoroughly for another 2 h, and set for the polyelectrolyte complexation step.

The polyelectrolyte complexation step involved 200 ml of pH-adjusted (4.6) chitosan stock solution was extruded dropwise with an adapted burette- syringe through a 20-gauze needle into a stirred prepared pre-gel mixture. The resulting nanoparticle solution with homogenous nano capsules was recorded as the translucent solution with the best

transparency observation and was stirred for 90 min at room temperature and set down for the lyophilized procedure to obtain a final dried weight of 2.782 g with a yield of 85.6 %

On the other hand, the control samples prepared contained chitosan/ alginate nano capsules with encapsulating NPK active nutrients, and the weight of dried nano capsules was 2.3075 g with a yield of 71%.

All tested trial samples were weighted after the lyophilization process. The yield analysis was calculated from the weight of dried nano capsules recovered as (W_1) and divided over the sum of the initial dry weight of starting materials used (W_2). The yield percentage was determined according to the following equation:

$$\text{Yield (\%)} = \frac{W_1}{W_2} \times 100 \quad (1)$$

Where :

W_1 = weight of dried nano capsules recovered .

W_2 = weight of the initial dry weight of nano capsules.

2.2.3 Homogenization, Purification, and Lyophilization Of Nano bio-fertilizer Capsules

The prepared nano bio-fertilizer capsules were homogenized at 10,000 r.p.m. in 5 min to prevent suspension overflow. Then, it was sonicated three times for 5 min each cycle; then, the suspension was allowed to settle and equilibrate overnight to achieve a complete ionotropic gelation polyelectrolyte complexation. Then, the suspended nano capsules were purified through filtration to remove any excess nano capsules, large aggregates, and undissolved NPK materials. Filtered nano capsule materials were transferred into a 250 ml glass-Prex container and sealed with a lid to be frozen overnight at -20°C . After the retentate material was frozen, the Pyrex lid was replaced with permeable tissue paper and placed again into a freezer dryer at -50°C for 72 h to sublimate all nanoparticle moisture. After that, all prepared samples were removed and weighed out: the control sample (2.3075 g) was white, and the cross-linked sample

(2.9148g) was light brown. All lyophilized trails were stored in an air-tight container in a freezer at -20°C until further characterization.

2.2.4 Encapsulation Efficiency of Nano bio-fertilizer

5 mg of each nano capsule suspension solution trail was centrifuged at 6000 r.p.m. for 30 minutes to separate the nano capsules from the aqueous medium containing the non-associated encapsulated materials. The suspension was left for 48 h in the dark under constant agitation to allow all entrapped active NPK nutrients to be available in the supernatant solution. The free materials in the supernatant were filtered with 0.2 µm membrane and vortexed for 10 sec. Then, each NPK nutrient was determined using ICP analysis for potassium, phosphorous ions, and CFU analysis for nitrogen ions. All trials were carried out in triplicate. The encapsulation efficiency (EE%) of the nanoparticles was calculated according to the following equation :

$$(EE\%) = \frac{\text{Total amount of NPK loaded} - \text{Free amount of NPK}}{\text{Total amount of NPK loaded}} \times 100 \quad (2)$$

2.2.5 Controlled Release of Active Nutrients from Nano bio-fertilizer

To investigate the controlled Release of NPK nano fertilizer behavior from synthesized nano capsules, 50 mg of each lyophilized trail sample nano capsules were transferred to a dialysis bag and then immersed in 100 ml citrate phosphate buffer solution with (pH 5.5). At certain intervals, 10 ml of the solution was taken for NPK concentration determination, and another 10 ml of citrate phosphate buffer solution was added into the beaker to maintain a constant initial solvent volume. The samples were kept at 30°C under gentle stirring at periodic intervals. These measurements were carried out in triplicate, and the data represent the average of these measurements. The amount of phosphorous and potassium ions concentrations were measured using ICP- MS, and nitrogen ions concentrations were measured using CFU analysis.

The percentage of accumulative controlled Release was calculated according to the following equation:

$$E = \frac{V_E \sum_{i=1}^{n-1} C_i + V_0 C_n}{m_0} \times 100 \quad (3)$$

Where:

E is the percentage of accumulative controlled Release (%).

V_E is the volume of sampling volume (ml).

V_0 is the initial volume of the medium buffer (ml).

C_i, C_n is the concentration of NPK nano fertilizer (mg/ml) for initial and at a certain time.

M_0 is the mass of the sample taken for measurement (mg).

2.2.6 Water Retention Behavior of Soil with and without Formulated Nano bio-fertilizer

This experiment was carried out to investigate soil's water retention behavior for formulated tested nano bio-fertilizers. A plastic cup containing 100 g of loamy sand soil and 10 g of lyophilized sample was mixed for both synthesized nano capsule trial samples. 50 ml of distilled water was poured, and the plastic cup was weighed as (W_0). For the control trials, a plastic cup containing 110 g of loamy sand soil and 50 ml of distilled water was poured, and the plastic cup was weighed as (W_0). In another reference of a plastic cup containing only 100 g of loamy sand soil without any sample, 50 ml of distilled water was added too, and the plastic cup was weighted as (W_1) and weighted and set as a reference each time.

All plastic cups were kept in a lab room with ambient room temperature and weighed daily as (W_t) over 30 days with 5 days intervals.

The water retention percent as (WR %) of soil was determined using the following equation:

$$(WR\%) = \frac{W_t - W_1}{W_0 - W_1} \times 100 \quad (4)$$

2.2.7 Particle Size and Zeta Potential Analysis

Particle size and zeta potential of nano bio fertilizer analysis were obtained by dynamic light scattering (DLS) and Malvern nano series zeta sizer instrument. 200 µg of each lyophilized tested sample was suspended in 2 ml of 0.2 µm filtered water, allowing total dissolution. Then, it was vortexed for 20 s and sonicated for 15 min. After that, the sample was filtered through a mciroyn glass vacuum filter with (10µm particle retention) and sonicated for 5 min to dissolve fine nanoparticles fully. Subsequently, a small portion of the sample was placed in a plastic cuvette and carried to the analyzer chamber. All analysis measurements were performed at a scattering angle of 90 °C, temperature of 25 °C, and refractive index of 1.590. For each trial, the collective 24 reading was the mean diameter of particle size and zeta potential with a standard deviation of 100 iterations.

2.2.8 Thermogravametric Analysis

(~20 mg) of each lyophilized sample was added into aluminum pans with a hole in the lid, and scanning was completed at a rate of 10 °C/ min from 0 °C to 700 °C with nitrogen purging and measured with Pt crucible in nitrogen gas flow (20 ml/min) with a heating rate of 5°C in the 25 -900 °C range. The program was managed by the STAR software v 10.00 (Mettler Toledo)

2.2.9 Enumeration of P. fluorescence in the Nano capsules

To estimate the viable counts of bacterial strain in the formulated nano capsules and the amount of viable bacterial strains without any contamination by measuring the releases encapsulated bacterial strain by resuspending 100 mg of nano capsules in phosphate-buffered saline (pH 7.0) for 40 min followed by homogenization. The total number of released bacterial strains was determined by the standard plate count method after incubating at 30 °C for 48 h. At every monthly interval, the cell densities in the nano capsules were enumerated using a similar method to study the cell loss upon storage. [82]

2.3 Synthesizing and Characterizing Chitosan-based Nanocomposites (Chitosan-based Photocatalyst Materials) and Testing In Vitro Antimicrobial Agents

2.3.1 Synthesis of Chitosan.ZnO

Zinc oxide (ZnO) nanoparticle synthesis was carried out according to a previously reported work [83] with some modifications. In brief, 1.4 g of zinc sulfate heptahydrate ($\text{ZnOSO}_4 \cdot 7\text{H}_2\text{O}$) was dissolved in isopropanol and subjected to continuous stirring for 12 hours while 50 ml of 1 M NaOH was slowly added dropwise. The resulting white suspension was centrifuged at 4000 r.p.m. for 20 minutes using a HERMLE Z 200 A Universal Compact Centrifuge. The resulting pellets were washed with distilled deionized water three times by adding 50 ml each time, followed by centrifugation at 4000 r.p.m. for 10 minutes. Finally, the product was recovered and dried in an oven at 100°C for 24 h to obtain dried white-colored ZnO nanoparticles kept for further use and functionalization with chitosan polymer.

A chitosan solution was prepared by dissolving 1 g of chitosan in 98 ml of distilled water containing 2 ml of concentrated acetic acid. The resulting mixture was stirred at 700 r.p.m at room temperature until a clear solution was obtained. After that, 0.0366 g of ZnO nanoparticles was added to 15 ml of chitosan solution, which was then subjected to sonication for 40 min. Subsequently, 1M of NaOH was added dropwise to the mixture until a pH of 10 was achieved, and the solution was stirred at 7000 r.p.m in a water bath at 60°C for an additional 4 h until it turned to an off-white gel color. The solution was centrifuged at 3000 r.p.m. for 15 minutes using a HERMLE Z 200 A Universal Compact Centrifuge and repeatedly washed with distilled water, then poured into a PVC plate and dried in an oven at 100 °C for 2 hours to remove water molecules. The result is an off-white thin film with a weight of 0.105 g, referred to as Ch.ZnO, for further characterization and application.

2.3.2 Synthesis of Chitosan. CNDs

Carbon nano-dots (CNDs) have been synthesized through a modified protocol originally reported by Sawalha et al.[84] This procedure utilized Olive Solid Waste (OSW) to obtain the CNDs particles. Initially, The OSW product was washed with boiled water to remove impurities, and then it was subjected to a pyrolysis process at 400°C for 1 hour,

generating carbon-based material. The resultant material was subsequently milled to a fine black powder.

After that, 100 mg of black powder was dispersed in a mixture of 10 ml of distilled water with 0.45% H₂O₂; the mixture was sonicated for 15 minutes using Elmasonic S 100 H sonicator, followed by refluxing for 100 minutes. The solution was centrifuged at 6000 r.p.m. for 20 minutes using a HERMLEZ 200 A Universal Compact Centrifuge. The supernatant containing CNDs particles was filtered through a 0.22 µm – filter syringe. Subsequently, the prepared CNDs solution was dialyzed through 1 KD membrane against distilled water overnight to remove any excess or unreacted reagents. Finally, the CNDs solution was lyophilized to obtain a light brown powder for incorporation with chitosan polymer.

To prepare the chitosan-CND nanocomposite, a chitosan solution was made by dissolving 1 g of chitosan in a mixture of 98 ml distilled water and 2 ml concentrated acetic acid, followed by stirring at 7000 r.p.m. until a clear solution was obtained at room temperature. Subsequently, 10 ml of CND (1mg/ml) solution was added to 20 ml of chitosan solution and then sonicated using an Elmasonic S 100 H sonicator for 30 minutes. After that, the solution was heated in a water bath at 80 °C for 5 hours. The obtained solution was centrifuged at 3000 r.p.m. for 20 minutes using a HERMLEZ 200 A Universal Compact Centrifuge. Then, it was washed several times with distilled water, poured onto a glass plate, and dried in an air oven at 100 °C till a tan-yellowish colored thin transparent film was obtained, weighing 0.173 g, which is referred to as Ch.CND for further analysis.

2.3.3 Synthesis of Chitosan. Hybrid (ZnO /CND)

The hybridization approach of the hybrid (ZnO /CND) nanocomposite was executed through a modified version of a previously reported procedure in the literature [85]. A green sol-gel method was carried out in a one-pot reaction. Specifically, ZnO (70 mg, 0.885 mmol) was dispersed in 10 ml of isopropanol in a 50 ml round bottom flask and stirred until completely dissolved. Next, 9 ml of CNDs solution (1mg/ml) was added to the flask, and the mixture was covered with aluminum foil and sonicated for 30 min at 80°C using an Elmasonic S 100 H sonicator. The mixture was kept stirred at room temperature overnight, and the obtained precipitate was separated by centrifugation at

300 r.p.m. for 10 min using a HERMLEZ 200 A Universal Compact Centrifuge. Next, the precipitate was washed with 30 ml of distilled water to remove unreacted CNDs and followed by dried at 60°C for 2 h. The obtained pale-yellow powder was referred to as a hybrid. It exhibited an increased absorption in the visible light region and influential energy conduction band, leading to massive photoluminescence.

For the incorporation of chitosan with hybrid material forming a heterogeneous photocatalytic material, the experimental procedure involved the dissolution of 0.1 g of chitosan in 16 ml of aqueous acetic acid (1% v/v), followed by the addition of 0.05 g of a hybrid material, and stirring the mixture for 1 h at room temperature until a homogenous dispersion was obtained. Subsequently, the resulting solution was heated in a water bath at 80°C for 4 h to initiate the hydrothermal reaction. The resulting product was then centrifuged at 10,000 r.p.m. for 10 minutes using a HERMLEZ 200 A Universal Compact Centrifuge, and the supernatant was filtered through a 0.22 µm filter membrane. The precipitate obtained was decanted onto a glass plate and dried in an air oven at 100 °C till a pale-tan colored thin transparent film was obtained, with a total of 0.0809 g, which is referred to as Ch.Hybrid for further characterization and antimicrobial identification.

2.3.4 Antimicrobial Activity

2.3.4.1 Microbial Strains

Antimicrobial activity performance of synthesized photocatalytic materials ZnO, CNDs, Hybrid, Chitosan, Ch./ZnO, Ch./CNDs, and Ch./Hybrid was investigated against a broad spectrum of gram-positive and gram-negative bacterial and fungal strains such as *Staphylococcus aureus* (ATCC25923), *Klebsiella pneumonia* (ATCC 13883), *Escherichia coli* (ATCC 25922), *methicillin-resistant Staphylococcus aureus* (MRSA) (DPC 5645), *Saccharomyces cerevisiae* (PMID 8849441), *Proteus vulgaris* (ATCC 13315), *Aspergillus funigatus* (ID18).

2.3.4.2 Preparation of Antimicrobial Stock Solution

The antimicrobial agent stock solutions for synthesized materials with a concentration of 1000 µg/ml of 10 % (v/v) DMSO were prepared using 13×100 mm sterile test tubes. Serial dilutions were prepared for each stock solution by transferring 0.5 ml from each

tube to another test tube containing 0.5 ml of 10 % (v/v) DMSO, resulting in a final volume of 1 ml. This process was repeated for a total of nine dilution sets obtained. 100 μ l of each diluted stock solution was collected and preserved to examine the antimicrobial activity. In order to ensure accuracy and reliability, the trials were conducted in triplicate for all tested synthesized materials and their respective stock solutions for both dark and sunlight conditions modes.[86]

2.3.4.3 Preparation of Microbial Suspension

The McFarland reference solution microbial suspensions were prepared according to the Clinical Laboratory Standards Institute (CLSI) protocol. 0.5 of McFarland reference solution was prepared by mixing 0.5 ml of 1.167 % (w/v) $\text{BaCl}_2 \cdot \text{H}_2\text{O}$ with 99.5 ml of 1% (v/v) H_2SO_4 and covered with aluminum foil for further use. For the microbial suspensions for each microbial strain, two to three counted colonies from a cultured plate were transferred to a sterile saline solution. The turbidity of microbial suspensions was adjusted using the prepared 0.5 McFarland reference solution, and their absorbance was measured at $\lambda = 630$ nm, setting pure water as a reference blank. The turbidity scale ranged from 0.08 to 0.1, correlated with a 1.5×10^8 CFU/ml microbial concentration. After that, 100 μ l aliquots of the adjusted inoculum solution were transferred to each well, considering the positive and negative control wells, and incubated overnight at 24 $^\circ\text{C}$. [86]

2.3.4.4 Agar Disk Diffusion Test Zone Inhibition Test

The zone inhibition assay was carried out 0.5mm diameter wells were made using a corker borer. The prepared materials 100 of 1 mg/ ml was added into the well; in the third well, chitosan was added as a control, and the plates were incubated at 24 $^\circ\text{C}$ for 24 h; duplicate tests were conducted for each mode, and the inhibition zones diameter were measured using the standard antibiotic zone scale for each sample tested. Each material's experimental procedure was carried out to determine the most effective concentration.[86]

2.3.4.5 Determination of Minimum Inhibitory Concentration (MIC)

The minimum inhibitory concentration for synthesized materials and chitosan as a control was carried out according to the CLSI guidelines. This method involves using a 96-well plate to prepare stock solution antimicrobial agents, with each well labeled according to the microbial strains tested, solution names, and their concentrations. Next, aliquots of 100 μ l of each microbial suspension and diluted antimicrobial solution were pipetted to the wells in serial order, considering the negative and positive control wells. Then, the plates were incubated at a constant temperature of 24°C for 24 hours, either in the dark or under sunlight, with the former covered by aluminum foil to maintain a dark environment. The test was performed in triplicate for each sample and mode. The MIC is known as the lowest concentration of the tested antimicrobial solution that can inhibit microbial growth, as per the guideline of the CLSI.[86]

2.3.4.6 Determination of Microbial Colonies Forming Unit Reduction (CFU)

This test utilized the surface plating technique to determine the number of viable colonies for all tested antimicrobial solutions at a constant known concentration employing the traditional method. Specifically, the microbial suspensions were first diluted to a concentration of 10^6 CFU/ml in a sterile 0.9 % saline solution. Then, 100 μ l aliquots of each diluted antimicrobial solution were surface-plated onto LB agar plates, along with 100 μ l aliquots of each microbial suspension. Subsequently, the plates were incubated for 24 hours at 24°C with continuous agitation. Following this, the colonies on all tested antimicrobial samples and controls were tallied, and the viable colony numbers were determined as log and percentage colony-forming units to determine the microbial colonies forming unit reduction. [86]

2.3.4.7 Glutathione Deficiency Test

The antioxidant activity of synthesized materials was determined by the DPPH free radical scavenging method. Briefly, a portion of 255 μ l of each synthesized material was separately dispersed in 50 mM bicarbonate buffer with a specific pH of 8.6. After that, 255 μ l of 0.4 mM of Glutathione (GSH) was added to each solution to induce the oxidation process. Positive control was about 0.4 mM of GSH oxidation with 1 mM H₂O₂, and negative control was about using a GSH solution only. All samples were wrapped with aluminum foil and agitated in a water bath shaker for 2 h with a speed of

150 rpm. After that, to measure the antioxidant activity, 15µl of 100 mM DNTB Ellman's reagent and 780 µl of 0.05M Tris-HCl were added to each sample. The GSH absorbance assays were measured spectrophotometrically at $\lambda = 412$ nm. All samples were conducted in triplicate for each dark and sunlight mode, and all results are reported as mean value \pm SD. The absorbance at $\lambda = 412$ nm was measured and used to calculate the antioxidant activity of each sample according to the following formula:[86]

$$\% \text{ loss of GSH: } ((\text{absorbance of negative control} - \text{absorbance of the sample}) / \text{absorbance of negative control}) \times 100 \%. \quad (5)$$

2.3.4.8 Time- Kill Kinetics

This test was performed according to previously reported methods[87] with some modifications. The minimum inhibitory concentration (MIC) of each tested sample was conducted in this experiment to determine if the nature of the inhibitory effect is time-dependent or concentration-dependent.

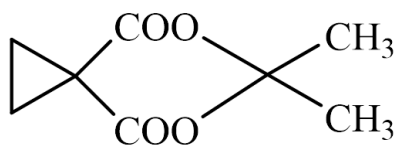
This test was performed in triplicate for dark and sunlight modes, where four tubes for each sample and test were conducted. A 1 ml volume of adjusted microbial inoculums (10⁶ CFU/ml) and tested sample were added to three tubes, and the fourth tube is considered the growth control. All tubes were agitated at 200 rpm and incubated at 24 °C. Subsequently, 100 µl of each tested sample was carried out to measure its turbidity for each microbial strain at $\lambda = 630$ nm at different varied time intervals (0, 4,6,8,10,12 h). The MIC of each sample was plotted against the time of killing for each strain.

2.4 Chitosan-based Composites (Chitosan-based Amino Acids Materials) are Active Plant Bio-stimulants with in Vitro Agricultural Applications

2.4.1 Synthesis of ACC(1- amino cyclopropane -1- carboxylic acid)

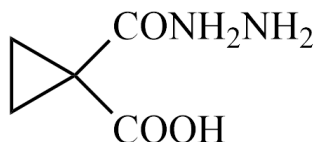
The synthesis of ACC was executed through a modified version of a previously reported procedure in the literature [88]

2.4.1.1 Synthesis of spiro [2,5].5,7- dioxo-6,6- dimethyl octane-4,8-dione



2.6 g of cyclopropane-1,1-dicarboxylic acid was mixed with 2.4 ml of acetic anhydride and (0.080 ml) of conc. (98%) H₂SO₄. The mixture was stirred in an ice-salt bath at 0 °C, then a 2 ml of acetone was added dropwise to the stirred mixture. The resulting clear solution was stirred for 3 hours and laid in a refrigerator overnight. After that, the solution was diluted with 30 ml of ice distilled water, and a white crystal was formed and filtered, washed twice with 30 ml portions of ice water. The obtained filtrate liquid was neutralized with a saturated solution of NaHCO₃ till pH=5, and another white crystal was filtered. The third patch of white crystal was extracted with ether (3*5)ml, and the ether was evaporated till the final white crystal. Three batches of white solids were dried to afford pure white crystal compound with a total of 2.9 g, yield (86%), melting point (62- 66)°C, TLC: R_f = 0.37(cyclo hexane: acetone (3:1(v/v))).

2.4.1.2 Synthesis of hydarzinocarbonyl cyclopropane-1-carboxylic acid

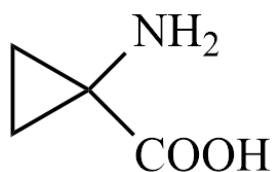


1.70 g of the white crystal of spiro [2,5].5,7- dioxo-6,6- dimethyl octane-4,8-dione was dissolved in 10 ml of absolute ethanol. Then 1 g of 85% hydrazine hydrate in 1 ml of absolute ethanol was added dropwise to the stirred solution. The resulting clear solution was left under stirring at ambient room temperature for four days, detecting the compound's spot on TLC until it disappeared under ultraviolet light. On the fourth day, a white needle crystal was formed and filtered, washed with 10 ml of absolute ethanol, and dried to give a solid white product with a weight of 1.44 g, yield (100 %), melting pint (151-154 °C), TLC: R_f=0.52 (ethanol).

IR (ν cm⁻¹): 3340(OH),3100-2900 (N-H, C-H),1640 (C=O) ,1531(O-H),1230(C-N).

¹HNMR (500 MHz, DMSO): δ 1.25 (s,4 H)

2.4.1.3 Synthesis of amino cyclo propane-1- carboxylic acid (ACC)



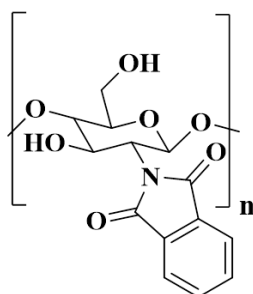
0.5 g of white crystal of hydrazine cyclopropane-1- carboxylic acid was dissolved in 1 ml of distilled water and 0.5 ml of conc. HCl was added dropwise. Then, it was poured into 91.5 g of crushed ice mixed with 2 ml of ether. The mixture was stirred for 1 hour, 0.57 ml of 34.5% NaNO₂ was added dropwise, and the reaction was carried in an ice-salt bath at 0 °C. After that, the ether layer was separated, and the aqueous layer was extracted by 1 ml of cold ether (2 times). The combined extracted portions were dried on anhydrous CaCl₂, and the resulting portion was mixed with 3 ml of toluene in a bath at 40 °C for 2 hours till all ether and N₂ were evaporated. Then, the mixture was carried to a shaker and 1.2 ml of conc. HCl was added dropwise for 1 hour. After that, toluene and CO₂ were removed under reduced pressure, and the obtained liquid residue was diluted with a small portion of distilled water and conc. HCl, with adjusting the pH value to (pH =1). The obtained white solid was purified and recrystallized with ethanol-water solution, then dried in a vacuum till a white product of ACC-hydrochloride was obtained with a weight of 0.26 g (50 %), melting point: 217-221 °C, TLC: R_f = 0.43(n-BuOH-ACOH-H₂O:6:2:2 v/v).

IR (ν cm⁻¹): 3031 (O-H, N-H), 2730(O-H),2393 (C-H),1579(C=O), 1405(C-H),1257(C-O),1317(O-H),1040(C-C-C).

¹HNMR (500 MHz, DMSO): δ 1.83 (s,2 H,CH),1.95(s,2H,CH)

2.4.2 Synthesis of Chitosan –ACC

2.4.2.1 Synthesis of N- phthaloyl chitosan



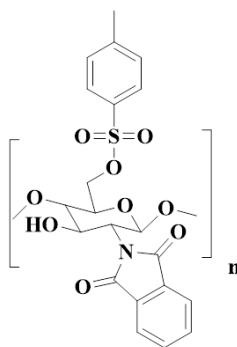
The N-phthaloylation of chitosan was conducted following a procedure previously reported in the literature [89] with modification as follows:

15 g of phthalic anhydride was dissolved in a mixture of DMF and distilled water (315 ml, 5% v/v) was added to 5g of chitosan, and the resulting yellow mixture was heated with stirring to 150 °C for one hour till it became as dark yellow gel mixture, this gel was broken with vigorous stirring under nitrogen at 120 °C for 15 hours. After the reaction was completed, the resulting mixture was cooled to room temperature and poured into ice water. The resulting pale tan precipitate was collected by filtration, washed with 500 ml methanol at room temperature for 3 hours, and filtered. The pale tan-colored product was dried under a vacuum overnight to give N-phthaloyl chitosan. (7.824g, 96.13 %, m.p. (299- 300)°C).

IR (ν cm^{-1}): 3420 (O-H), 2933 (C-H), 2133 (C-NH₂), 1775, 1712 (phthalimidio), 1657, 1369 (N-H), 1104, 1065 (pyranose), 1032 (C-N), 721 (phthaloyl arom.).

¹H NMR (500 MHz, DMSO): δ 7.9-7.5 (m, N-phthaloyl), 3.9 (s, 1H, C₁H a numeric), 3.8 (s, 2H, C₂H, C₄H), 3.4 (s, 2H, C₃H, C₅H), 3.45 (s, 1H, OH), 2.9 (q, 2H, J=7Hz, C₆H)

2.4.2.2 Synthesis of 6-O-tosyl-N-phthaloyl chitosan



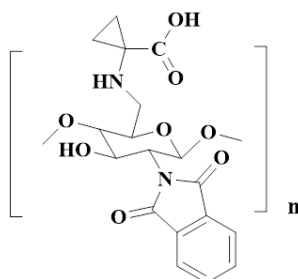
The acylation synthesis approach of N-phthaloyl chitosan using toluene-4-sulfonyl chloride (TsCl) was employed based on the strategy a procedure previously reported in the literature [89] with modification as follows:

2g of N-phthaloyl chitosan was slurred in 50 ml of DMAc and stirred for two hours at 100 °C in order to the exclusion of moisture; after cooling 2.5g of NaH was added in order to activate the hydroxyl groups at C₆ (primary hydroxyl group, most reactive alcohol) atoms on the chitosan surface for subsequent surface functionalization. The mixture was continued to stir until a clear and viscous solution was obtained under nitrogen conditions. Afterward, the solution was cooled to 0 °C, followed by the gradual addition 11.5 ml of triethyl amine, 5 ml each time; the mixture was allowed for stirring for 15 min, then the reaction temp was raised to 5 °C, followed by dropwise addition of a solution 19 g of TsCl in 10 ml DMSO along 45 min duration, resulting with a reddish brown mixture which was stirred vigorously at 5-10 °C for 15 h. Upon completion of the reaction, the mixture was decanted into 200 ml acetone and stirred for 40 min. The obtained precipitated polymer was washed with distilled water (two times, 200 ml) and subsequently with methanol (three times, 200 ml) and acetone (two times, 50 ml) at room temperature for 20 minutes and filtered. The tan-colored product was dried under a vacuum overnight to give. (2.532 g, 86.89% m.p. (239- 241) °C).

IR (ν cm⁻¹): 3379 (O-H), 2921(C-H), 1774,1715(phthalimidio), 1620,1187(S=O), 1045,1006 (pytanose), 1032(C-N), 815(C-O-S), 718(phthaloyl arom.)

¹HNMR (500 MHz, DMSO): δ 7.9-7.8 (m, N-phthaloyl), 7.75(d,2H,J=7.6 Hz,Ar-Ts), 7.46 (d,2H,J=7.6 Hz,Ar-Ts), 3.40 (s,1H,C₁H anumeric), 3.8 (s,2H,C₂H,C₄H), 3.30 (s, 2H,C₃H,C₅H), 2.9 (q,2H,J=7Hz,C₆H)

2.4.2.3 Synthesis of N-phthaloyl chitosan ACC

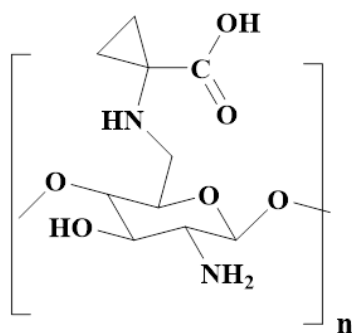


200 mg of 6-*O*-toysl-N-phthaloyl chitosan was mixed with 300 mg of ACC compound in the solid state under an argon vacuum, where the vacuum was inserted, then argon with repeating this step three times. After that, 15 ml of DMF solvent was added, and the mixture was stirred in a water bath at 80 °C under nitrogen conditions for 5 hours. The resulting mixture was cooled to ambient room temperature and poured into ice water. The resulting pale orange precipitate solid was filtrated and washed with 20 ml distilled water and 50 ml methanol. The pale orange-colored product was dried under a vacuum overnight to give N- ph. chitosan ACC product (133.64mg, 78.12%,)

IR (ν cm^{-1}): 3030- 3415 (O-H,N-H), 2929(O-H, C-H), 1774,1715(phthalimidio), 1713(C=O), 1655 (C-N amide),1062,1006 (pytanose), 1390,1104 (C-N), 1040(C-C-C),721(phthaloyl arom.).

^1H NMR (500 MHz, DMSO): δ 7.9-7.6 (m, N-phthaloyl), 7.76 (s,1H,COOH), 5.42(s,1H,CHNH), 3.86 (s,1H,C₁H a numeric), 3.7 (s,2H,C₂H,C₄H) , 3.4 (s, 2H,C₃H,C₅H), 2.95 (q,2H,J=7.2Hz,C₆H),1.9 (d,2H,CH)

2.4.2.4 Reduction of N- phthaloyl of chitosan ACC mild de-protection



100 mg of N- ph. chitosan ACC was dissolved in 10 ml of hydrazine monohydrate, stirred at 50 °C for 14 h in nitrogen, and then poured into 250 ml of ice water. The product was collected by glass filtration, washed with ethanol in a soxhlet extractor for 4 hours, and then with methanol at 40 °C for 1 hour. After that, the obtained solid compound was dried.

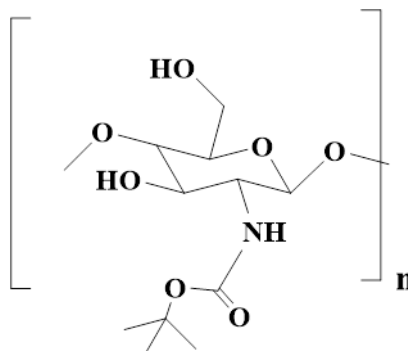
The pure product was obtained with soxhlet extraction as one of the standard techniques for extracting impurities from the required solid product, where the obtained product with 54 mg was transferred to the extractor, and 150 ml of ethanol was placed in a round bottom flask. The system temperature was raised gradually until the ethanol evaporated, condensed above the desired sample, and covered completely. The ethanol washed the sample and passed with residues through the column back to the round flask bottom. The process was carried out for 3 hours, and then the ethanol was displaced with 150 methanol for another 1 hour with the same protocols. The recovered sample was dried to give chitosan –ACC (53.13 mg,76.9%).

IR (ν cm⁻¹): 3404 (N-H primary), 3030 (O-H,N-H), 2929(O-H, C-H), 1712(C=O), 1650 (C-N amide, C=O),1062,1019 (pytanose), 1277,1104 (C-N), 900-1040(C-C-C).

¹HNMR (500 MHz, DMSO): δ 7.7 (s,1H,COOH), 3.76 (s,1H,C₁H anumeric), 3.7 (s,2H,C₂H,C₄H) , 3.4 (s, 2H,C₃H,C₅H), 2.95 (q,2H,J=7.2Hz,C₆H),1.24 (d,2H,CH)

2.4.3 Synthesis of Chitosan-based –Amino acids

2.4.3.1 Synthesis of N-Boc chitosan

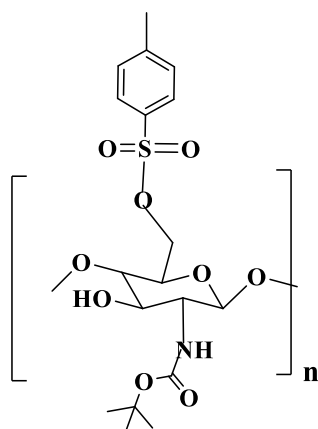


20 mg of chitosan was dissolved into 6 ml of water: dioxane (1:1), until it became a clear solution, then 10 μ l of triethyl amine was added via a syringe dropwise to the solution. After 15 min, 200 mg of di-*t*-butyl di-carbonate (Boc) was added gradually while the reaction mixture was stirred. The reaction mixture was capped with a rubber cap and stirred at ambient temperature for 10 h. After completion of the reaction, the solvent was removed by rotary evaporation, then washed twice extensively with 15 ml of DCM: acetone, dried over anhydrous Na₂SO₄, and concentrated under reduced pressure to give the N-Boc chitosan as a clear pale yellowish viscous oil, which, upon standing solidified into a yellowish solid product to provide (28.795 mg, 97.084%).

IR(ν cm⁻¹) : 3349 (N-H), 2928- 2800 (C-H), 1651 (C=O, C-N amide), 1557 (N-H bend,in-plane), 1375(C-H), 1319 (C-N stretch), 1070 (O-C=O), and 648 (N-H bend out of plane).

¹HNMR (500 MHz, DMSO): δ 8.22 (s,1H,NH), 3.92 (s,1H,C₁H anomeric), 3.84 (s,2H,C₂H,C₄H) , 3.39 (s, 2H,C₃H,C₅H), 2.95 (q,2H,J=7Hz,C₆H), 1.12(t,9H,J=7.1 Hz, BOC).

2.4.3.2 Synthesis of 6- O- Tosyl-N-Boc chitosan



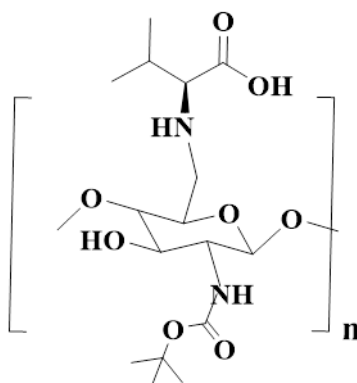
In a typical procedure, the acylation synthesis approach of N- Boc chitosan using toluene-4- sulfonyl chloride (TsCl) was conducted as follows:

20 mg of N- Boc chitosan was slurred in 20 ml of DCM and stirred for 30 min till it dissolved at ambient room temperature under the exclusion of moisture. After cooling the reaction mixture to (0-5)^oC, 0.3066 μ l of triethyl amine was added dropwise to the solution. After 15 min, 0.41943 mg of tosyl chloride dissolved in 10 ml of cold DCM was added dropwise via a syringe to the reaction mixture. The color of the mixture turned pale orange during stirring for 16 h at ambient room temperature in a water bath. The polymer product was obtained by removal of the solvent by rotary evaporation, then washed with ice water (five times, 20 ml) and subsequently with acetone (three times, 20 ml) at room temperature for 20 min and filtered. The pale orange colored product was dried in vacuum desiccation overnight to give (30.095mg, 88.62%)

IR(ν cm^{-1}): 3340-3560 (N-H), 2987- 2709 (C-H), 1594 (C=O, C-N amide, tosyl aromatic.), 1474 (N-H bend in-plane), 1372(C-H), 1319 (C-N stretch), 1172 (S=O),1070 (O-C=O), 816 (C-O-S), and 681 (N-H bend out of plane).

¹HNMR (500 MHz, DMSO): δ 9.63 (s,1H,NH), 7.5(d,2H,J=7.6 Hz,Ar-Ts),7.14 (d,2H,J=7.6 Hz,Ar-Ts), 4.01(bs,1H,C₁H a nomic), 3.94(bs,2H,C₂H,C₄H), 3.39-3.35(m,2H,C₃H,C₅H), 3.09 (q,2H,J=5Hz,C₆H), 2.29(s,3H,CH₃),1.19(t,9H,J=5.5 Hz, BOC).

2.4.3.3 Synthesis of 6- O- Valine-N-Boc chitosan



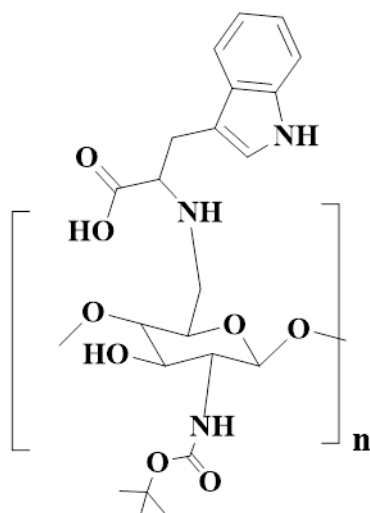
35 mg of 6- O- tosyl-N-Boc chitosan in 10 ml of DCM was added to 40 mg of L-valine. The resulting solution was allowed to stir under reflux in a water bath at 40°C. The color of the mixture turned dark yellowish during the stirring for 12 hours. After that, the solvent was removed by rotatory evaporation, and the resulting mixture was dissolved in distilled water, filtered, and washed with water (five times, 30 ml) and ethanol (two times, 20 ml) before being dried and concentrated to leave a yellow-tinged waxy solid (25.059 mg, 85.55%),

IR(ν cm^{-1}) : 1500- 3500 (inter and intramolecular hydrogen bond),3340 -2972 (N-H) (COO), 2928- 2800 (C-H), 2632(O-H,N-H-O).1681 (C=O, C-N amide, N-C=O, C-N sec, terti. amide), 1564 (N-H bend,in-plane, COO), 1395(C-H, O-H bend, COO), 1328 (C-N stretch), 1286 (C-O stretch),1172 (C-O),1064 (O-C=O, C-O), 946 (C-C-O),773(C-C), and 683 (N-H bend out of plane).

^1H NMR (500 MHz, DMSO), δ : 8.5 (s,1H,COOH), 7.5(d,1H,J=7.2Hz,NH), 7.13(d,1H,J=7.2Hz,NH), 4.14(m,1H,CHanomeric), 3.78(m,2H,C₂H,C₄H), 3.68 (s,2H,C₃H,C₅H), 3.07(q,2H,J=6.6 Hz,C₆H), 2.17-2.16(m,1H,CHNH),

2.1-2.08 (m,1H,CH(CH₃)₂), 1.18(t,9H,J=7.2 Hz,BOC),0.97-0.91 (m,6H,CH(CH₃)₂)

2.4.3.4 Synthesis of 6- O- Tryptophan-N-Boc chitosan

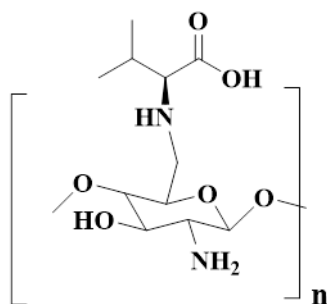


30 mg of 6- O- tosyl-N-Boc chitosan in 10 ml of DCM was added to 408 mg of Tryptophan. The reaction mixture was allowed to stir under reflux in a water bath at 40°C for 16 h. The color of the mixture turned to be dark brown color. After that, the solvent was removed by rotatory evaporation, and the resulting mixture was dissolved in distilled water, filtered, and washed with water (five times, 30 ml) and ethanol (three times, 30 ml) before being dried and concentrated to leave a dark brown solid (23.819 mg, 94.88%)

IR(ν cm^{-1}) : 1500- 3500 (inter and intramolecular hydrogen bond), 3302 -2975(N-H) (COO), 2975 (C=N, C-H), 2928- 2800 (C-H), 2630(O-H), 2359 (C=N),1731 (C=C, arom.) 1665 (C=O, C-N amide, N-C=O, C-N sec. amide,COO), 1590(N-H bend,in-plane,H₂N-H),1457(C-H), 1395(C-H, O-H bend, COO), 1356(C-N arom aime), 1210 (C-O stretch),1166 (C-O),1064 (O-C=O, C-O),1010 (C-O) and 683 (N-H bend out of plane).

¹HNMR (500 MHz, DMSO), δ : 11.05(s,1H,COOH), 7.61(d,1H,J=10.2 Hz,Ar), 7.51(d,1H,J=6.05Hz,Ar),7.37(d,1H,J=5.5Hz,NH),7.25(s,1H,CHindole),7.22(s,1H,NH), 7.13(d,1H,J=5.5Hz,NH),7.08(t,1H,J=5.6Hz,Ar),6.99(t,1H,J=5.6Hz,Ar),3.71(s,1H,C1Ha nomic),3.35(d,2H,J=5.8Hz,C₂H,C₄H),3.32(d,2H,J=5.7Hz,C₃H,C₅H),3.14(q,1H,J=5.8 Hz,COO), 3.01(q,2H,J=5Hz,C₆H),2.29(s,2H,CH),1.17(t,9H,J=10Hz,BOC).

2.4.3.5 De-protection of 6- O- Valine chitosan

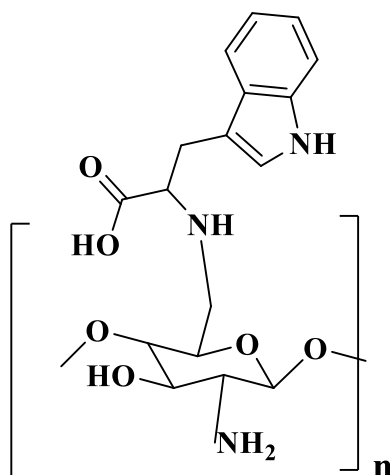


(10 mg) of 6- O- Valine-N-Boc chitosan in methanol (2 ml) was treated with 0.5 ml of tri-fluoro acetic acid for 6 h at room temperature. The solvent was removed in vacuo, and the crude was concentrated to leave a light yellow-tinged viscous solid material (6.631 mg, 94.52 %).

IR(ν cm^{-1}): 1500- 3500 (inter and intramolecular hydrogen bond), 3389 ((N-H, primary) (COO)), 2928- 2800 (C-H), 1774 (C=O, C-N amide, N-C=O, C-N sec. amide), 1712 (C=O, COO) 1642 (C-N sec. amide), 1390(C-H, O-H bend, COO), 1110 (C-N),1065 (O-C=O, C-O, NH_3^+), 951(C-C-O),721(C-C).

^1H NMR (500 MHz, DMSO), δ : 5.18(s,1H,NH), 5.04 (d,1H,J=5Hz,CH anomeric),4.94(d,1H,J=10Hz,C₃H), 4.93-4.36(m,1H,C₅H), 4.79-4.73 (m,2H,C₂H,C₄H), 3.90(t,J=10Hz,2H,C₆H),3.56(s,1H,CH(CH₃)),1.23(s,1H,(CH₃)₂).

2.4.3.6 De-protection of 6- O- Tryptophan chitosan



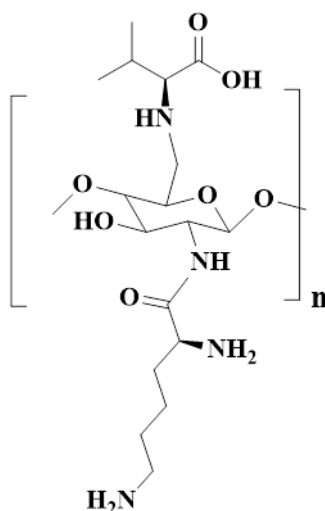
(10 mg) of 6- O- Tryptophan chitosan in methanol (2 ml) was mixed with 0.5 ml of tri-fluoro acetic acid for 6 h at room temperature. The solvent was removed in vacuo, and the crude was concentrated to leave a light brown viscous, sticky gel material (5.84 mg, 72.719 %).

IR(ν cm^{-1}): 1500- 3500 (inter and intramolecular hydrogen bond), 3390 (N-H primary), 3031 -2975(N-H) (COO), 2938 (C=N, C-H), 2928- 2800 (C-H), 2630(O-H), 2359 (C=N),1738 (C=C, arom.) 1667 (C=O, C-N amide, N-C=O, C-N sec. amide, COO), 1514(N-H),1460(C-H), 1444(C-H, O-H bend, COO), 1340(C-N arom. aime), 1190 (C-O stretch),1166 (C-O),1058 (O-C=O, C-O),1058 (C-O).

^1H NMR (500 MHz, DMSO, δ): 11.07 (s,1H,COOH),8.27 (s,2H,NH₂), 7.57(d,1H,J=8Hz,Ar),7.49(d,1H,J=5.6Hz,Ar.),7.37(d,1H,J=8Hz,NH),7.23(s,1H,CHindole),7.12-

7.07(m,1H,Ar),7.02(t,1H,J=7.6Hz,Ar),4.12(bs,1H,C₁Hanomeric),3.66(s,1H,C₂H),3.85(s,1H,C₄H),3.27(d,2H,J=6.1Hz,C₃H,C₅H),3.08(q,2H,J=5Hz,C₆H),2.29(s,1H,CHNH),1.23 (s,2h,CH₂CH).

2.4.3.7 Synthesis of 6- O- Valine chitosan N- Lysine

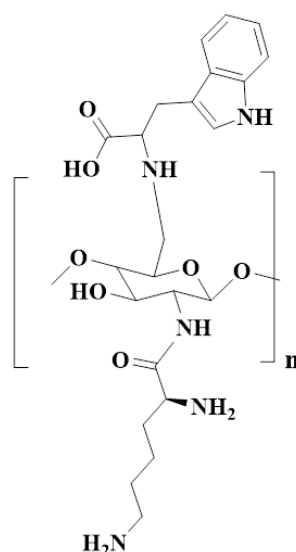


(50 mg, 1.1eq) Lysine was dissolved in 20 ml of DCM and degassed by bubbling nitrogen for 30 min till it dissolved completely. Subsequently, EDC (72 mg) and NHS (43 mg), where the resultant solution was incubated in a water bath at 37°C with stirring for two h. After that, an appropriate amount of 6- O- valine chitosan (10 mg, 1.1 eq) already dissolved in 10 ml of DCM was added to the above solution. The resultant reaction mixture was allowed to stir under the same condition for 16 h for amide coupling bridging formation or reductive amination. The resulting yellowish solid product was vacuumed and washed with 20 ml distilled water: acetone and vacuumed to give a dried product with (12.364 mg, 87.19 %).

IR(ν cm^{-1}): 1500- 3500 (inter and intramolecular hydrogen bond), 3100 ((N-H, primary) (COO)), 2928- 2800 (C-H), 1780(C=O, C-N amide, N-C=O, C-N sec. amide), 1712 (C=O, COO), 1650 (C-N sec. amide), 1560 (N-H),1473(COO), 1390(C-H, O-H bend, COO), 1135 (C-N),1078 (O-C=O, C-O, NH_3^+), 1010(C-C-O),721(C-C).

^1H NMR (500 MHz, DMSO): δ 8.29 (s,1H,COOH), 8.16 (bs,1H,NH), 7.49(d,2H,J=7.6Hz,NH₂), 7.12(d,2H,J=7.6Hz,NH₂),4.68(bs,1H,C₁H anomeric), 3.94 (s,1H,C₂H), 3.73 (bs,2H,C₃H,C₅H), 3.62 (s,1H,C₄H), 3.15 (s,1H, CHNH), 3.08(q,5H,CH₆),2.49(s,4H,2CH₂),2.27(s,4H,2CH₂), 2.19-2.13(m,2H, CHNH , CHNH), 1.18(t,6H,J=5Hz,CH₂CH₃),0.97(t,6H,J=5.5Hz,2CH₃).

2.4.3.8 Synthesis of 6- O- Tryptophan chitosan N- Lysine



(50 mg, 1.1eq) L-lysine was dissolved in 20 ml of DCM and degassed by bubbling nitrogen for 30 min until it dissolved completely. Subsequently, EDC(72 mg) and NHS (43 mg), where the resultant solution was incubated in a water bath machine at 37 °C with stirring for two hours. After that, an appropriate amount of 6- O- tryptophan chitosan (10 mg, 1.1 eq) already dissolved in 10 ml of DCM was added to the above solution. The resultant reaction mixture was allowed to stir under the same condition for 16 h for amide coupling bridging formation or reductive amination. The resulting black-colored solid product was vacuumed and washed with 20 ml water: acetone and vacuumed to give a dry product with (9.045mg, 70.83 %).

IR(ν cm^{-1}): 1500- 3500 (inter and intramolecular hydrogen bond), 3294 (N-H primary), 3031 -2975(N-H) (COO), 2969 (C=N, C-H), 2928- 2800 (C-H), 2693(O-H), 2480 (C=N),1777 (C=C, arom.) 1735 (C=O, C-N amide, N-C=O, C-N sec. amide,COO), 1648 (C=O), 1565(N-H),1481(C-H), 1481 (COO),1444(C-H, O-H bend, COO), 1261 (C-N arom. amine), 1204 (C-O stretch), 1068 (O-C=O, C-O),700-900 (C-H).

^1H NMR (500 MHz, DMSO): δ 10.86(s,1H,COOH), 8.31(s,2H,NH₂),8.15-7.92 (m,2H,Ar),7.50(s,2H,NH),7.3(s,1H,CHindole),7.13-6.95(m,2H,Ar),4.5(s,1H,C₁H anomeric),4.11(s,1H,C₂H),3.24(s,1H,C₃H)

3.03-2.99 (m,2H,C₄H,C₅H),2.69 (s,2H,C₆H) ,2.64 (s,4H,2CH₂), 2.59 (s,4H,2CH₂), 1.7 (s,2H,CH₂), 1.18(t,1H,J=10Hz,CHNH),0.99(s,1H,CHNH).

2.4.4 Kaiser Test

To quantify the amine groups after de-protection synthesis Preparation of Kaiser test solutions:

First, a potassium cyanide solution at a concentration of 1 mM: water was prepared by dissolving 2 ml of the solution in 98 ml of pyridine. A 0.043 mM phenol solution was obtained by dissolving 40 g of phenol in an absolute ethanol solution. A 0.28M ninhydrin solution in absolute ethanol was prepared in the dark for all tests. The extinction coefficient of chitosan was measured and calculated to be 1×10^{-4} .

Analyte-tested solutions were prepared from the stock solution by weighing 2 mg of each tested material in a test tube. The Kaiser reagent solutions were added in each tested tube as 75 μ L of phenol, 75 μ L of ninhydrin, and 100 μ L of potassium cyanide, respectively. A blank tube containing all Kaiser reagent solutions without tested materials was realized; also, another blank tube containing 1 ml of the 60 % ethanol solution was set for absorption calibration. The tubes were sealed with aluminum foil and parafilm and sonicated for 5 min using an Elmasonic S 100 H Sonicator. Then, the mixtures were heated at 120 °C for 10 minutes and cooled to room temperature, diluted with 1 ml of 60 % ethanol. Supernatants were carefully twice filtered with a glass filter containing cotton fibers with 1 ml of 60% ethanol in the repeated filtration step, and noticeable color for each tested material was reported. Absorption spectra of the supernatant were recorded at 570 nm by using UV-Vis absorption spectra (Beckman Coulter DU 800 Spectrophotometer). Experiments were repeated and triplicated three times to ensure the results' accuracy. Handling the de-protection of prepared materials followed the same protocol mentioned above. The spectral absorption data were used to calculate and quantify free primary amine groups in μ mol/ gram for each 1 g of the synthesized material. The following equation is applied to determine for each 1 g of chitosan how much of NH₂ in (μ mol/ gram) value is available:

Amount of NH_2 ($\mu\text{mol/gram}$) =

$$\frac{\text{Absorbance of sample} - \text{absorbance of blank} \times \text{dilution factor} \times 10^6}{\text{Extinction coefficient} \times \text{amount of sample tested}} \quad (6)$$

Dilution factor = 2.25

Extinction coefficient = 10^{-4}

Amount of sample tested = 2 mg

2.4.5 Plant Cultivation and Growth Condition

Seeds of six-row Barley (*Hordeum vulgare* L. cv. Olsok) seeds were surface sterilized in 10 % (v/v) hydrogen peroxide for 20 min, then soaked in distilled water for 15 h at ambient room temperature; after noticeable enlargement of the seeds in their sizes, they were left to germinate on moist cotton in a flat glass dish covered with a transparent plastic bag for three days. The dish was kept in the daylight at approximately 25-29°C, and the plastic bag was opened once daily to aerate the seedlings. After sprouting, seedlings with 2-5 cm high shoots were prepared for cultivation. The tested synthesized materials were utilized and specified in this experiment by weighing 0.05g of each dried sample and inserting them into sterilized tea bags.

After the sprouting process of Barley seeds, the cultivation process was prepared by setting a triplicate trial for each tested synthesized sample with 27 identical polyethylene brown pots with dimensions (10 x 9.5 x 7 cm) for each tested trial sample with triplicate and filled with 700 g of sand with plastic beads in the bottom of each pot. The prepared material in tea bags was placed 4 cm deep in each classified pot, and randomly, ten uniform seedlings were spread over it in each pot, followed by cover with about 10 cm surface layer of sand. All pots were moisturized with deionized water with the application of respective treatments. The pots were carried under natural light, temperature, and humidity conditions. During this period, the day and night temperatures ranged between 25 to 30°C, 16-18 h of supplemental natural light, and relative air humidity was 40 % (day = night). Experiments were performed in April – June, and the sand moisture was maintained at 80 % of the maximum water-holding capacity gravimetrically with one daily irrigation with distilled water. Neither the growth conditions nor the experimental conditions were axenic. After the emergence of

untreated and treated trials, the plant height and weight were quantified in cm as a plant growth parameter at 15 and 30 days. Also, the chlorophyll content, amino acid content, and photosynthesis performance value were noted and measured. The trials were classified as follows: control as an untreated trial, chitosan, L- valine, Tryprotphan, L- lysine, chitosan- valine, chitosan- Tryptophan, L-Lysine chitosan L- valine, and L- lysine chitosan Tryptophan trails.

2.4.5.1 Sample Data Collected

In this study, 81 samples were selected in the morning and were taken randomly for analysis. The sample analysis was identified as leaf shoots and roots analysis with a ruler meter for plant growth analysis, and the leaf diameter was also determined similarly. Wet mass and dry biomass of leaf-shoots and roots for selected samples were determined after the harvest process, where firstly, The roots were thoroughly washed with distilled water and immediately dipped into three aliquots of 0.5 mM CaCl₂, then gently blotted with tissue paper to remove any residuals. Then, samples were allowed to stand air dry overnight on tissue paper. Their wet biomass was weighed, while its dry biomass was determined by placing the sample in a weighted aluminum foil in a drying oven set at 80°C for 18 hours, then cooled in a vacuum desiccator to prevent the moisture from uptaken and reweighted as dry biomass weight.

2.4.5.1 Measurement of Plant Photosynthesis with PAM Fluorometry

Plant photosynthesis was measured to investigate the role of prepared materials in enhancing the photosynthesis process; the measurement was conducted using pulse amplitude-modulated fluorometry (LUCAM, Fluor cam version 15.1.0). All trails were dark adapted for 30 minutes before analysis.

The F₀ minimum fluorescence was adjusted to 0.10-12.03 million ± 0.042 by changing the fluorescence rate of a single non-modulated saturating 0.672 s light pulse used for F_m measurements. Then, F_s were measured after 30 seconds using non-modulated 640-700 nm actinic radiation. After this step, plants were left for 14 minutes to ensure the fluorescence reached a steady state. A single non-modulated saturating 0.6 s light pulse was excited every minute to measure the F_m in the presence of actinic light. All final resulting parameters (F_v/F_m) were obtained to examine the effect of amino acids on the

performance of the plant photosynthesis process as another parameter indication for its promoting plant growth and optimizing obtaining biomass.

Chapter Three

Results and Discussion

3.1 Nano bio-fertilizer Capsules

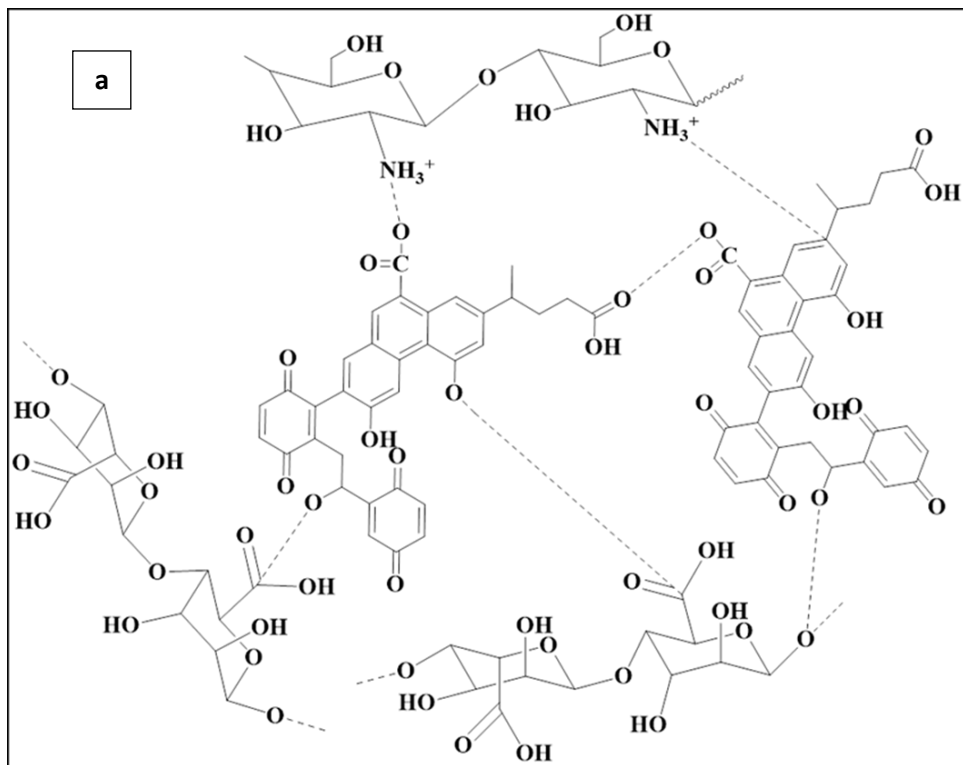
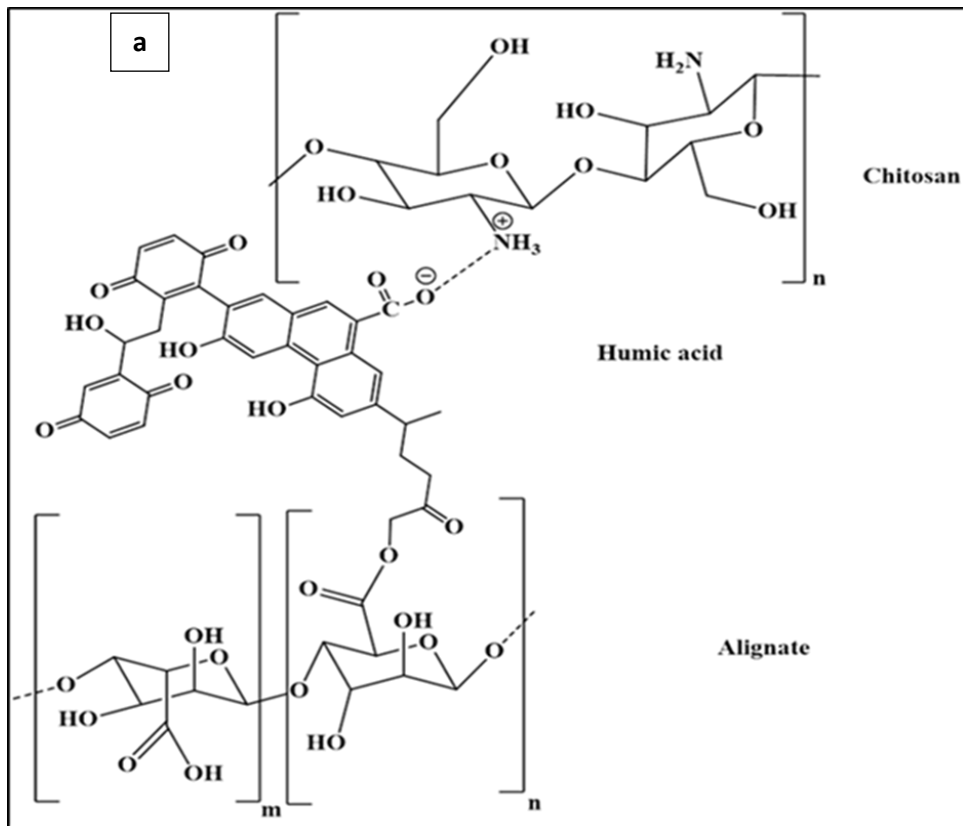
3.1.1 Synthesis and Characterization of Nano capsules

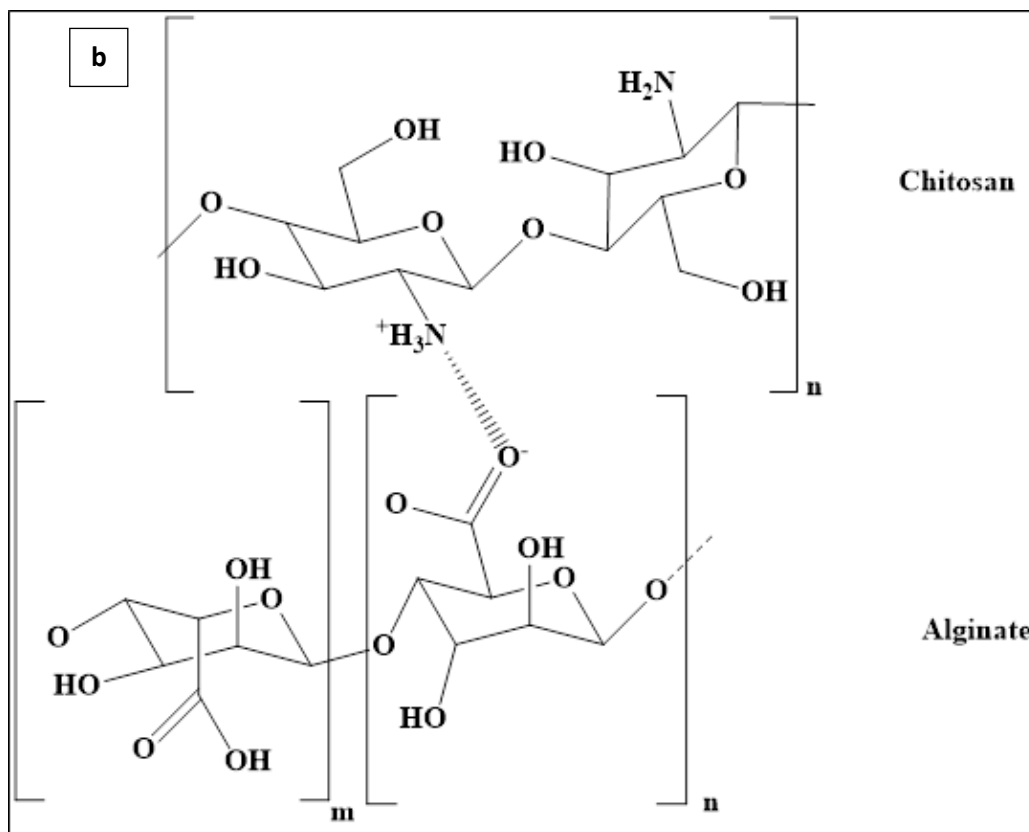
Nano bio-fertilizers are pivotal in modern agriculture, presenting a revolutionary approach to enhance nutrient availability, soil fertility, and overall crop productivity sustainability. Combining the strengths of nano fertilizer and bio-fertilizer technologies will offer innovative solutions with targeted nutrient delivery alongside beneficial microorganisms, ensuring sustained release at nano-sized encapsulated materials and improved uptake efficiency. Besides that, the benefit of bio-fertilizer techniques is that they shield the encapsulated microorganism from environmental stressors, enabling controlled release over time. Embracing nano bio-fertilizers can be a viable alternative to conventional agro-fertilizers and pesticides, effectively reducing nutrient loss through leaching and volatilization, thereby minimizing environmental pollution. The adoption of nano bio-fertilizers presents immense potential in addressing environmental resource security challenges while promoting eco-friendly farming practices, where this cutting-edge field represents a crucial area for ongoing research and development in agriculture.

This research synthesized novel nano bio-fertilizer capsules consisting of (Ch./Alg.) cross-linking with humic acid. These nano capsules were loaded with essential agro-nutrients (NPK) and beneficial microorganisms from the (*P. Fluorescence*) strain, all at the nano scale level. These novel capsules are referred to as (Ch./Alg.HA.NPK) or as (Ch./Alg.HA.NPK.PGPR) nano capsules. The diagrammatic representation of their proposed interaction is shown in Figure 5.a.b. For comparative analysis, another controlled nano capsules of (Ch./Alg.NPK.PGPR) or (Ch.Alg.NPK) nano capsules, without any cross-linking agents. This was done to elucidate the impact of cross-linking on the stability of the nano capsules and the controlled release of the entrapped materials.

Figure 5

(a) Suggested (Ch./Alg.HA.NPK.PGPR) nano capsules interaction, (b) Suggested (Ch. /Alg. NPK.PGPR) nano capsules interaction





In this study, the synthesized nano capsules were created using the ionotropic gelation polyelectrolyte method (IG-PEC). This method aimed to prepare nanoparticles that could encapsulate nano scale-sized active (NPK) fertilizer alongside beneficial microorganisms (*P. Fluorescence*). The process involved coating NPK fertilizer and (*P. Fluorescence*) with chitosan and alginate nanoparticle polysaccharides through cross-linking with humic acid in an aqueous solution. This humic acid cross-linking brought about several improvements: enhancing nano capsule stability, providing a suitable environment for selected PGPRs strain maintenance, and promoting adhesion between the two coating interfaces, making it more rigid and stable. This resulted in the highest potential payload of active (NPK) fertilizer and beneficial microorganisms (*P. Fluorescence*) at the smallest scale with a prolonged release effect to the targeted site, as illustrated in the following sections. These newly developed nano bio-fertilizer capsules have the potential to address numerous challenges in the agriculture sector and promote environmentally friendly crop production practices. Besides that, it reduces the reliance on traditional agrochemical fertilizers, offering a controlled and efficient method for delivering and releasing active (NPK) fertilizer and valuable materials.

Optimizing processing parameters of the prepared nano capsules of chitosan/alginate cross-linked with humic acid and its IG-PEC method has been adopted with the most stable mass ratio formulation, smallest particle size, surface charge, and highest encapsulation efficacy (EE). The particle size, zeta potential, and encapsulation efficacy %(EE) for control (Ch./ Alg. NPK) nano capsule and (Ch./Alg. HA.NPK) nano capsule were measured to investigate the cross-linking effect on improving the nano capsule particle size, potential surface charge and encapsulation efficacy. The particle size and zeta potential of nano capsules play a crucial role in nanoparticle suspension's stability to increase its targeted materials' encapsulation. Nano capsules with a 50-500 nm diameter have been proven to have the best nano capsules properties.[90] The size distribution of nanoparticles depends on the molecular weight, concentration, and ratio of chitosan with other polymers and the cross-linking agents. The sign of zeta potential with ζ -potential more than -30 mV dictates the stable main ionic charge of the nano capsules' surface. The (Ch./ Alg. NPK) nano capsules show an average particle size of $(316.3 \pm 1 \text{ d.nm})$ (Figure S2, Appendix B), an average ζ -potential of $(-24 \pm 1.4 \text{ mV})$, and an average (EE) of $(65 \pm 0.99)\%$. The (Ch./ Alg. HA.NPK) nanocapsules show an average particle size of $(450.9 \pm 0.530 \text{ d.nm})$ (Figure S2, Appendix B), an average ζ -potential of $(-33 \pm 0.95 \text{ mV})$, and an average (EE) of $(87 \pm 1.2)\%$. The (Ch./Alg. NPK) nano capsules show smaller average particle size, higher average zeta potential charge value, and lower encapsulation efficacy percentage than (Ch./Alg. HA. NPK) nano capsules.

The results of (Ch./Alg. NPK) nano capsules reveal that these particular nanocapsules exhibit limited stability and are prone to sedimentation over a defined timeframe, which was further validated through observations of settlement in approximately one month. Meanwhile, their particle size can be ascribed to amino groups within chitosan and hydroxyl alginate in stoichiometric ratios conducive to nano capsule formation. Nonetheless, the reduced encapsulation efficacy can be attributed to the preferential presence of NPK-negative ions, such as NO_3^- and PO_4^{3-} , on the surface of the nanoparticles rather than being predominantly encapsulated within the capsules. [91]

This is also manifested in the elevation of the zeta potential value, which is intricately linked to the prevailing van der Waals interactions between the polysaccharide components, chitosan, and alginate, surpassing the influence of electrostatic repulsion in

the ionotropic gelation polyelectrolyte method (IG-PEC) employed for preparation. In this context, chitosan typically assumes a dispersed arrangement due to the repulsion from its positively charged amino NH_3^+ groups in the polymer structure. Consequently, this structural disposition enhances the adsorption capacity for negatively charged ions, particularly the active NPK materials, onto the nanoparticles' surface. This interaction, in turn, exerts a direct impact on the stability of the nanocapsules.

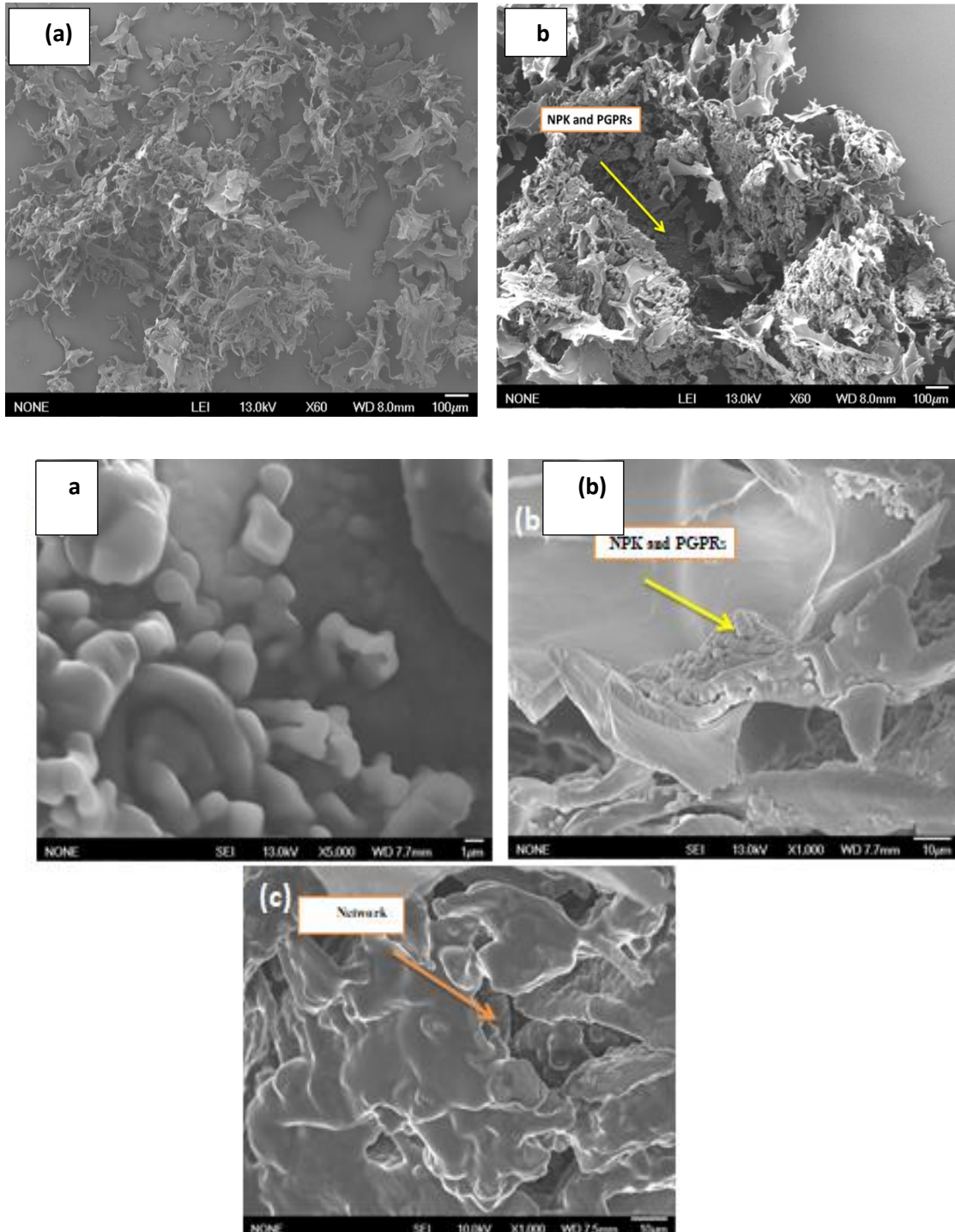
Meanwhile, the (Ch./Alg.HA.NPK) nanocapsules show larger particle sizes, higher encapsulation efficacy, and higher zeta potential value. The larger particle size can be ascribed to the role of humic acid in the formation of the organized network and plays a crosslinker upon formulating the nanocapsules in the ionotropic gelation polyelectrolyte method (IG-PEC) preparation method, where humic acid increased the availability of negatively charged hydrophilic carboxylate groups in the solution, which means more active carboxylate groups are ready to be linked with amino groups of chitosan polymer, as illustrated in Figure.6. Consequently, the electrostatic interaction between chitosan and alginate materials will be the dominance over van der Waals interaction by entrapping more NPK fertilizer at the nano scale in its internal matrix, producing more extensive and less dense particles with strong repellent forces and higher encapsulation efficacy percentage. Furthermore, the heightened zeta potential exhibited by these nanocapsules plays a pivotal role in determining the potential allocation of chitosan within the dispersion particles. Notably, humic acid demonstrates a preferential orientation towards alginate, as opposed to chitosan, effectively bolstering the stability of the interfacial matrix. Notably, the NPK fertilizer assumed an ionic configuration, specifically NO_3^- and PO_4^{3-} ions. This particular ionic composition could potentially lead to interactions between these ion groups and the internal matrix constituted by humic acid and alginate, with minimal absorption occurring on the surface of the nanocapsules. Consequently, the NPK fertilizer entrapped within the emerging internal network modulates the surface charge, enhancing encapsulation efficiency. This phenomenon indicates that the formulated nano fertilizer possesses the essential attributes requisite for effective utilization in agronomic contexts.

3.1.2 Surface Structure and Morphology Analysis

The surface structure and morphologies of (Ch./Alg.NPK.PGPRs) nanocapsules and (Ch./Alg.HA.NPK.PGPRs) nanocapsules were studied using the scanning electron microscope (SEM) technique. Figures 6.a. and b show alternatively the surface structure and morphologies for (Ch./Alg.NPK.PGPRs) nanocapsule and (Ch./Alg. HA.NPK. PGPRs) nanocapsule. As shown in Figure 6.a., the (Ch./Alg.NPK.PGPRs) nanocapsules were not of distinct spherical shape; they appear less physically stable and seem to have porosity and hollowness.

Figure 6

a. (a) Surface of (Ch. Alg.NPK.PGPRs) Nano capsule, (b) inside the matrix of nanocapsule with the appearance of entrapped NPK and PGPRs. b. (a) Surface appearance of (Ch. Alg. HA.NPK. PGPRs), (b) inside the matrix of nanocapsule with the appearance of entrapped NPK and PGPRs, (c) Network of cross-linking inside the nanocapsule with embedded entrapped materials



Meanwhile, the Figure 6. b. (Ch./ Alg. /HA.NPK.PGPRs) most resembled a spherical shape with a spherical shell and core type regular arrangement, as well it appeared to be smooth in its shell appearance, which means chitosan was able to sufficiently coat these nanoparticles with efficient loading of NPK materials and PGPRs strain.

This change in morphology between (Ch./ Alg. /HA. NPK.PGPR) and (Ch./Alg. NPK.PGPRs) nanocapsules can be attributed to the incorporation of alginate with chitosan and its cross-linking effect with humic acid, where the existence of amorphous products with interconnected porous network able to increases with the presence of active ingredients to be distributed on contact surface area and within the hydrogel network pores of formulated nanocapsules, leading to more active nutrient absorption in the preparation method. Also, it should be noteworthy that the interlinked pore of the humic acid, as cross-linked, can delay the dissolution of the loaded entrapped targeted materials as revealed in the release profile and result in the slow release mechanism behavior.

3.1.3 FT-IR Spectral Analysis

Fourier Transform Infrared Spectroscopy (FTIR) is a powerful analytical technique for analyzing various materials' molecular composition and structure. FTIR can provide valuable insights into chitosan and alginate's chemical characteristics and their cross-linking with humic acid molecules in the formulation of nano bio-fertilizers.

Figure S3 in Appendix B shows the FT-IR spectra of Chitosan, Alginate, and Humic acid, and for both (Ch. Alg. NPK) and (Ch. Alg. HA. NPK), as indicated by the H.A. shows noticeable change as a cross-linked fertilizer formulation proceeds to completion of nanocapsules formation.

Its FT-IR spectra results are similar to those obtained in other studies for chitosan polymer. The chitosan spectrum shows firm functional group peaks at 3368 cm^{-1} and 656 cm^{-1} , corresponding to the N-H and O-H stretching frequency of glucosamine and intermolecular hydrogen bonding. Significant peaks at 2885 and 2900 cm^{-1} are allocated to C-H symmetric and asymmetric stretching. These bands are the main characteristics of typical chitosan polysaccharides. Other peaks at 1651 cm^{-1} and 1546 cm^{-1} correspond to the C – O stretch in the primary alcohol group. The absorption peak

at 1376 cm^{-1} is allotted to C-N glucose stretching of primary amine, while those at 1404 cm^{-1} and 1424 cm^{-1} are allotted to CH_2 and CH_3 symmetrical deformation, respectively.

Alginate is a linear polymer derived from brown seaweeds. The FTIR study of alginate provides information on its molecular structure and functional groups. Alginate, like chitosan, has distinct peaks in the FTIR spectrum: The carbonyl (C=O) stretching vibration of the carboxyl groups in alginate corresponds to the peak at approximately 1566 cm^{-1} . The asymmetric stretching vibration of the alginate carboxylate group (COO^-) corresponds to the peak at 1411 cm^{-1} . The peak shows the stretching vibration of the C-O bond in the carboxylate group at 1249 cm^{-1} . The peak at around 1249 cm^{-1} corresponds to the stretching vibration of the C-O bond in the carboxylate group. The peak at about 1095 cm^{-1} corresponds to the stretching vibration of the C-O-C bond in alginate.

The resulting spectrum obtained from the FTIR analysis of humic acid will show characteristic absorption peaks corresponding to different functional groups in the sample. Some standard absorption bands observed in the FTIR spectrum of humic acid include carboxylic acids with a peak around 1700 cm^{-1} , indicating the presence of carboxylic acid groups ($-\text{COOH}$). The peak bands around 1650 cm^{-1} indicate the presence of aromatic rings, and the peak at 2930 cm^{-1} indicates the presence of aliphatic hydrocarbon chains. The hydroxyl ($-\text{OH}$) group peak is around 3350 cm^{-1} .

(Ch. Alg.) nanocapsule: The FT-IR analysis of the chitosan-alginate complex revealed a shift in the amide carbonyl group to 1628 cm^{-1} and a shift in the chitosan amino group to 1566 cm^{-1} , indicating the interaction between chitosan and alginate.

(Ch.Alg.HA) nanocapsule: Combining chitosan with alginate and humic acid creates new interactions and compatibility between these components. FTIR analysis aids in understanding these interactions and probable chemical reactions by studying changes in functional groups. The FT-IR analysis of the Chitosan with Alginate and Humic Acid complex revealed a shift in the amide carbonyl group to 1651 cm^{-1} , a shift in the chitosan amino group to 1542 cm^{-1} , a shift in carboxylic acid groups ($-\text{COOH}$) to 1734 cm^{-1} , and shift in the hydroxyl ($-\text{OH}$) groups to 3420 cm^{-1} . These variations can be

attributed to hydrogen bonding, electrostatic interactions, or other types of chemical bonding.

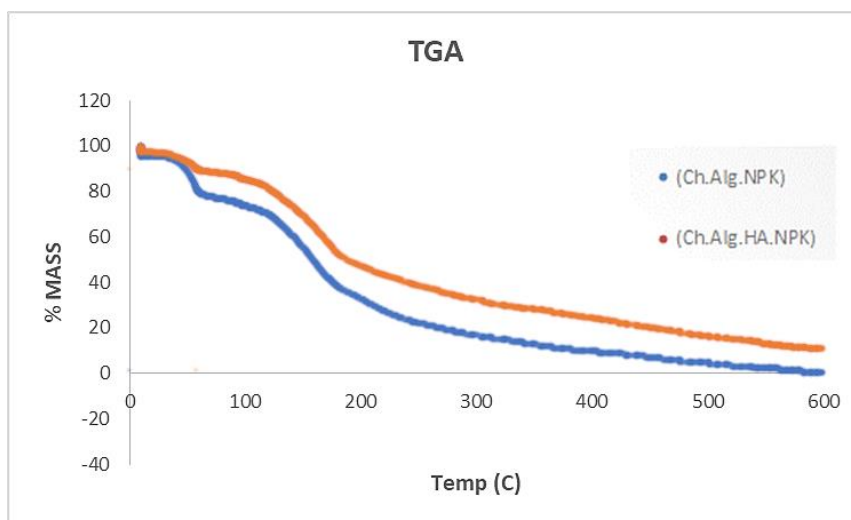
In summary, FTIR analysis of chitosan, alginate, and chitosan with alginate and humic acid provides precise information about their molecular composition, functional groups, and possible interactions. Researchers can analyze the FTIR spectra to gain insights into these materials' structural properties and chemical behavior, which is valuable for agricultural purposes.

3.1.4 Thermogravimetric Analysis

TGA is a thermal analysis technique that analyzes the thermal behavior of materials as their temperature changes. TGA can offer significant information about thermal stability, breakdown behavior, and compatibility, as shown in Figure 7 for (Ch. Alg) and (Ch. Alg. HA) nanocapsules.

Figure 7

TGA analysis for (Ch. Alg. NPK) and (Ch. Alg. HA.NPK) nanocapsules



TGA analysis of (Ch. Alg. NPK) nanocapsules entails submitting the sample to a controlled temperature increase and measuring the accompanying weight changes. The TGA curve derived often exhibits the following significant features:

- Weight loss at first: The TGA curve may show a minor reduction in weight at lower temperatures due to the evaporation of moisture adsorbed on the sample's surface.

- Primary decomposition stage: Chitosan-alginate polymers are thermally decomposed in a multi-step process. The TGA curve typically displays a significant weight loss during the main breakdown stage. The polymeric backbone of chitosan and alginate degrades, yielding volatile degradation products such as carbon dioxide, carbon monoxide, and water vapor. The study shows that alginate-chitosan composite can experience weight losses ranging from 30% to 85.7% when subjected to temperatures between 100°C and 400°C.
- Residue formation: A residue may remain after the major breakdown step, often consisting of inorganic components or burned material. This residue's weight reveals information about the thermal stability of the leftover alginate fragments and the presence of contaminants.

TGA analysis of (Ch. Alg. HA.NPK) nanocapsule provides information about the thermal behavior of the composite and any interactions among the components. The TGA curve for the alginate-chitosan-humic acid composite may resemble the following extra features:

- Interaction and compatibility: Compared to the above analysis, the TGA curve may reveal differences in breakdown behavior and heat stability. The study shows that (Ch. Alg. HA.NPK) nanocapsule composite can experience weight losses ranging from 10% to 61.1% when subjected to temperatures between 100°C and 400°C. This suggests that alginate, chitosan, and humic acid interact via hydrogen bonding and chemical interactions.
- Synergistic effects: Chitosan and Humic acid can alter the thermal stability of the composite. Synergistic effects, in which the combination of components improves overall thermal stability, can be noticed as a greater decomposition temperature or lower weight loss than the other nanocapsule.
- Residue formation: The composition of the residue following thermal degradation may differ in the composite. The residue may contain chitosan, humic acid, and any leftover alginate fragments.

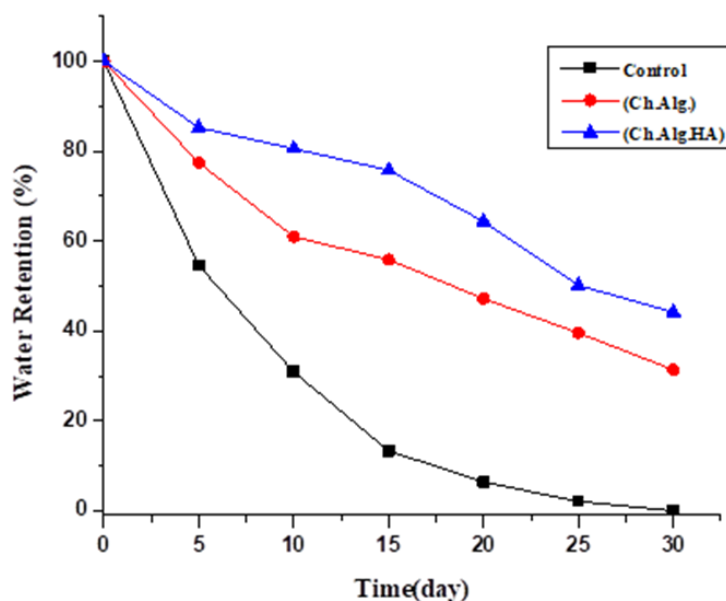
In conclusion, the TGA study of (Ch. Alg. HA.NPK.PGPRs) nanocapsule can provide insights into thermal stability, breakdown behavior, and potential interactions among the components.

3.1.5 Water Retention Behavior of Nano capsules in Soil

The water retention behavior of synthesized (Ch. Alg. NPK) and (Ch. Alg. HA.NPK) nano capsules were studied in loamy sand soil, as shown in Figure 8 and Table S1 in Appendix B.

Figure 8

Water Retention of Formulated (Ch.Alg.NPK.PGPRs) and (Ch. Alg. HA.NPK.PGPRs) nano capsules



Notably, the prepared (Ch./Alg. HA.NPK.PGPRs) nanocapsules increased the water retention percentage with 44.2% of the soil more than the (Ch. Alg. NPK.PGPRs) nanocapsules of 31.4% for the studied period. These findings revealed that humic acid with the hydrophilic carboxylate groups that cross-linked and incorporated with chitosan and alginate nanoparticles in the hydrogel network of formulation enhances the absorption of water molecules inside the nanocapsules and preserves it for a more extended period, and thus improve the water retention behavior. As a result, using these nano bio fertilizer capsules in farming practices can decrease irrigation frequencies and enhance its sustained and prolonged release.

3.1.6 Nano bio-fertilizer Release Studies

The cumulative release profile for synthesized nanocapsules formulation was performed as a function of time in pH solution and is presented in Figure 9 a. b.c and Tables S2, S3, S4 in Appendix B., for Nitrogen, Phosphorous, and Potassium, respectively. The controlled cumulative release profile is defined as the rate of active substances released from the nanocapsules, where the nanocapsules are able to control the release of entrapped target materials and provide multiple functional benefits; usually, the nanocapsules are made of polysaccharide materials with particular barrier properties for manipulating and controlling the release of entrapped materials.

The controlled release profile can be classified into two modes: sustained or delayed. The sustained release is designed as the release of entrapped materials in constant release with maintaining concentration to the target site. The delayed release is designed to delay the release of entrapped materials to a point where the release is required. The release of active NPK nutrients and bacterial strains in this research will be initiated by using a buffered solution stressor with (a pH of 5.5) to stimulate the soil media.[92]

Implementing the release profile in vitro conditions assures the nanocapsules' functionality and the release behavior of entrapped materials in actual agriculture applications with similar environmental conditions. Also, it can validate the type of diffusion release mechanisms as a cumulative release or percentage release of encapsulated materials at a particular time.

The release profile of these active NPK nutrients and bacterial strains has shown to undergo two phases within this stressed buffered solution. The first phase is about the initial burst release of encapsulated materials, and the second phase is the uniform controlled release in a sustained manner. This effect occurs when water is absorbed into the nanocapsules, where the large concentration of entrapped active NPK materials will be attached near the surface of the particle membrane, allowing it to undergo the first phase of rapid release.[92, 93]

After that, the second phase occurred with the diffusion of entrapped active nutrients from the inner compartment and core in the first-period intervals. Then, over time, the nanocapsules degraded to release the entrapped active NPK nutrients and bacterial

strain, where the release involves three steps: absorption of the solution into a loaded nanocapsule system, swelling of the inner matrix, conversion of the glassy polysaccharide polymer into a rubbery matrix, and finally diffusion of the active nutrient and microorganism from the rubbery matrix, which is faster than matrix erosion. [92, 93]

The chitosan polymer membrane acts as a barrier to control the release of active substances, and the diffusion mechanism limits the diffusion of active substances by controlling their diffusion from its location in the matrix to the surface of the nanocapsules. Mainly, the Diffusion mechanism is controlled by several factors, such as temperature, the solubility of nanocapsules and their permeability, and the vapor pressure effect of the membrane.

Slow-release kinetics of the active NPK nutrients were analyzed for both prepared nano bio-fertilizer capsule trials by immersing it in the stressed buffered (pH 5.5) solution. The result of N, P, and K slow release from the nano bio-fertilizer capsules is shown in Figure 9. a, b,c, respectively, where two curves belong to (Ch. Alg. HA.NPK) nanocapsules and (Ch. Alg..NPK) nanocapsules. [46, 93]

Figure 9

(a) Nitrogen Cumulative Release (%) profile for synthesized nanocapsules,(b) Phosphorous Cumulative Release (%) profile for synthesized nanocapsules,(c) Potassium Cumulative Release (%) profile for synthesized nanocapsules

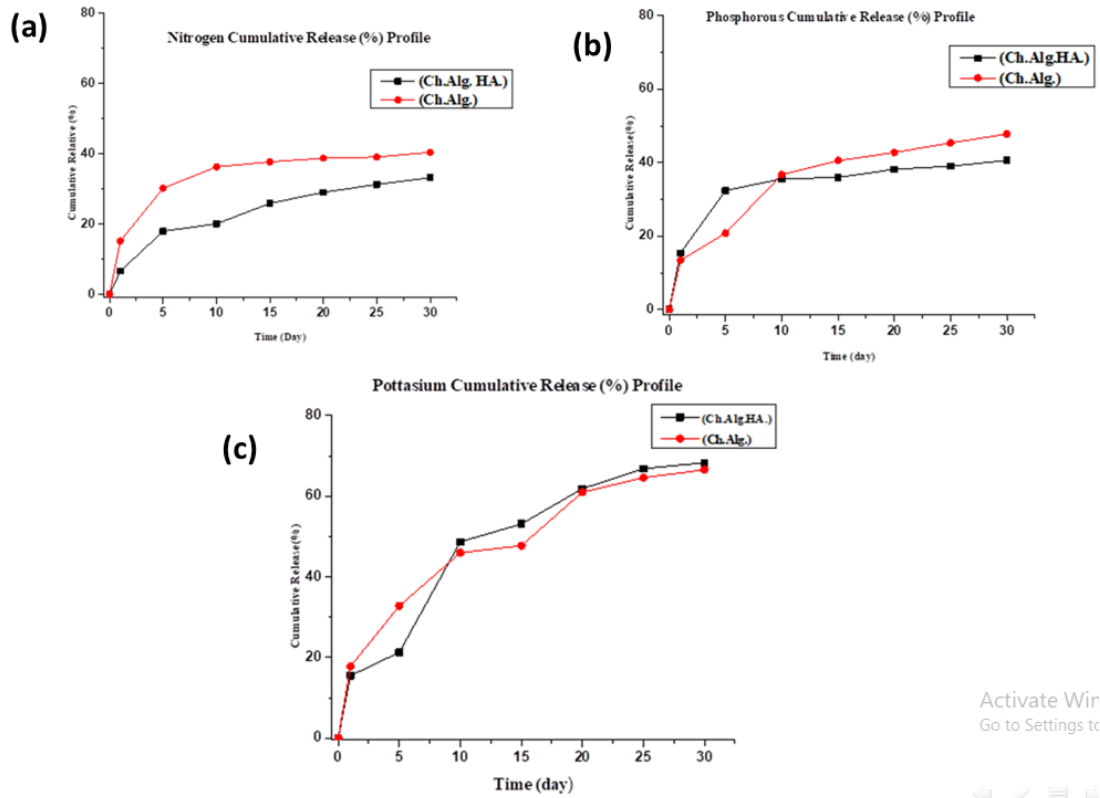


Figure 9.a. shows the cumulative nitrogen release profile of (Ch./Alg. HA.NPK) nanocapsules show a preferable sustained release behavior in a controlled manner compared to the curve of the (Ch./Alg..NPK) nanocapsules; this can be related to the role of humic acid which worked a barrier effect in releasing the entrapped components. It is shown that ((Ch./Alg. HA.NPK) nanocapsules cumulative nitrogen release profile was approximately 33.2 % within 30 days compared to (Ch./Alg.NPK), which was about 40.44% within the same study period. These results indicate the efficient role of humic acid in controlling the release of ionic nitrogen compounds and altering its release to be sustained with prolonged effect.

Figure 9.b. shows the cumulative phosphorous release profile of (Ch./Alg. HA.NPK) nanocapsules also shows a preferable sustained release behavior in a controlled manner compared to the curve of the (Ch./Alg..NPK) nanocapsules; this can be related to the role of humic acid which worked a barrier effect in releasing the entrapped components. It is shown that ((Ch./Alg. HA.NPK) nanocapsules cumulative phosphorous release profile was approximately 40.7 % within 30 days compared to (Ch./Alg.NPK), which was about 47.8% within the same study period.

Figure 9.c. shows the cumulative potassium release profile of (Ch./Alg. HA.NPK) nanocapsules and preferable sustained release behavior in a controlled manner compared to the curve of the (Ch./Alg..NPK) nanocapsules. It is shown that ((Ch./Alg. HA.NPK) nanocapsules cumulative potassium n release profile was approximately 68.3 % within 30 days compared to (Ch./Alg.NPK), which was about 66.56 % within the same study period. It is noticed that the cumulative release of (Ch. Alg. NPK) was less than (Ch. Alg. HA.NPK). This may be attributed to the small size of potassium ions and the ease of release of larger nanocapsule sizes from formulated pores in its network; also, the positive charge enhances its release where there is no interaction with the chitosan surface.

On the other hand, the curves showed that nitrogen nutrient was slowly released compared to other phosphorous and potassium nutrients.

The slow release of nitrogen can be explained by the ionic bond force between chitosan nanoparticles on the surface with the negative nitrogen ions when it reaches the surface at the diffusion phase. In contrast to potassium ions, they inhibited the fast release and were followed by phosphorous ions, which may also be affected by the formulation of ionic bonds formed between these ions and chitosan nanoparticles on the surface. However, these ionic bonds seemed less stable than nitrogen ionic bonds, which are visualized in their cumulative release profile. [94]

On the other hand, the number of bacterial strain inoculums was also measured, and it was found that the number of high viability bacterial cells slightly decreased to 1.7×10^{10} CFU /g with minimum cell loss; this indicated that nanocapsules were capable of releasing cells for more than six months.

Also, The kinetic release for all cumulative releases of entrapped active nutrients for both synthesized nanocapsules was analyzed by Korsmeyer and Peppas module as shown in Tables S2, S3, S4, and Figures S4, S5, S6 in Appendix B.[95] The release profile for each nutrient was fitted into the Korsmeyer Peppas model Equation (7) as follows :

$$\frac{M_t}{M_0} = K_{kp} t^n \quad (7)$$

Where :

$\frac{M_t}{M_0}$ = is the released fraction of active nutrients at time t

K_{kp} = is a constant incorporating characteristics of nanocapsule

(n)= diffusional exponent, as indicative of the transport mechanism

The linearization of all graphs for all nutrients for both synthesized nanocapsules samples generates an equation of the line: y –the axis is the log of cumulative release, and the x-axis is the log of time. The linear equation shows the slope as the release exponent(n) as the release mechanism, and the y-intercept is log release and its rate constant.[96] Suppose the diffusion exponent (n) value for the release of fertilizer is $n \leq 0.5$. In that case, it means that the active nutrient release mechanism approaches a Fickian diffusion-controlled sustained release module, whereas if the n value is equal to $n= 1$, it indicates that the active nutrient release approaches the zero-order mechanism transport. Meanwhile, if the n value is between 0.5 and 1, it shows that active nutrient release is anomalous non-Fickin diffusion.

It can be seen from Tables S2, S3, S4, and Figures S4, S5, and S6 in Appendix B that all NPK nutrients have a release mechanism (n) that lies between 0.4 and 0.8; the nitrogen diffusional exponent for (Ch.Alg.HA. NPK) was approximately 0.5, which means it follows the Fickian diffusion-controlled sustained release module; whereas, the (Ch. Alg. NPK) 's nitrogen release diffusional exponent (n) was approximately 0.6, which means the nitrogen release is anomalous non-Fickin diffusion module.

For the phosphorous release, it shows that the diffusional exponent(n) for (Ch. Alg.HA.NPK) and(Ch.Alg.NPK) nanocapsules is also approximately equal to 0.5, which means both nanocapsules release follow the Fickian diffusion-controlled sustained release module.

Finally, for the potassium kinetic release, diffusional exponent (n) intersects with their release behavior, and the highest cumulative release for both synthesized nanocapsules is approximately equal to 0.7, whose transport mechanism is a non-Fickin diffusion module.

This diffusional exponent of all active nutrients for both synthesized nanocapsules indicates controlled and matrix-based releases.[97] Besides that, the high value of the y -intercept supports the profile that release undergoes stress-solution conditions.

The prepared (Ch. Alg. HA.NPK.PGPRs) nanocapsule in this research work exhibits several advantages compared with the controlled synthesized (Ch. Alg. NPK. PGPRs) nanocapsule. The one-step preparation process of this novel nano-bio fertilizer loaded with active nutrients and beneficial microorganisms loaded by in-situ simple polymerization technique can significantly reduce the production cost of these prepared nanocapsules formulations. Using a humic acid molecule not only advances the cross-linking forming between chitosan and alginate polysaccharides but embeds a high amount of encapsulated material, enhancing the water absorption capacity and providing a release property.

Finally, using such nano bio-fertilizer products not only can be an alternative to conventional agrochemical fertilizers but can also increase the quality and quantity of agricultural products by improving crop fertility and soil water conservation.

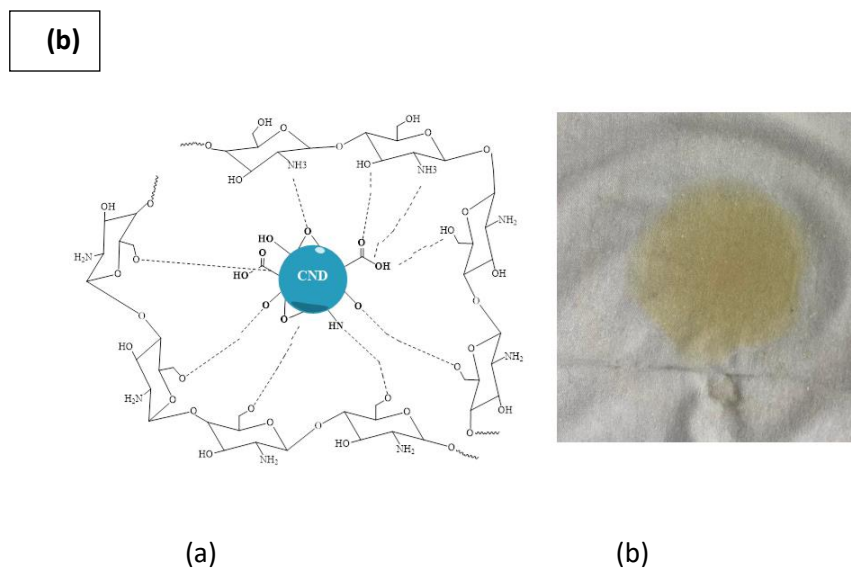
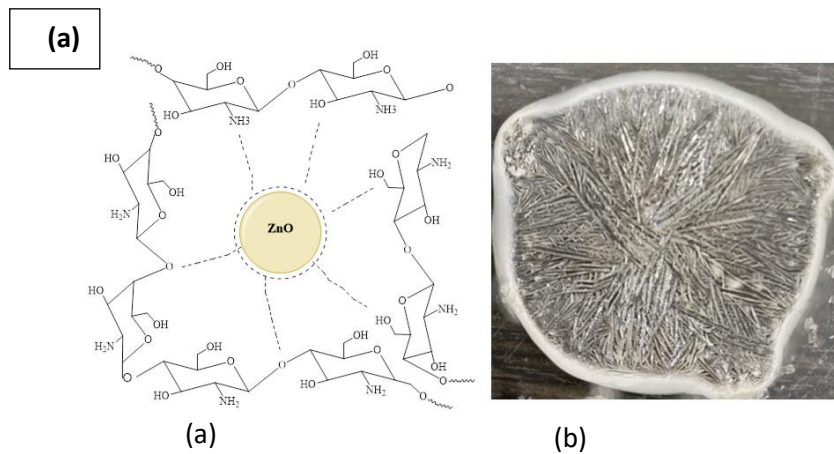
3.2 Synthesis and Characterization of Chitosan-based Photocatalytic Composites

This section will discuss the synthesis and characterization of chitosan-based photocatalytic materials. The synthesis of Ch. ZnO composite was carried out with two synthesis routes; firstly, the synthesis of ZnO nanoparticles by the direct precipitation method yielded nearly 68%. After that, uncapped ZnO nanoparticles and chitosan were fabricated chemically via co-precipitation technique, obtaining Ch. ZnO white forming

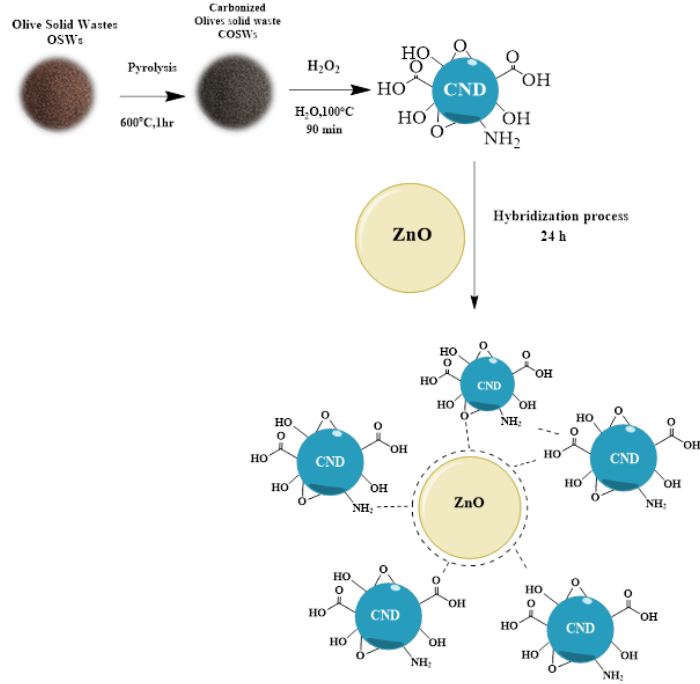
film, as shown in **Figure 10. a.b.c** with its proposed interaction of chitosan with ZnO nanoparticles.

Figure 10

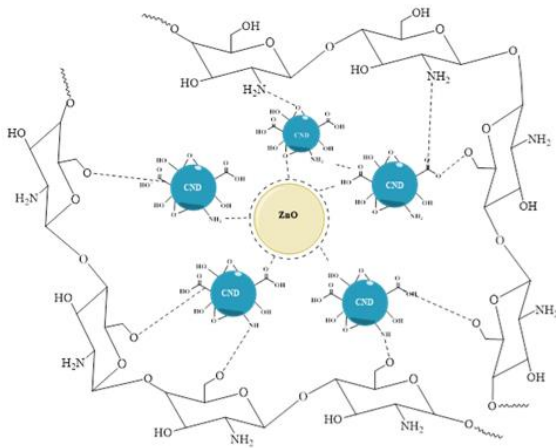
(a).: (a) The Ch. ZnO white forming film,(b) The structural interaction of Ch.ZnO (b). : (a) The Ch.CNDs pale yellowish film,(b) The structural interaction of Ch.CNDs. (c)(a).: CNDs and ZnO-CNDs hybrid preparation summary. (c)(b): (a) The Ch.Hybrid yellowish film,(b) The structural Chitosan/ Hybrid(ZnO-CNDs) Interaction



(c) (a)



(c) (b)



(a)



(b)

On the other hand, the Ch. CNDs consist of the CNDs synthesis by combined top-down and bottom-up methods depending on pyrolysis and oxidation routes with a yield of about 10 %. Then, the CNDs were incorporated with chitosan polymer in a simple solution casting method in one pot reaction, giving a Ch. CNDs with pal yellowish film, as shown in Figure 10.b. with its proposed interaction of chitosan with CNDs nanoparticles.

Meanwhile, The Hybrid composite was prepared by a sol– gel method by combining CNDs and ZnO nanoparticles at the nanometer molecular level, resulting in a pale-yellowish powder of the Hybrid product with a yield of 84.4%. During the synthesis route, the hybrid composite was thought to be formed by the absorption of CNDs particles on the ZnO surface. The CNDs particles create a weak van der Waals or hydrogen bond linkage interaction between ZnO nanoparticles, as shown in Figure 10.c.(a.b.).

After that, the hybrid material was mixed with chitosan polymer through a simple solution casting method, and chitosan offered a suitable matrix for the Hybrid to be localized on its surface, forming an interaction linkage between the primary amine and hydroxyl groups of chitosan with CNDs surface freely functional groups, leading to a yellowish film, as shown in Figure 10.c.(b)

3.2.1 Atomic Force Microscope Analysis

The morphology and size of all prepared materials ZnO, CNDs, Hybrid, Ch. ZnO, Ch. CNDs, Ch. Hybrid was studied by AFM instrument. Figure S1.a.(a.b) in Appendix C shows the CNDs nanoparticles were well dispersed with a size range of 0.84 to 5 nm and an average size of 2.3 ± 0.9 nm.

Figure S1 a.(c.d) shows the ZnO nanoparticles show a size range of 10 to 30 nm with an average of 23.5 ± 3.2 nm. The hybrid material ranges from 40 to 180 nm, averaging 105 ± 26 nm. Notably, the hybrid material size is more significant than both combined materials; this can be attributed to two main reasons: the agglomeration phenomenon with an electrostatic interaction between the hybrid particles, as noticed in the AFM image of Figure S1 a (e.f) in Appendix C and the successive absorption of CNDs on the surface of ZnO nanoparticles.

On the other hand, For Ch. ZnO, the AFM image in Figure S2.(a) in Appendix C shows that the addition of ZnO nanoparticles resulted in a more rough surface and was homogeneously distributed in the matrix, where chitosan polymer played an excellent binding agent for ZnO nanoparticles, leading to a Ch. ZnO film with small aggregates like dendritic floc–like appearance structure and nearly rod-in shape of ZnO on the chitosan surface could affect the material's properties. It revealed the presence of well-

dispersed ZnO nanoparticles on the chitosan surface, contributing to an increase of surface with an average of 4 μ m. This proves that successfully incorporating ZnO nanoparticles within the chitosan polymer matrix, adhered firmly, improves the resulting composite film's physical properties and antimicrobial activity.

For the Ch. CNDs composite, the AFM image in Figure S2. (b) in Appendix showed the Ch. CNDs film possessed a relatively smooth surface. The Ch.CNDs show a well-dispersed CNDs particle with pineapple rings in shape on the surface of the chitosan polymer matrix with a size range of 18.8-19.8 nm and an average size of 19.3 ± 0.89 nm; this evidence indicates successful incorporation and good interfacial compatibility between CNDs and chitosan polymer. This composite material's apparent interaction between chitosan and CNDs can be described through various suggested mechanisms, including electrostatic attractions, physical interactions, and chemical bonding.

The specific type of interaction depends on factors such as the main functional groups present on the chitosan polymer as amine and hydroxyl groups, and the main surface functional groups exist of CNDs particles as (carboxyl, hydroxyl, amine) groups. Accordingly to each combined material, three main suggested interaction mechanisms can be explained and worked aligned for this pineapple shape as follows: electrostatic interaction of a positively charged chitosan polymer due to the presence of amino groups, and CNDs carry a net negative charge or possess charged functional groups on their surface.

Electrostatic attraction between both materials can promote dispersion and stabilization within the composite. Hydrogen bonding as chitosan contains hydroxyl and amino groups, which can form hydrogen bonds with functional groups that exist on the CNDs surface, then the possibility of another hydrogen bonding forming between CNDs particles which corporate together in circle form. These hydrogen bonding also contribute to the interfacial adhesion between chitosan and CNDs.

The covalent bonding interaction mechanism is another suggested possible interaction for this phenomenon between reactive functional groups. Specifically, the amino groups on chitosan are hypothesized to undergo a reaction with the carboxylic acid groups located on the surface of carbon nanodots (CNDs). This chemical process is anticipated to create an amide covalent linkage, effectively connecting the two components.

On the other hand, The Ch. Hybrid morphology as appeared in the AFM image, as shown in Figure S2.(c) in Appendix C, shows a heterogenous distribution in the chitosan matrix surface, where the hybrid material shows a good dispersion in water, forming a homogenous suspension solution due to the hydrogen bonding forming between surface freely functional groups on CNDS surface and water molecules.

Furthermore, an additional advantage arises from effectively integrating chitosan polymer as an exceptional binding agent within hybrid materials, forming a hetero-photocatalyst composite. The arrangement of pineapple rings validates the CNDS' absorption onto the ZnO surface, while the presence of unfettered functional groups on the CNDS' surface significantly enhances their interaction with the chitosan matrix. These interactions align with the elucidated mechanisms of interaction proposed earlier.

3.2.2 X-Ray Diffraction

To further confirm the formation of hybrid materials between ZnO and CNDS material, the XRD patterns of ZnO, CNDS, and hybrid crystal structures are shown in Figure S3 in Appendix C.

For the ZnO case, the XRD pattern confirms the typical hexagonal Wurtzite crystal structure with the prominent characteristic diffraction peaks at $2\theta^\circ = 32^\circ, 34.68^\circ,$ and $36.53^\circ, 47.87^\circ, 57^\circ$ which corresponded to (100), (002), (101), (102), and (110) planes respectively.[98]

The CNDS case shows a diffraction peak at $2\theta^\circ = 25.6^\circ$, corresponding to (002) graphitic plane originating from the amorphous CNDS shape.[99] For the hybrid material, there is a slight shift in the main diffraction lines to lower degrees, and an increase in full width of half maximum (FWHM) for $2\theta^\circ$ from 0.53° to 0.64° of (101) crystal plane has been observed, and this proves the absorption of CNDS on the ZnO surface lattice components.[100] Also, the broadening of the (101) diffraction peak leads to a smaller crystallite size of 13.64 nm compared to 16.48 nm of ZnO nanoparticle as calculated from the Debye- Scherrer equation (Eq.) for (101) of hexagonal wurtzite of ZnO and Hybrid (ZnO/CNDS), [101] as follow:

$$D_{crystallite\ size} = \frac{k\lambda}{\beta \cos\theta} \quad (8)$$

Where :

λ is the wavelength of the x-ray ($\lambda = 1.5406 \text{ \AA}$).

$k = 0.94$.

θ = is the half-diffraction angle of (101)

β = is the FWHM in radius

This noticeable decrease in the crystallite size of ZnO is due to the combination with CNDs in forming a Hybrid composite, which is located with peaks at $2\theta = 31.77^\circ$, 34.47° , 36.25° , which corresponds to (100), (002), and (101), respectively. [102] Also, this can be related to those of the hexagonal shape structure. [103] The lattice constants a, b, c , and the plane d -spacing can be calculated using the following Eqs. , and also by using Bragg's Equation [104]

$$a = b = \frac{\lambda}{\sqrt{3}} \times \frac{1}{\sin \theta_{100}} \quad (9)$$

$$c = \frac{\lambda}{\sin \theta_{002}} \quad (10)$$

$$d_{spacing} = \frac{\lambda}{2 \sin \theta_{101}} \quad (11)$$

The obtained values of a, b, c , and d for ZnO and Hybrid are summarized in Table (1) below:

Table 1

Hexagonal lattice constants and Bragg's spacing of ZnO and Hybrid

	$a=b$	c	c/a	$d_{spacing}$ (Bragg)
ZnO	3.2269	5.1691	1.6018	2.4580
Hybrid	3.2496	5.1996	1.6000	2.4760

The obtained calculated parameters of the lattice constants a,b,c, and the plane d-spacing show a modification with an increase in the lattice constants as observed between ZnO and Hybrid material in Table (1); this for sure referred to the presence of CNDs on the surface of ZnO and also the enlargement of d- spacing could propose a relatively high density of ZnO stabilized with CNDs particles leading to forming Hybrid composite.[104]

Meanwhile, for XRD of Ch.ZnO, Ch.CNDs, and Ch. Hybrid is not listed or discussed due to the appearance of chitosan peaks over the photocatalyst peaks, and thus, the value of the XRD patterns did not appear.

3.2.3 FT-IR Spectra

The FT-IR technique acquired the chemical functional groups of all synthesized materials, where the FT-IR spectra of ZnO, CNDs, Hybrid, and Ch. Hybrids are illustrated Figure S4 in Appendix C.

The FT-IR of the ZnO nanoparticles spectrum shows prominent characteristic bands at 550 cm^{-1} , 698 cm^{-1} , 920 cm^{-1} , and 3238 cm^{-1} , which are allotted to the Zn-O bond and formation of ZnO.[85, 105]

The CNDs spectrum shows a significant peak at 3300 cm^{-1} corresponding to the N-H /O-H groups and peaks at 28100 cm^{-1} corresponding to C-H stretching. Also, 1600 cm^{-1} and 1390 cm^{-1} peaks are attributed to the C=O /C=C and C-H binding, respectively. The peak at 1070 cm^{-1} is mainly related to the C-O-C group, where functional groups on the CNDs surface are responsible for chemical and electrostatic linkage with ZnO and chitosan polymer. [106, 107]

The hybrid spectrum reflects the hybridization that occurred between ZnO and CNDs, where there is a minor shift of CNDs peaks to beaks 2818 cm^{-1} , 2900 cm^{-1} , 1630 cm^{-1} , and 1375 cm^{-1} , which are related to C-H stretching, C=O/C=C and C-H bending, respectively.[108] Also, a slight shift to a peak related to ZnO to be at 780 cm^{-1} instead of 698 cm^{-1} and a broadening of the peak at 930 cm^{-1} as an indication of occurred linkage of Zn-O-C through hydroxyl and carboxylic groups exists on CNDs surface, which also contributes to good dispersion and high stability with increasing its

negative charge ζ - potential from -20 ± 1.5 to be -28 ± 2.1 mV in phosphate buffer solution (PBS @ pH~7.4).[108]

The chitosan spectrum shows strong functional group peaks at 3368 cm^{-1} and 656 cm^{-1} , corresponding to the N-H and O-H stretching frequency of glucosamine and intermolecular hydrogen bonding. Significant peaks at 2885 and 2900 cm^{-1} are allocated to C-H symmetric and asymmetric stretching. These bands are the main characteristics of typical chitosan polysaccharides. Other peaks at 1651 cm^{-1} and 1546 cm^{-1} are corresponding to the C-O stretch in the primary alcohol group. The absorption peak at 1376 cm^{-1} is allotted to C-N glucose stretching of primary amine, while those at 1404 cm^{-1} and 1424 cm^{-1} are allotted to CH_2 and CH_3 symmetrical deformation, respectively.

When chitosan is combined with a hybrid composite, the FT-IR spectrum shows a broad peak at 3800 cm^{-1} corresponding to the amide linkage that occurred between the free amine group of chitosan with carboxyl groups exist on CNDs surface, where it is evident that the amine peak of chitosan has been shifted to this new observed peak which confirms the formation of new bonds. Other significant sharp peaks at 2990 cm^{-1} and 2884 cm^{-1} are attributed to C-H stretching in asymmetric and symmetric, respectively.

The slight shift of peak at 1630 cm^{-1} to 1539 cm^{-1} confirmed the existence of C=O /C=C groups of CNDs molecules and assigned to C=O in the carboxyl group, which participates in amide formation with chitosan polymer. as well, another indication of is the slight shift of C-H bending peak from 1375 cm^{-1} to be 1394 cm^{-1} .

The appearance of a new sharp peak at 1050 cm^{-1} can be related to the C-O stretch on the CND's surface and chitosan skeleton. The broadened peak of linkage of Zn-O- C at a 930 cm^{-1} has been decreased due to the formation of a new sharp peak at 1050 cm^{-1} , which confirms the absorption of CNDs on the surface of ZnO and participation of CNDs ' functional group in the linkage with chitosan polymer.

The FT-IR of Ch. ZnO spectrum is shown in Figure S5 (a) in Appendix C. The spectrum shows low-intensity peaks at 3075 cm^{-1} , 1552 cm^{-1} , 1444 cm^{-1} , and 1018 cm^{-1} , corresponding to NH_2 and OH vibrational stretching, CH_2 group, C=O, and C-O-C linkage, respectively. These peaks confirm the existence of chitosan polymer with a

significant shift due to the presence of ZnO and its interaction. Some additional spectral peaks related to the ZnO nanoparticles in the same spectrum confirm the blending of chitosan with ZnO.

Also, the FT-IR of Ch.CNDs spectrum is shown in Figure S5 (b) in Appendix C. The Ch.CNDs show an intense vibrational peak in the (3200 - 3500) cm^{-1} ranges attributed to the N-H and O-H stretching vibration found in CNDs and chitosan. Furthermore, the characteristic peak in 2727 cm^{-1} is attributed to the acetyl group, and 1708 cm^{-1} and 1645 cm^{-1} are related to C=O for Ch.CNDs film.

The presence of typical peaks of CNDs and chitosan in the IR spectrum of the product demonstrated the successful synthesis of Chitosan with CNDs film. A weak peak at 1708 cm^{-1} indicates that some of the O-H groups in chitosan form ester – COO⁻ moiety also absorption peaks at 1651 cm^{-1} , 1547 cm^{-1} , 1424 cm^{-1} , and 1404 cm^{-1} peaks have been shifted to be 1645 cm^{-1} , 1389 cm^{-1} , 1273 cm^{-1} , and 1014.87 cm^{-1} with the disappearance of 1376 cm^{-1} of C-N indicate the new linkage formation. These new peaks indicate the grafting of chitosan and synthesized Ch.CNDs form and confirm the interaction.

Besides that, the RAMAN spectrum for the Hybrid, as shown in Figure S6 in Appendix C., proves the successful hybridization of ZnO- CnDs as indicated by the existence of D and G bands at approximately 1390 cm^{-1} and 1600 cm^{-1} , which originated from the graphite CNDs structure absorbed on the surface of ZnO nanoparticles.

3.2.4 Optical Properties of Synthesized Materials

Figure S7 a.b. in Appendix C shows the optical properties of prepared ZnO, CNDs, Hybrid, Ch.ZnO, Ch.CNDs., and Ch.Hybrid by performing UV- Vis spectral acquisition.

ZnO, and Ch. ZnO with white color, where ZnO shows only one absorption band in the UV- region at 370 nm with a cutoff at the edge at 397 nm, which is related to its high energy band gap.

On the other hand, the UV-Vis analysis of Ch. ZnO was obtained, where chitosan typically exhibits a broad peak in the UV region between 200-300 nm, known as the $\pi-\pi^*$ transition. This peak is attributed to the transitions between the non-bonding electrons on the nitrogen atom and the antibonding electrons in the acetyl or hydroxyl groups. Besides that, it shows a tail extending in the visible region, where these absorption features arise from electronic transitions involving chromophoric groups present in chitosan, as well as conjugated double bonds.[109] [110, 111]

When chitosan and ZnO combine to form a photocatalyst composite, the UV-Vis spectrum will combine the characteristic absorption features of these combined materials. Therefore, the absorption peaks rely on their preparation method, concentrations, and processing conditions. The observed UV-Vis spectrum shows the peak undergoes a characteristic peak at a range of 223 – 259 nm, which is observed.[109]

The UV-Vis spectra for CNDs and Ch.CNDs were also acquired with colored forming and transparent under daylight, where CNDs often exhibit strong absorption in the UV-region with a shoulder at 225 nm, which arise from $\pi-\pi^*$ transitions of aromatic sp^2 hybridized carbon core. As well its spectrum shows a tail extending toward the visible region.[112-114]

The Ch.CNDs often display in the UV region absorption peaks due to the $\pi-\pi^*$ transitions, which involve the excitation of electrons from the filled π - orbitals to the unfilled π^* orbitals of the carbon-based structures. Typically, these transitions occur at lower energy levels than traditional transitions in organic molecules. The exact peak location ranged between 205- 265 nm, with the highest typically observed around 250 - 290 nm. The composite of combined chitosan with CNDs exhibits extending tail absorption peaks in the Vis- region arising from various electronic transitions, including $n-\pi^*$ transitions and charge transfer interactions. Mainly, the transitions involved the excitation of electrons from non-bonding orbitals (n) to π^* orbitals, or it can be described as from the donor groups to acceptor groups. [84, 113-115]

On the other hand, the Hybrid (ZnO/CNDs) and Ch. Hybrid shows the apparent color and is transparent under daylight. The Hybrid UV- Vis analysis indicates the absorption features of CNDs and ZnO in the UV and Vis region with an absorption peak at 370 nm

and a strong UV absorption peak. These results confirm the contribution of CNDs in enhancing the optical properties of ZnO and visible light harvesting of the hybrid composite. It is the same as when chitosan is combined with hybrid materials, generating hetero photocatalytic composites with distinguishable optical properties as observed in the UV- Vis spectrum and shifting the position of the absorption peaks with enhancing the overall absorption intensity, where significant absorption peaks located at a range between 207 -229 nm, and another absorption peak at 289 nm as a slight shift from absorption peak of Hybrid as alone, with a tail extending in the visible region. [53, 110] These significant absorption intensities in the UV- Vis region could serve with the unique optical contribution of hetero photocatalytic composites in different applications.[116]

Moreover, the direct band gap of ZnO and Hybrid (ZnO/CNDs) was recalculated from Uv- Vis spectra by *Tauc's* plot by applying the Equation [116, 117]

$$(\alpha h\nu)^2 = B(h\nu - E_g) \quad (12)$$

Where:

α is the absorption coefficient,

$h\nu$ is the photon energy as ($h\nu = 1240/\lambda$)

λ is the wavelength

B is constant

E_g is, the band gap energy.

Figure S7 (b) shows the plotting of $(\alpha h\nu)^2$ versus $(h\nu)$ with a linear extrapolation to $(h\nu)$ at $(\alpha h\nu)^2 = 0$, where band energy can be obtained. ZnO exhibits a large band gap with a numerical value of (3.1 eV). This large band gap can be attributed to the cut-off edge and the absence of visible light absorption. Meanwhile, when the Hybrid formed, the band gap decreased to (2.8eV) due to forming an intermediate energy level above the ZnO valence band.[118] . It promoted the ZnO photocatalytic activity in the visible light region to be more efficient as an antimicrobial agent.

3.2.5 Antimicrobial activity

The relative antimicrobial activity for studied materials ZnO, CNDs, Hybrid, Chitosan, Ch./ZnO, Ch./CND, and Ch./Hybrid was evaluated against a broad spectrum of gram-positive and gram-negative bacterial strains and fungal strains using various in vitro antimicrobial laboratory methods such as disc diffusion method, minimum inhibitory concentration (MIC), reduction of the colony- forming units, and time – killing kinetics. All antimicrobial methods were carried out under dark and sunlight conditions to assess the role of the existence or absence of light irradiation in enhancing the antimicrobial inhibition mechanisms.

Firstly, the antimicrobial activity was qualitatively screened using the disk diffusion methods under dark and sunlight modes, measuring the mean diameter of inhibition zones developed around tested samples. All tested samples were studied in triplicate. The obtained data are listed in Table (2) and Table (3).

Table 2

Size comparisons of inhibition zone for ZnO, CNDs, and Hybrid for different bacterial and fungal strains under sunlight and dark modes

Microbial strains	Gram Type	mm of Inhibition Zone (Mean \pm SD)					
		ZnO		CNDs		Hybrid	
		Dark	Sunlight	Dark	Sunlight	Dark	Sunlight
<i>E. coli</i>	-ve	23 \pm 4	27 \pm 3	23 \pm 4	27 \pm 4	22 \pm 3	26 \pm 3
<i>S. aureus</i>	+ve	24 \pm 3	29 \pm 1	17 \pm 2	25 \pm 1	27 \pm 2	36 \pm 3
<i>K. pneumonia</i>	-ve	26 \pm 3	33 \pm 1	15 \pm 3	25 \pm 3	30 \pm 2	35 \pm 1
<i>MRSA</i>	+ ve	14 \pm 1	21 \pm 3	14 \pm 4	19 \pm 3	25 \pm 1	30 \pm 1
<i>P. aeruginosa</i>	-ve	19 \pm 2	25 \pm 2	13 \pm 2	19 \pm 4	19 \pm 1	26 \pm 1
<i>Mold</i>	-	26 \pm 1	30 \pm 2	20 \pm 1	30 \pm 2	30 \pm 1	38 \pm 1
<i>S. cerevisiae</i>	-	28 \pm 3	31 \pm 3	22 \pm 2	29 \pm 1	31 \pm 2	37 \pm 1
<i>A.s fumigatus</i>	-	20 \pm 3	26 \pm 3	20 \pm 3	28 \pm 1	30 \pm 1	35 \pm 1

As Shown in the Table (2), ZnO nanoparticles show better antimicrobial activity under sunlight than in dark conditions. In the sunlight condition, a clear inhibitory zone ranged from (21-33) mm; meanwhile, in the dark condition, its inhibition zone ranged from (14-26) mm, less than the sunlight condition.

The CNDs particles exhibit lower antimicrobial activity than ZnO nanoparticles in their inhibitory activity. Even though it shows better antimicrobial activity under sunlight than in dark conditions, where its inhibition zones ranged from (19-30) mm in sunlight condition, but in the dark condition its inhibition zone ranges from (13-23)mm, which indicates more qualitative results of the inhibitory effect of these synthesized materials.

Undoubtedly, combining ZnO and CNDs particles leads to a synergistic effect of forming hybrid materials, which plays a vital role in its antimicrobial activity. The effect of hybrid material also varied between the dark and sunlight conditions, where in the dark condition, its inhibitory zone ranged from (15-31)mm, and in sunlight condition, its inhibitory zone ranged from (25-38) mm, which depicts qualitatively how much the photo-irradiation enhances the microbial colonies effectively.

Table 3

Size comparisons of inhibition zone for Chitosan, Chitosan/ZnO, Chitosan/CNDs, and Chitosan/Hybrid for different bacterial and fungal strains under sunlight and dark modes

		mm of Inhibition Zone (Mean \pm SD)							
Microbial Strains	Gram Type	Chitosan		Chitosan/ZnO		Chitosan/CNDs		Chitosan/Hybrid	
		Dark	Sunlight	Dark	Sunlight	Dark	Sunlight	Dark	Sunlight
<i>E.coli</i>	-ve	23.4 \pm 0.30	35.6 \pm 0.77	33.2 \pm 0.49	41.2 \pm 0.39	29.3 \pm 0.35	39.4 \pm 0.36	40.2 \pm 0.44	49.6 \pm 0.20
<i>S. aureus</i>	+ve	34.5 \pm 0.18	40.5 \pm 0.29	40.1 \pm 0.34	45.2 \pm 0.45	36.4 \pm 0.28	41.5 \pm 0.43	43.7 \pm 0.10	52.8 \pm 0.19
<i>K.pneumonia</i>	-ve	37.6 \pm 0.29	44.2 \pm 0.73	41.2 \pm 0.48	47.1 \pm 0.33	37.9 \pm 0.18	43.7 \pm 0.26	50.2 \pm 0.28	54.3 \pm 0.63
<i>MRSA</i>	+ve	31.4 \pm 0.31	39.7 \pm 0.44	34.2 \pm 0.60	44.4 \pm 0.23	33.5 \pm 0.73	40.8 \pm 0.22	45.9 \pm 0.70	50.1 \pm 0.22
<i>P.aeruginosa</i>	-ve	28.9 \pm 0.72	30.8 \pm 0.52	32.1 \pm 0.94	36.2 \pm 0.64	29.3 \pm 0.66	33.6 \pm 0.92	39.8 \pm 0.39	42.4 \pm 0.52
<i>Mold</i>	-	32.9 \pm 0.53	39.5 \pm 0.61	44.2 \pm 0.88	49.3 \pm 0.55	40.9 \pm 0.37	44.4 \pm 0.27	43.3 \pm 0.63	54.7 \pm 0.42
<i>S. cerevisiae</i>	-	36.1 \pm 0.73	43.7 \pm 0.43	44.4 \pm 0.76	48.7 \pm 0.92	43.5 \pm 0.28	45.2 \pm 0.45	44.7 \pm 0.84	55.1 \pm 0.32
<i>A. funigatus</i>	-	37.5 \pm 0.43	42.4 \pm 0.50	43.2 \pm 0.37	47.4 \pm 0.19	40.2 \pm 0.19	44.4 \pm 0.25	42.7 \pm 0.12	54.9 \pm 0.22

Table (3) shows that chitosan exhibits antimicrobial activity against a broad spectrum of microbial strains; the type of chitosan, molecular weight, and several physiochemical properties are attributes of this activity.

As shown in Table (3), the inhibition zone diameter for Ch./ZnO reveals better antimicrobial activity under sunlight mode than in dark mode. , where in the dark condition, its zone mean diameter ranged from (33.2-44.4) mm. Meanwhile, it ranged from (41.2-49.3) mm under sunlight irradiation. The photo-irradiation enhanced the Ch./ZnO photocatalyst activity for inhibiting the gram-positive and gram-negative bacterial strains and fungal strains. On the other hand, Ch./CND exhibits higher antimicrobial activity than chitosan but lower than Ch./ZnO materials under both dark and sunlight modes, where for dark mode, its inhibition zone mean diameter ranged from (29.3-43.5) mm, and in sunlight mode, its inhibition zone ranged from (33.6-45.2) mm. These obtained values indicate the discrepancy of inhibitory effect for the tested microbial series .

Certainly, the Ch. Hybrid showed a significant zone inhibition diameter compared to other tested samples; this can be attributed to the synergistic effect of incorporation of ZnO with CNDs forming the hybrid materials, which was deposited on a chitosan matrix, and hence more stability formed, giving more surface area to interact with microbial walls and inhibit their growth. The efficiency of its antimicrobial activity varies between dark and sunlight modes. In dark mode, zone inhibition ranged from (39.8-50.2) mm. In sunlight mode, an evident zone inhibition ranged from (49.6-55.1) mm, which depicts qualitatively how much the microbial colonies inhibited drastically with prolonged sunlight irradiation .

The antimicrobial activity of synthesized materials was evaluated by determining their minimum inhibitory concentration (MIC) in the presence and absence of sunlight irradiation against a broad spectrum of different microbial strains, as observed in Table (4) and Table(5). The experiment included the exposure of microbial strains to a series of diluted aqueous prepared stock antimicrobial solutions with setting chitosan material as the control solution since all synthesized materials consist of chitosan as the backbone set.

Table 4

Minimum inhibition concentration of microbial growth (MIC) values ($\mu\text{g/ml}$) of ZnO, CNDs, and Hybrid under sunlight and dark modes

Microbial Strains	Microbial growth (MIC) values ($\mu\text{g/ml}$)					
	ZnO		CNDs		Hybrid	
	Dark	Sunlight	Dark	Sunlight	Dark	Sunlight
<i>E. coli</i>	31.5	15.6	62.5	31.5	31.5	7.8
<i>S. aureus</i>	31.5	15.6	125	62.5	15.6	7.8
<i>K. pneumonia</i>	31.5	15.6	125	62.5	31.5	15.6
<i>MRSA</i>	125	62.5	125	125	62.5	31.5
<i>P. aeruginosa</i>	125	62.5	250	125	125	31.5
<i>Mold</i>	31.5	15.6	62.5	31.5	15.6	7.8
<i>S. cerevisiae</i>	31.5	15.6	62.5	31.5	15.6	7.8
<i>A. fumigatus</i>	62.5	31.5	62.5	31.5	15.6	7.8

As shown in Table (4), the MIC concentrations of ZnO under dark mode ranged to (31.5-125) $\mu\text{g/ml}$, and under sunlight mode ranged to (15.6-62.5) $\mu\text{g/ml}$. For CNDs, its MIC concentration in the absence of light was (62.5-250) $\mu\text{g/ml}$ and was more effective under sunlight mode at (31.5-125) $\mu\text{g/ml}$. However, the Hybrid composite shows an outstanding performance, and the MIC concentration approves its efficiency under dark mode to be in the range of (15.6-62.5) $\mu\text{g/ml}$, but it shows more inhibition microbial effect in the presence of light to be in the range of (7.8 – 31.5) $\mu\text{g/ml}$. These findings prove the synergistic effect of CNDs inseparably bound to ZnO nanoparticles and enhancing the photocatalytic phenomena effect.

Table 5

Minimum inhibition concentration of microbial growth (MIC) values ($\mu\text{g/ml}$) of Chitosan, Chitosan/ZnO, Chitosan/CNDs, and Chitosan/Hybrid under sunlight and dark modes

Microbial Strains	Gram Type	Microbial growth (MIC) values ($\mu\text{g/ml}$)							
		Chitosan		Chitosan/ZnO		Chitosan/CNDs		Chitosan/Hybrid	
		Dark	Sunlight	Dark	Sunlight	Dark	Sunlight	Dark	Sunlight
<i>E.coli</i>	-ve	250	125	15.6	7.8	31.25	15.6	15.6	3.91
<i>S. aureus</i>	+ve	125	62.5	7.8	3.91	15.6	7.8	7.8	1.95
<i>K.pneumonia</i>	-ve	125	62.5	7.8	3.91	31.25	15.6	7.8	3.91
<i>MRSA</i>	+ve	500	125	31.25	15.6	62.5	31.25	31.25	7.8
<i>P.aeruginosa</i>	-ve	500	250	62.5	31.25	125	62.5	31.25	15.6
<i>Mold</i>	-	250	62.5	15.6	7.8	31.25	15.6	7.8	3.91
<i>S. cerevisiae</i>	-	125	31.25	15.6	7.8	31.25	15.6	7.8	1.95
<i>A. funigatus</i>	-	125	31.25	31.25	15.6	31.25	15.6	7.8	1.95

As shown in Table (5), The Ch. ZnO showed practical MIC values under sunlight modes more than dark modes as MIC values in a range of (3.91- 15.6) $\mu\text{g/ml}$ compared to a dark MIC range of (7.8-62.5) $\mu\text{g/ml}$, even though, its performance was less than Ch.Hybrid but still more effective than Ch.CND. The Ch.CNDs were not as effective as Ch.ZnO and Ch.Hybrid, its MIC in the absence of light was in a range of (15.6-125) $\mu\text{g/ml}$, but its MIC was better in the presence of light irradiation to be in a range of (7.8-62.5) $\mu\text{g/ml}$, even still less than Ch./Hybrid, which this confirms the synergistic effect of combined moieties.

The MIC for Ch. Hybrid in the absence of light was found to be in a range of (7.8-31.25) $\mu\text{g/ml}$, and the microbial growth was more inhibited under photo light irradiation at MIC concentrations of a range (1.95-15.6) $\mu\text{g/ml}$. This outstanding performance can be ascribed to the hybrid synergistic effect of CNDs material and ZnO nanoparticles; the electrostatic interaction of the Hybrid with chitosan polymer endowed the as-prepared Ch.Hybrid heterogeneous photocatalyst film gives high tensile strength and superior UV-Vis blocking photocatalytic properties. Thus, they become excellent potential active antimicrobial agents.

Moreover, ZnO, CNDs, Hybrid, Ch.ZnO, Ch.CNDs, and Ch.Hybrid were shown to alter the antimicrobial activity by colonies forming units and their percentage in the absence and presence of photo-light irradiation. Table S6 in Appendix C shows the log for the number of colonies in the absence and presence of antimicrobial agents, and Table S4 in Appendix C shows the percent colonies reduction. The resulting colonies forming units (CFU) reduction in microbial growth for ZnO in dark conditions give a $\text{Log}_{10}\text{CFU}$ ranging from (0.04- 0.14) and growth inhibition percentage (8-28%). In contrast, the sunlight mode exhibited higher antimicrobial activity, its $\text{Log}_{10}\text{CFU}$ ranging from (0.13-0.4) with an inhibition percentage growth (of 36-78%). For CNDs particles in dark mode, it shows a $\text{Log}_{10}\text{CFU}$ (0.02-0.18) and an inhibition growth percentage (4-24%), but in sunlight mode, it shows a noticeable antimicrobial activity with a $\text{Log}_{10}\text{CFU}$ (0.08-0.4) and an inhibition growth percentage of (16-60 %). Even though these results of both ZnO and CNDs prove that ZnO undergoes different ROS mechanism routes.

On the other hand, the Hybrid composite shows effective $\text{Log}_{10}\text{CFU}$ and percentage inhibition growth compared to other moieties. In the dark mode, the $\text{Log}_{10}\text{CFU}$ is (1.55-2.49) and inhibition growth (97.2-99.6%), whereas in the presence of photo-light irradiation, its $\text{Log}_{10}\text{CFU}$ (2.09-4.39) and inhibition growth (99-99.99%). These results depict how the synergistic effect plays an efficient role in enhancing antimicrobial activity.

Thenceforwards, Table S7 in Appendix C shows the resulting counted colonies as $\text{Log}_{10}\text{CFU}$ for Ch. ZnO, Ch.CNDs, and Ch.Hybrid under dark and sunlight conditions to assess their effect in both modes. Also, the results of colonies forming unit reduction performance studies are collected in Table S4 in Appendix C, which shows it as inhibition growth percentage). Tested antimicrobial agents resulted in the highest photo-induced micro biocide efficiency, the Log_{10} CFU. Its inhibition growth percentage increased to be in the case of Ch.Hybrid under sunlight (1.921-4.398) and (97.2-99.99%), respectively, compared to Ch.ZnO with a Log_{10} CFU range of (0.3187-2.398) and an inhibition growth percentage (60- 99.6%), while for Ch.CNDs its $\text{Log}_{10}\text{CFU}$ was in a range of (0.3979-1.398), and an inhibition growth percentage of (60- 98 %). Also, under the dark mode, in other words, in the absence of in-action photocatalytic mechanisms, the value of Ch.Hybrid is still higher than its comparative studies materials but less in value than exposure under photo light irradiation trails, where Ch. Hybrid values of $\text{Log}_{10}\text{CFU}$ and inhibition growth percentage were (1.398-4.398) and (97.2-99.99%), respectively. Meanwhile, the Ch.ZnO and Ch.CNDs $\text{Log}_{10}\text{CFU}$ values were (0.1938-1.398) and (0.301-1.222), with an inhibition growth percentage of (36-96%) and (36-94%), respectively. These obtained results validate the photo-induced micro biocide efficiency of being advanced with the synergistic effect of hybrid material combining CNDs and ZnO moieties, also how the incorporation and functionalization routes with chitosan polymer lead to a drastic decrease in the number of viable microbial cells, mainly for the illuminated Ch./Hybrid results compared to others, points to a great potential of utilizing such a prominent heterogeneous photocatalyst film as effective antimicrobial agents.

3.2.6 Time killing

The time-killing procedure provides information on the nature of the inhibitory effect with a reasonable length of time required for an effective killing kinetic with a certain amount of antimicrobial agent concentration. As depicted in Table (6) and Table (7), each of the studied materials within the context of their minimum inhibitory concentration behaves differently in the time required to kill a given fraction of the specific type of microbial population. The exposure time of the tested antimicrobial agent in contact with tested microbial strains was counted until a complete microbial inhibition occurred in the absence and presence of light irradiations .

As shown in Table (6), the ZnO nanoparticles exhibit an inhibitory effect ranging from 3 to 6 hours under dark conditions. CNDs and Hybrid exhibit the same inhibitory effect in light's absence, ranging from 2 to 4 hours. Whereas Hybrid shows a marked inhibitory effect under sunlight conditions ranging from 1 to 2 hours, and ZnO and CNDs exhibit the same inhibitory effect ranging from 1 to 3 hours. Seemly, the Hybrid composite could drastically suppress microbial growth in the presence of light within a limited period. These results can be attributed to photo light irradiation's role in enhancing photocatalytic mechanisms and forming reactive oxygen species. [107]

Table 6

Kill Time kinetic of ZnO, CNDs, and Hybrid for different bacterial and fungal strains under sunlight and dark modes

Microbial Strains	Gram Type	ZnO		CNDs		Hybrid	
		Dark	Sunlight	Dark	Sunlight	Dark	Sunlight
<i>E.coli</i>	-ve	6h	3h	4h	2h	4h	2h
<i>S. aureas</i>	+ve	4h	2h	3h	2h	2h	1h
<i>K.pnemounia</i>	-ve	3h	2h	3h	1h	2h	1h
<i>MRSA</i>	+ve	6h	3h	5h	3h	3h	2h
<i>P. aeruginosa</i>	-ve	3h	1h	4h	2h	2h	1h
<i>Mold</i>	-	3h	1h	2h	1h	2h	2h
<i>S. cerevisiae</i>	-	3h	2h	2h	1h	2h	1h
<i>A. fumigatus</i>	-	4h	2h	3h	2h	2h	1h

On the other hand, Table (7) shows that Ch.ZnO exhibited a marked inhibitory effect in the presence of light irradiation with a range from (25 min - 2 h), whereas in the absence of light, it takes longer as noticed to be in a range from (50 min - 4:10 h); this demonstrates the effect of light in activating the role of oxidative defense mechanisms, and thus accelerate its kill of kinetic time. On the other hand, Ch.CNDs inhibition effect required longer for an effective microbial killing than Ch.ZnO in the absence of light as a range from (1:20 h - 4:40 h); this can be attributed to resistance of some microbial strains in the first stage for its mechanism of action as an antimicrobial agent, but its photophysical and photochemical processes were advanced in the presence of light which is correlated with time of killing to be in the range of (40 min -2:35 h), even it is still less in value than Ch.ZnO for specific microbial strains; this aligned with the nature of each material and its photocatalyst precursors.

Table 7

Kill Time kinetic of Ch.ZnO, Ch.CNDs, and Ch.Hybrid for different bacterial and fungal strains under sunlight and dark modes

Microbial Strains	Gram Type	Ch.ZnO		Ch.CNDs		Ch.Hybrid	
		Dark	Sunlight	Dark	Sunlight	Dark	Sunlight
<i>E.coli</i>	-ve	3 h	1:15 h	4:05 h	1:40 h	2:10 h	50 min
<i>S. aureus</i>	+ve	50 min	35 min	1:20 h	47 min	50 min	30 min
<i>K.pneumonia</i>	-ve	1:20 h	40 min	2 h	55 min	1:30 h	45 min
<i>MRSA</i>	+ve	4:10 h	2 h	4:40 h	2:35 h	2:20 h	1:15 h
<i>P.aeruginosa</i>	-ve	3:05 h	1:50 h	4:20 h	2:10 h	1:50 h	1h
<i>Mold</i>	-	50 min	25 min	1:20 h	50 min	55 min	25 min
<i>S. cerevisiae</i>	-	1:15h	30 min	1:33h	1:10 h	1:10 h	30 min
<i>A. funigatus</i>	-	50 min	35 min	1:30 h	40 min	50 min	20 min

A drastic kinetic of kill for a time required for significantly suppressed microbial growth was notified with Ch.Hybrid in both the presence and absence of photo irradiation, even though the light irradiation advances its heterogeneous photocatalyst approaches. In the absence of light mode, the range of time was from (50 min- 2:20 h), and for the presence of light, primarily microbial strains were fully inhibited in a custom period that ranged from (25 min -1:15 h); this is ascribed to a natural synergistic effect of combined ZnO and CNDs materials, and how emerged with chitosan metric forming a heterogeneous photocatalyst film with distinguished antimicrobial properties.

3.2.7 Glutathione Deficiency Test

The mechanism of antimicrobial activity for prepared interested samples has been extensively studied in the presence and absence of light to explain their mechanism of action under both modes. All synthesized materials exhibited different mechanism action modes and antimicrobial activity towards gram-positive and gram-negative bacterial and fungal strains under dark and light modes. This difference in their antimicrobial mechanism routes can be attributed to the type of photocatalyst materials and those incorporated with chitosan, thus enhancing its chemical modification and antimicrobial effectiveness.

According to the in vitro glutathione deficiency lab test, Figure S8 and Figure S9 in Appendix C showed that the loss of glutathione percentage results in the presence and absence of light irradiation modes. Figure S8 shows the glutathione percentage in dark

mode for ZnO (62 %), CNDs (83%), Hybrid (88.2%), chitosan (78.2%), Ch./ZnO (81.9%), Ch./CNDs (86.5%), and Ch./Hybrid (91.5%).

Meanwhile, as evident in Figure S9, a remarkable glutathione percentage was obtained upon exposure to photo light irradiation conditions for ZnO (81.1%), CNDs (85.5%), Hybrid (95%), chitosan (88.9%), Ch./ZnO (93.4%), Ch./CNDs (90.9%), and Ch./Hybrid (96.8%), respectively. Herein, the Ch./Hybrid showed the highest oxidation values percentage in both modes, indicating the synergistic effect of incorporating chitosan with two photocatalytic moieties, leading to a compelling heterogeneous photocatalyst film with different precursor antimicrobial approaches.

The most common action modes of the mechanism of chitosan with antimicrobial properties in the presence or absence of light are defined in different aspects, which are: chitosan with its mucoadhesive properties able to form a film on the microbial cell porins, and thus blocks the exchange of nutrients, even can promptly open tight epithelial junction of a microbial cell wall, all this leading to microbial death; chitosan polymer consists of positive charges (NH_3^+) groups and negative charges (OH^-), which can disrupt the microbial cell membrane and its molecular functions; chitosan molecules based on their molecular weight can penetrate the microbial porins and affect RNA/DNA synthesis, leading to its death .[119]

On the other hand, For ZnO and Ch./ZnO, various microscopic investigations were revealed to explain their antimicrobial mechanisms under dark and light irradiation conditions. For dark conditions, its antimicrobial activity is unrelated to its photocatalytic activity, neither reactive oxygen species (ROS) generation nor oxidative transfection stress. It only relies on the Zn^{+2} ions generated when the Ch./ZnO film is attached to the microbial cell walls, where Zn^{+2} ions can interfere with microbial cytoplasm and destroy the microbial cells. Meanwhile, when Ch./ZnO is irradiated under sunlight, ZnO nanoparticles have broad oxidative defense mechanisms.[120, 121]

Its photocatalyst mechanism is derived from their superior photocatalytic properties, where the electron transition from the valence band to the conduction band generated in the electron-hole pair in which the electron and holes reacted with glutathione peroxidase and molecular scavengers, generating reactive oxygen species such as hydroxyl radicals (OH^\bullet), superoxide anions ($\text{O}_2^{\bullet-}$), hydrogen peroxide (H_2O_2), and

singlet oxygen ($^1\text{O}_2$). These highly active free radicals control the antimicrobial oxidative mechanism that could damage the cells of microbes, destroy the internal microbial structure, and eventually achieve an antimicrobial effect.[53, 121]

The antimicrobial mechanism for CNDs and Ch./CNDs as active antimicrobial agents relies mainly on the dispersion of CNDs on the chitosan surface and how their surface charged, surface-functionalization, and precursors advance the role of both merged materials against the microbial defense. In the absence of photo-irradiation, the Ch./CNDs, mainly CNDs, possess a specific limited antimicrobial activity, where Ch./CNDs film can be adsorbed onto microbial surface cell wall, leading to biological isolation and preventing microbes from spreading or consuming nutrients, thus this disturbing their physiological metabolism, causing to the destruction of microbes. Besides that, CNDs can penetrate the microbial wall and bind to its RNA and DNA via non-covalent interactions, changing their structures and leading to disruption and microbe death.[123 ,122] [123]

In the other part of the Ch./CNDs antimicrobial process, it was found, according to obtained results, that light irradiation enhances its antimicrobial effect since CNDs act as photosensitizers, which possesses excellent oxidative defense mechanism, generating reactive oxygen species through two main photochemical processes. The first type of this process relies on the electron transfers from CNDs particles after the absorption/excitation process to the surrounding substrates (O_2 , H_2O), leading to oxidative radicals substrates ($\text{O}_2^{\cdot-}$). The second type depends on the cycles of photophysical and photochemical processes, and the energy is directly transferred to the ground state with singlet oxygen generation for different reactive oxygen species generation. Therefore, the ROS induct the oxidative damage of microbial strains .

In the meantime, the antimicrobial effect of Hybrid and Ch./Hybrid has not been reported yet. As shown in Fig., the Ch./Hybrid has the highest glutathione values under dark and sunlight modes with a noticeable increment of glutathione deficiency percentage; undoubtedly, this can be attributed to the synergistic effect of heterogeneous photocatalyst components, even though these results were more significant compared with composite hybrid material alone. Chitosan polymer offers a suitable matrix for hybrid material to spread thoroughly and distribute homogeneously in

the film, thus increasing surface defects and surface charge and gaining high stability with good diverse photostability.[122]

Mechanistically, ZnO and CNDs' dual effect induces and advances the microbial killing procedure under dark and sunlight conditions. This also could be ascribed to the positive effect of CNDs on the photocatalytic performance of ZnO, where CNDs can either act as a photosensitizer or as a photoelectron reservoir for semiconductor electrons. Indeed, for heterogeneous photocatalyst components, the high distribution of hybrid material onto the chitosan matrix increases the hybrid capacity, improving the photocatalytic process. [122]

As a result, when heterogeneous photocatalyst components are irradiated with sunlight, the CNDs materials can reduce the interfacial transfer time through the generation of an intermediate energy level above the valence band ZnO, leading to a decrease in its band gap to 2.8 eV to improve its absorption in UV- visible regions, where it is accounted for higher performance of hybrid materials. Moreover, as ZnO is a surface-confined process, the CNDs have high adsorption capacity through hybridization. Incorporating with chitosan polymer is another beneficial effect, leading to a more effective heterogeneous photocatalyst effect.[120]

3.3 Characterization and Chemical Modification of Chitosan as Plant bio-stimulant

Chitosan consists of covalent glycosidic bonds that link repeated monomer units, and it includes a 3-position secondary hydroxyl group ($C_3\text{-OH}$), a 6-position primary hydroxyl group ($C_6\text{-OH}$), a 2-position amino group ($C_2\text{-NH}_2$), and sometimes N- acetylamino groups. The 3-position secondary hydroxyl group ($C_3\text{-OH}$) and N-amino acetyl groups are considered relatively stable compared to the above chemically active groups and have high steric hindrance that cannot efficiently react or even rotate freely for chemical modifications. However, The 2-position amino group ($C_2\text{-NH}_2$) and a 6-position primary hydroxyl group ($C_6\text{-OH}$) are the most chemically active groups responsible for various chitosan derivatives with different chemical reactions and modifications.[124]

When a chemical reaction occurs in chitosan polymer, the primary hydroxyl group is always more active than the secondary hydroxyl group; if any compound has a primary amino group and primary hydroxyl group, the amino group is more chemically active than the hydroxyl group. Therefore, in chitosan polymer, the (C₂-NH₂) amino group generally has the most significant activity, so the reaction activity of the three groups is usually ranked as (C₂-NH₂), (C₆-OH), and (C₃-OH).[124]

A common problem in chitosan, when it undergoes chemical functionalization and modification, is that the amino and primary hydroxyl groups will interfere with the chemical reaction; thus, unwanted functionalized chitosan product is obtained with unwanted introduced functional groups on the chitosan polymer. However, this problem was avoided by introducing a protective group to either amino or hydroxyl groups, which is not selected for chemical modification in the required reaction. Therefore, when a chemical reaction is set up for modification of chitosan polymer, different reaction conditions should be considered: types of chemical modification reaction, the purpose of the chemical reaction, type of protective groups, reaction conditions, and chemical reagent. [125]

There are diverse chemical modification reactions for chitosan that can occur in the hydroxyl or amino or both amino and hydroxyl groups; if the chemical reaction is conducted at amino groups, then it is an N-modified chitosan derivatives compound result, and if the chemical reaction is conducted at hydroxyl group it is an O- modified chitosan derivatives compound, and if the chemical reaction occurred for both amino and hydroxyl groups, then it becomes an N, O- modified chitosan derivatives.[125]

The general purpose of synthesizing chitosan derivatives is to advance the role of chitosan and its main functionalized groups in their implemented applications; thus, incorporating amino acids in chitosan polymer is to advance their role in stimulating plant growth and production in different agriculture purposes.

Chitosan is a tremendous polymer candidate for different functional group delivery, as figured out in recent research results. Chitosan polymer structure allows for functionalization with diverse beneficial amino acids within polymer matrix at the 2-position amino group (C₂-NH₂) and a 6-position primary hydroxyl group (C₆-OH). As

a result, this will diversify its implementation and promote agronomic and physiological agriculture parameters via dual effective and advanced performance.

In this research work, chitosan polymer is considered a suitable carrier and reservoir for amino acids, offering a large surface area, promoting its absorbance in the plant growth cycle, and providing nutrient absorbance and uptake.

Besides that, chitosan effectively protects amino acid compounds from environmental degradation effects such as evaporation, harsh pH media, depletion, and consumption risks. Also, when amino acids are incorporated with chitosan polymer, the release of amino acids will be effectively controlled within its constant biodegradability, leading to enhanced therapeutic efficacy and reduced uncontrolled consumption. Thus, this synthesis route and application can increase product shelf life and alleviate their degradation by promoting plant growth and development.[126]

Mainly, the reaction pathways focus on substituting chitosan at the (C_2-NH_2) or (C_6-OH) position, leading to a product with a random functionalization pattern. Also, if the (C_2-NH_2) amine group in the chitosan backbone is incorporated with amino acid, it would not be conducive for further amino group modification, and it may be needed for more synthesis processes, which makes it not a feasible solution. Therefore, blocking the amine group was taken, where a usual (C_2-NH_2) is blocked with a phthalic anhydride group, giving an N-phthaloyl group. Then, the (C_6-OH) position was converted to p-toluene sulfonic acid ester to ease the nucleophilic displacement reaction, yielding terminal amino acid derivatives while preserving the (C_2-NH_2) group. This type of reaction was carried out in this research to functionalize chitosan with synthesized plant precursor amino acid (1- amino cyclopropane-1-carboxylic acid) compound for enhancing the beneficial microorganism growth in soil, leading to soil fertility. [127].

The chitosan functionalized with ACC compound was synthesized through a series of chemical reaction approaches to achieve a modified chitosan with ACC compound on the (C_3-OH) positions. This compound was obtained by firstly blocking the amine groups in chitosan polymer with N- phthaloyl group as the amine protective group, subsequently followed by tosylation of the primary hydroxyl groups in chitosan to tosylate ester to increase its activity toward further substitution reactions with diverse

functional groups. After that, the tosyl group was replaced with ACC compound, as indicated by specific reaction reagents and conditions. Then, a de-protection process was applied to the N-phthaloyl amine group using a hydrazine reagent with mild de-protection conditions to obtain the desired final chitosan ACC product without affecting the carboxyl groups of ACC groups.

N-phthaloyl is a commonly protective amine group utilized in many research types in modifying chitosan and protecting its amine groups for the specific modification chitosan reactions demand, mainly if the reaction requires a modification to occur only at primary hydroxyl groups of chitosan polymer. The tosylation process also considers another standard method for acylation of the primary hydroxyl groups with the tosyl group for further functionalization to expand its applications, where it involves converting primary hydroxyl groups to tosylate ester. Then, it undergoes subsequent substitution reactions with amino acids as a functional group example. This procedure method efficiently achieved the desired protection of amino groups and the tosylation of primary hydroxyl groups. The resulting compound usually exhibited stability and enhanced reactivity towards selected functional group reactions, developing various compounds with tailored properties. [89]

This synthesis approach can significantly expand the application of such a derivative for another substitution on the (C_2-NH_2) group. Even though N-phthaloyl chitosan is still the standard method for amine blocking, it is considered a versatile approach for (C_6-OH) tosylation and nucleophilic substitution. Also, the N-phthaloyl group's unblocking process usually occurs using a hydrazine compound. However, if this approach is selected, it may affect the amino acid functionalized chitosan at the (C_6-OH) position, where there is an acute chance of a reaction of the carboxylic acid with a hydrazine compound in the unblocking stage, giving unfavorable side products. Moreover, such a sequence reaction is inefficient as an excess amount of organic solvents is consumed for the precipitation of the product, which requires a long time to complete. The de-protection process of N- the phthaloyl group, where harsh reaction conditions and reagents are required as using hydrazine compound with higher reaction temperature, sometimes affects the functionalized group. This type of reaction method now suffers from some main drawbacks, and it becomes necessary to develop new pathways for efficiently synthesizing functionalized chitosan.[89]

Concerning the extraordinary properties and application of amino acid-functionalized chitosan for agriculture purposes, in this research, a novel efficient synthesis method for amino acid-functionalized chitosan was conducted through the following reaction sequences: new N-blocking method using (di-tert-butyl-di-carbonate) BOC component for the first time as blocking reagent for (C_2-NH_2) in chitosan polymer with efficient reaction conditions, then, subsequently followed with the tosylation of (C_6-OH) of chitosan to p- toluene sulfonic acid esters (tosyl chitosan), then it was functionalized with amino acid through nucleophilic substitution pathway at the tosyl position. After that, chitosan was unblocked using a few millimeters of Tri-fluoro acetic acid at a particular efficient time, then another functionalization of amino acid at the (C_2-NH_2) position after de-blocking was carried out using the addition reaction. This potential pathway with two different amino acids functionalized chitosan was suitable for controlling reaction pathways and conditions with efficient attenuation results. [128]

A Kaiser test was performed to validate the new N-protection and de-protection method of chitosan with Boc reagents and compare it with N-phthaloyl compounds for both N-blocking and de-blocking methods to validate amine protection and de-protection. The indication of amine protection was validated by measuring the absorbance of the prepared solution containing the N-blocked chitosan product and calculating the number of free amino groups (in Micromol) that exist for each 1 g of chitosan polymer. Also, the result color of each solution was another indication of successful amine blocking, where the appearance of a faint blue color was related to an entirely successful amine protection process, and the appearance of a very intensive dark blue color indicated poor amine protection process and more free amine have still existed in the chitosan polymer. The calculated results with color indication are illustrated in Table (S1) in Appendix D below for both N-blocking approaches.

Also, The Kaiser test was carried out for the de-protection process after functionalization of chitosan at the C_6-OH position to ensure complete de-protection in the synthesis process with a very intensive dark blue color, indicating successful de-protection and availability of free primary amine, which reacted with ninhydrin tested compounds. [129]. Table (S1) in Appendix D below also shows the calculated data for de-blocking of amine, with detection of the appeared color, as follows:[129, 130]

3.3.1 Application of chitosan-ACC to enhance the growth of fluorescence pseudomonas bacterial strain

Chitosan and 1- amino cyclopropane-1- carboxylic acid were noticed for their potential to enhance plant growth-promoting rhizobacteria (PGPR), mainly the fluorescence pseudomonas, as presented in vivo research work.

Figure S.1 in Appendix D shows that each petri plate contains the tested materials as Chitosan, ACC, and Chitosan-ACC. It is noticed that both chitosan and ACC trials have promoted the growth of the PGPR strains, and the available colonies were counted. In contrast, the combination of these two compounds has promoted these bacterial growths to reach an uncountable number in the tested plate, indicating the dual functionality of both compounds in enhancing these beneficial bacterial strains as these PGPR strains can colonize the rhizosphere and promote plant growth through various mechanisms, as well, the chitosan enhances the stability of ACC compound within its matrix with less solubility effect and more surface appearance.

In this vivo study, the effect of chitosan-ACC on the inoculation and growth of fluorescence pseudomonas bacterial strain, shedding light on its role in stimulating their growth and activity and indirectly enhancing plant growth under biotic and abiotic conditions. This compound significantly increases colony-forming units (CFUs) and, in return, will be able to enhance the production of growth-promoting substances such as indole-3- acetic acid (IAA), siderophores, and volatile organic compound organic compounds (VOCs), which are known to influence plant growth positively.[127]

These findings highlight the potential of the chitosan-ACC compound in enhancing the growth and activity of PGPR bacteria as beneficial bacterial strains. The ability of chitosan-ACC to stimulate the production of plant growth-promoting substances and regulated ethylene levels provides valuable insights into its role in promoting plant-microbe interactions. Further research studies are warranted to explore the in vivo effects of these compounds on plant growth and their potential agriculture application as biofertilizers and biocontrol agents in agriculture systems.

3.3.2 Agronomic Parameters

Amino acids are crucial in stimulating plant growth and production, influencing various agronomic and physiological parameters. As shown in Table (8), the effect of tested traits on the following agronomic parameters: (A) shoot length (cm) after 15 days (B) shoot length (cm) after 30 days (C) Measurements of root length (cm) after 30 days (D) diameter (E) the number of internodes

Table 8

Effect of amino acids treatments on the root and shoot length system for (A) shoot length (cm) after 15 days, (B) shoot length (cm) after 30 days, (C) Measurements of root length (cm) after 30 days (D) diameter (E) number of internodes

#	Treatments	(A) Measurements of stem length (cm) after 15 days \pm SD.	(B) Measurements of stem length (cm) after 30 days \pm SD.	(C) Measurements of root length (cm) after 30 days \pm SD.	(D) Diameter (mm) after 30 days \pm SD.	(E) Number of internodes \pm SD
1	Control	7 \pm 0.034	13 \pm 0.053	9 \pm 0.034	5 \pm 0.033	5 \pm 0.013
2	Chitosan	10 \pm 0.011	20 \pm 0.046	15 \pm 0.066	6.4 \pm 0.019	7 \pm 0.044
3	L-Valine	9 \pm 0.078	11 \pm 0.089	13 \pm 0.021	9.2 \pm 0.028	6 \pm 0.052
4	L- Tryptophan	11 \pm 0.039	16 \pm 0.103	22 \pm 0.067	6.6 \pm 0.052	7 \pm 0.091
5	L-Lysine	14 \pm 0.027	25 \pm 0.033	16 \pm 0.014	5.2 \pm 0.088	7 \pm 0.014
6	Val.Ch	13 \pm 0.019	24 \pm 0.075	22 \pm 0.103	10.2 \pm 0.014	11 \pm 0.032
7	Tryp. Ch.	19 \pm 0.022	33 \pm 0.019	30 \pm 0.086	8.7 \pm 0.091	9 \pm 0.063
8	Val. Ch. Lys.	21 \pm 0.031	36 \pm 0.090	29 \pm 0.071	17 \pm 0.041	14 \pm 0.018
9	Tryp. Ch. Lys.	40 \pm 0.104	59 \pm 0.20	36 \pm 0.013	14.5 \pm 0.025	10 \pm 0.021

Apparently, The dual functionality of chitosan with two amino acids enhances plant agronomic and physiological parameters. The plant trail treated with (Tryp.Ch.Lys.) compound has a significant plant agronomic development over other treated trails. Both combined amino acid material contributes to its role in a synergistic effect in this biostimulation process. As a result, these naturally based agrochemical products can perhaps alleviate the usage of conventional agrochemical products and thus reduce different environmental issues. The effectiveness of these amino acid functionalized chitosan traits were arranged regarding their efficiency and performance as: (Tryp.Ch.Lys.), (Val. Ch. Lys), (Tryp.Ch.), (Val.Ch.), Chitosan and control traits.

Undoubtedly, The chitosan polymer matrix offers various advantages for this functionalization approach: Firstly, promoting plant growth with its nontoxic, biodegradability, and biocompatibility properties. Secondly, chitosan is an excellent carrier and reservoir for most compounds, increasing their efficiency with a prolonged release effect. Thirdly, chitosan offers a large surface area, which means abilities for diverse functional groups. Fourth, chitosan with its different hydrophilic group, the chitosan polymer structure increases the absorbance of functionalized amino acids to plants and nutrient uptake, thus promoting their performance for specific agricultural purposes.

Specifically, As shown in Table (8), the significant agronomic parameters of (Try. Ch. Lys.) compound can be ascribed to the synergistic effect of both L-lysine and L-tryptophane amino acid. Apparently, L- lysine works in promoting stem growth, and L-tryptophan enhances root growth, as illustrated with the measurement of each amino acid separately, where the L- lysine trait shows the highest stem elongation measurement amongst each non-functionalized amino acid trait as (25 mm) after 30 days. Meanwhile, the L-tryptophan trait shows the highest root elongation with a measurement of (22mm). However, L- the valine trait shows the lowest value in stem and root elongation, but its effect was observed for leaves diameter and number of internodes measurements to be as (10.2mm) and (11), respectively, which will be discussed in the physiological part.

L-lysine compounds significantly improved agronomic parameters related to stem elongation, as shown in Table (8) for these traits containing L-lysine amino acid in their formulations. Furthermore, L-lysine functionalized with chitosan-treated plants improved stem development more than other free L-lysine amino acids, meaning that chitosan enhances the role and stabilization of L-lysine amino acids and its prolonged effect during plant growth. [131]

L-lysine, an essential amino acid, has been identified as a critical regulator in promoting stem elongation in plants. Its role in plant growth and development can be attributed to several mechanisms: L-lysine amino acid is a precursor for synthesizing the most crucial growth-promoting plant hormones, such as gibberellins. These gibberellin hormones play a vital role in enhancing cell elongation by stimulating the synthesis of cell wall-degrading enzymes and increasing cell wall extensibility.[132, 133]. Second, L-lysine is vital in plants' nitrogen metabolism, mainly synthesizing nitrogenous compounds, including nucleotides, chlorophyll, and other amino acids. The nitrogenous compounds directly affect the stem elongation of plants. Therefore, L-lysine compounds contribute to efficiently utilizing these nitrogen compounds, promoting plant growth and stem elongation. Thirdly, with its amino acid structure, L-lysine serves in plant growth protein synthesis as a building block for regulating cell division and elongation processes. These proteins contribute to the organization of cell division and cell cytoskeleton. Thus, providing plants with L-lysine amino acids will effectively promote the synthesis of essential hormones and proteins for promoting stem elongation.[133]

On the other hand, L-tryptophan functionalized chitosan traits show significant agronomic parameters when compared with L- tryptophan free amino acid trait, mainly for root elongation measurements, which means chitosan was able to enhance the role of l- tryptophan in plant growth for a prolonged effect.[134] Thus, L-tryptophan amino acid can enhance plant growth and development due to its involvement in various physiological processes. However, it can have a significant impact on increasing the shoot length and elongation, as reported in Table (8) for all separated tested treatment trials, which mainly was visualized for both (Tryp. Ch.) and (Tryp.Ch. Lys.) traits, can serve as a precursor for auxin (IAA) biosynthesis in plants and as essential for beneficial plant microbes interaction in the root rhizosphere, which are primary determinates of plant health and soil fertility. The rhizosphere represents a highly

dynamic interaction between plant roots and beneficial soil microorganisms; in the rhizosphere, molecular communication between microorganisms and their plant has pronounced positive effects on plant growth and health. Thus, shoot elongation by L-tryptophan amino acid can achieve this approach. [134, 135]

Table (8) also shows the leaves' diameter and number of internodes for (Val.Ch.Lys.). The leaf diameter for (Val.Ch.Lys.) was (17mm), which is relatively higher in value than (Try.Ch.Lys.) as (14.5mm). These results mean that L-valine amino acid aligned with other incorporated amino and chitosan in affecting the internal plant genotypes responsible for cell elongation and chlorophyll production in leaves; thereby, more photosynthesis fluorescence activity occurred.[136] Also, it was higher in value than the (Val.Ch.) trait, which assures the influential incorporation role of all combined materials even though the internode measurement of (Val.Ch.Lys.) trait was (14) higher than (Try.Ch.Lys.) with a (10). As apparent, L-valine amino acid increases the internode numbers in contrast to L-tryptophan, which decreases the internode numbers; also, the internode number of the (Val.Ch.Lys.) trait is still higher in value than the (Val.Ch.) trait, which is related to the dual effect of all combined materials.

Table (9) shows the effect of amino acids treatments on another agronomic parameter as plant biomass, which is classified as (A) plant wet mass (g), (B) plant dry mass (g), and (C) moisture content for Barely Plant trails after 30 days.

Table 9

Effect of amino acids treatments on the growth system for (A) wet mass (g), (B) dry mass (g), (C) moisture content for Barely Plant trails after 30 days

#	Treatments	(A) Measurements of root + shoot wet mass (g) after 30 days \pm SD.	(B) Measurements of root + shoot dry mass (g) after 30 days \pm SD.	(C) Moisture Content (%)
1	Control	72.7 \pm 0.032	63.8 \pm 0.046	12.24
2	Chitosan	89.7 \pm 0.150	62.5 \pm 0.066	30.32
3	L-Lysine	120.5 \pm 0.065	85.4 \pm 0.110	29.12
4	L- Valine	105.6 \pm 0.934	78.9 \pm 0.046	25.28
5	L-Tryptophan	92.4 \pm 0.210	73.3 \pm 0.053	20.67
6	Val.Ch.	172.2 \pm 0.196	102.4 \pm 0.033	42.21
7	Tryp.Ch.	165.8 \pm 0.0636	98.8 \pm 0.096	40.41
8	Val.Ch.Lys.	269.5 \pm 0.0470	120.3 \pm 0.0107	55.37
9	Tryp. Chi.Lys.	255.3 \pm 0.126	123.7 \pm 0.201	51.79

$$\text{Moisture Content (\%)} \text{ Formula} = \frac{\text{Wet weight} - \text{Dry weight}}{\text{wet weight}} \times 100 \% \quad (12)$$

Table (9) shows the effect of amino acids treatments on another agronomic parameter as plant biomass, which is classified as (A) plant wet mass (g), (B) plant dry mass (g), and (C) calculated moisture content for Barely plant trails after 30 days, based on Equation (12). As noticed (Val. Ch. Lys.), the trait shows the highest moisture content compared to other traits. The dual functionalities of amino acids can explain this effect in enhancing plant biomass and moisture content. Mainly, L-valine traits show significant moisture content value compared to other amino acid traits, which can be revealed the role of L-valine amino acid in significantly increased fresh weight compared to dry weight and moisture content. These results mean valine compound treatments have no significant effect on plant leaf morphology. This differential effect probably occurs because the aerial part continues to grow, while the roots have already ceased growing due to the immediate treatments with L- valine amino acid and L- lysine in promoting the moisture content, which means it is an excellent potential for water shortage solution. [137]

The results clearly show that barley plants can be influenced by adding amino acids and taking up all amino acids; they also indicate that root amino acid uptake occurs as recorded. L-valine works in fruit development at the early stages.

3.3.3 Physiological Parameters

Photocatalytic activity of plants is one of the tested physiological parameters that revealed the chlorophyll fluorescence performance, which allows the visualization and study indirectly of different genetic functional levels such as primary light reactions, pigment performance level, dark enzymatic stroma reaction, and thylakoid electron transport reaction. Therefore, the photosynthetic fluorescence parameter analysis is considered necessary for evaluating and detecting plant mortality performance in response to tested traits.

Table 10

Photocatalytic activity measurement for treated trials

#	Trails Treatment	PAM F_v/F_m
1	Control	0.601
2	Chitosan	0.681
3	L-Valine	0.708
4	L-Tryptophan	0.675
5	L-Lysine	0.690
6	Tryp.Ch.	0.739
7	Val.Ch.	0.780
8	Tryp.Ch.Lys.	0.779
9	Val. Ch.Lys.	0.849

The measurements are usually presented as the primary photochemistry yield of the second photosynthetic reaction center (PSII), referred to as (F_v/F_m). The typical primary photochemistry yield of PSII (F_v/F_m) measurement fell into (0.5 to 0.7), indicating the typical performance of plants' photosynthesis process. If it increases within the range of (0.7 – 0.9), it indicates that plants usually undergo high photosynthetic performance and plant mortality activity. This study's results for all randomly selected plant traits ranged between typical photosynthesis and high fluorescence activity values.

Generally, As shown in Table (10), all trait plants treated with amino acid compounds show higher photosynthetic fluorescence values than the control plant trail. The highest increment of (F_v/F_m) was most apparent for the (Val. Ch. Lys) compound as the highest in value (0.849) compared to other plants' traits. It was noticeable that the photosynthetic fluorescence value of (Val. Ch.) was (0.780), slightly higher than (0.739) of (Tryp. Ch.) compounds, and for free amino acids, L-valine amino acids show the highest value compared to other tested amino acids. Thus, L--valine amino acid and its compounds contribute to the plant's photosynthetic activity, where it seems to enhance the photosynthetically active radiation in plans, which is absorbed by chlorophyll- protein and accessory pigments of chlorophyll- proteins compound complexes, and it migrates to the photosynthetic reaction centers, so the conversion of the quantum photosynthetic process.

Besides that, it was also noticed as another plant photocatalytic activity of the (Val. Ch. Lys) and (Val. Ch.) compounds was associated with their effect on early grain production; meanwhile, other traits of their extinguished contributions were associated with plant agronomic parameters as illustrated in above sections. Therefore, this study research shows that the L-valine compound primarily contributes to plant physiological parameters as a plant genotype chlorophyll promotor more than promoting plant agronomic indicators. These results are in good agreement with the results of the study by Li, Suhong, et al. on the mechanism of concentration-mediated inhibition of peach tree shoot growth, 2020, where in this study, the results showed the role of valine amino acid with its inhibition effect to the peach seedling growth with a noticeable increase in the fruit growth stage.[138]

On the other hand, chitosan-treated trials show a slightly significant adaptation photosynthetic activity compared to the control trial, where chitosan polymer is also considered a tremendous polymer candidate for amino acid delivery, figured out in the study results. Chitosan polymer is a suitable carrier for amino acids, offering a large surface area and amino acid availability for crop production. Also, the chitosan polymer structure allows it to be functionalized with diverse amino acids within one resulting compound, thus enhancing their synergistic role as plant bio stimulants and nutrient uptake performance.[139] [140, 141]

Additionally, as amino acids are functionalized on chitosan matrix, their release will be controlled with a prolonged sustainable effect; thereby, such a preparation process can reduce the usage of agronomic amount, and their biodegradability occurs in a sustained life-long manner.[140, 141]

Amino acids can be affected by various environmental degradation issues; therefore, chitosan is an excellent candidate for carrying amino acid compounds acting as a reservoir and protecting from degradation mainly due to environmental factors such as evaporation, harsh pH's media, prolonged release, and biodegradability. Thus, this synthesis route and application can increase product shelf life and alleviate their degradation by promoting plant growth and development. [141]

Chapter Four

Discussions and Conclusions

Conclusion

Organic farming is an up-to-date such as natural organic fertilizers and pesticide compounds, nano fertilizer and nano pesticides systems, and bio-fertilizer systems. This viable recent agriculture system delivers fresh and natural farm products using modern scientific and technical progress for developing agricultural activities to alleviate environmental pollution. Several natural and synthetic polysaccharide polymers have recently gained remarkable attention in this research field. Some innovative methodologies are being searched to introduce new natural organic materials that functionalize polymer formulations as alternative compounds to conventional fertilizers and pesticides. Also, other methodologies concentrate on synthesized smart nano-based polymers as nanocarriers and nanosensors for innovative delivery and release of active nutrients and pesticides in a sustained, controlled process, aiming to improve crop production by reducing the various hazardous impacts of these substances.

This research focuses on the utilization of chitosan in the synthesis of innovative nano bio-fertilizer capsules, aiming to deliver active agro nutrients, namely Nitrogen, Phosphorous, and Potassium ions (NPK), along with beneficial plant growth-promoting rhizobacteria (PGPRs) microorganisms. These entrapped components are coated using innovative cross-linking of chitosan and alginate with humic acid through ionic gelation and polyelectrolyte complexation technique. The synthesized (Ch.Alg.HA.NPK.PGPRs) nanocapsules show resembled spherical shape nanocapsules with an interconnected porous network regular type arrangement with a particle size of (450.9 d.nm.), ζ -potential of (-33mV), and encapsulation efficiency (87%). The thermal stability of these nanocapsules shows a percentage mass residuals of more than 25% at 600 ° C, indicating these capsules' stability for an efficient time in soil. Besides, its water retention capability percentage was 44.2%. The release test behavior of entrapped materials shows a cumulative release percentage of N, P, and K ions to be 33.2%, 47.8%, and 68.3%, alternatively within 30 days. Also, the release mechanism using the kinetic module of the Korsmeyer- Peppas mathematical model shows a Fickin diffusion controlled release module governs the release of N and P ions with a

diffusional exponent = 0.5, and the non-Fickian diffusional module governs the release of K ion with a diffusional exponent = 0.7. The findings provide insights into implementing nano bio-fertilizers to efficiently deliver agro-nutrients, which can contribute to agricultural productivity and sustainability.

On the other hand, the functionalization of chitosan with photocatalyst materials has emerged as a promising approach to developing bio pesticides. This research focuses on the functionalization of chitosan with three different photocatalyst materials: ZnO, carbon nanodots (CNDs), and a hybrid of (CNDs/ZnO), and their potential role as active antimicrobial agents against a broad spectrum of bacterial and fungal strains under dark and sunlight condition. Functionalized chitosan photocatalyst materials' resulting morphological, structural, and optical properties were examined using FT-IR, AFM, XRD, RAMAN, and UV-Vis instruments. Chitosan-Hybrid photocatalyst composite was synthesized with a ζ - potential of -33 mV. The Hybrid composite synthesized of (ZnO-NPs) and (CNDs) The sol-gel method synthesized a Hybrid composite, and CNDs were obtained from solid olive waste by pyrolysis and chemical oxidation, and ZnO nanoparticles were prepared from the precipitation method. CNDs absorbed in the ZnO surface led to the formation of a hybrid nanocomposite with a ζ - potential to be -28 mV and a size of 105 nm. Also, the CNDs enhance the visible-light photocatalyst of ZnO, showing a decrease in the energy band gap from 3.1 to 2.8 eV, where CNDs play an intermediate energy level above the valence band of ZnO. After that, chitosan was combined with Hybrid nanocomposites by a simple co-precipitation method, forming Ch.Hybrid composite with a ζ - potential to be -33 mV and strong optical properties in the UV- Vis spectrum indicates the successful combination of those moieties. The Ch. Hybrid exhibits distinguishable antimicrobial activity with the presence of photo-light irradiation within minimal inhibitory concentrations (1.95-15.6) $\mu\text{g/L}$, and the inhibition growth percentage was 99.99%, an inhibition zone ranged from (49.6-55.1) mm, and the kill time kinetic was 25 min to 1:15 h. The glutathione oxidation test was also investigated to depict the antimicrobial activity mechanism, showing that the high efficiency of antimicrobial activity is direct to its ROS-forming ability in the presence of photo-light irradiation with a glutathione deficiency oxidation percentage of (96.8%). This research's findings demonstrate the synthesized hetero-photocatalyst composite's ability as a potential antimicrobial agent in agriculture applications.

Finally, the potential of functionalizing chitosan with amino acids as PGPRs and plant bio stimulant products was also determined. A PGPR precursor named 1- amino cyclopropane-1- carboxylic acid (ACC) was synthesized and functionalized with chitosan. The chitosan functionalized ACC was conducted through chemical reactions to achieve a modified chitosan with ACC compound on the (C₃-OH) positions. This compound was obtained by firstly blocking the amine groups in chitosan polymer with N- phthaloyl group as the amine protective group, subsequently followed by tosylation of the primary hydroxyl groups in chitosan to tosylate ester to increase its activity toward further substitution reactions with diverse functional groups. After that, the tosyl group was replaced with ACC compound, as indicated by specific reaction reagents and conditions. Then, a de-protection process was applied to the N-phthaloyl amine group using a hydrazine reagent with mild de-protection conditions to obtain the desired final chitosan ACC product without affecting the carboxyl groups of ACC groups. The effect of synthesized chitosan-ACC as PRPRs precursor was evaluated in vitro petri-plate method, indicating an efficient PGPRs (*P. fluorescence*) growth and thus enhancing soil fertility.

On the other hand, the functionalization of chitosan with other amino acids as a plant bio stimulant was achieved through a novel synthesis approach. Different amino acids(L- valine, L- Tryptophan, and L- Lysine) functionalized chitosan were synthesized using the following reaction sequences: new N-blocking method using (di-tert-butyl-di-carbonate) BOC component for the first time as blocking reagent for (C₂-NH₂) in chitosan polymer with efficient reaction conditions, then, subsequently followed with the tosylation of (C₆ - OH) of chitosan to p- toluene sulfonic acid esters (tosyl chitosan), then it was functionalized with amino acid through nucleophilic substitution pathway at the tosyl position. After that, chitosan was unblocked using a few millimeters of Tri-fluoro acetic acid at a particular efficient time, then another functionalization of amino acid at the (C₂-NH₂) position after de-blocking was carried out using the addition reaction. The resulting compounds were categorized as (Ch.Val., Ch.Tryp., Val.Ch.Lys. Tryp.Ch. Lys.). This potential pathway with two different amino acids functionalized chitosan was suitable for controlling reaction pathways and conditions with efficient attenuate results. The structural characteristics were also determined using FT-IR and NMR instruments. The plant agronomic and physiological

parameters associated with these materials were examined. It is found that (Try.Ch.Lys.) has significant agronomic parameters among all other synthesized traits related to stem and root elongation to be (59cm) and (36 cm) within 30 days, respectively.

Meanwhile, (Val.Ch. Lys.) improves the growth of leaves diameter by (17 mm) and increases the number of internodes to 19, which indicates its role as a regulator of chlorophyll synthesis; also, it shows to enhances the moisture content by 55.37%. Besides that, (Val.Ch. Lys.) promotes the physiological plant production with an (Fv/Fm) to be 0.809 more than the regular value of (Fv/Fm) = 0.7, which indicates significant adoption of photosynthetic activity. The findings provide insight into using these bio-stimulant products in agricultural applications.

In conclusion, utilizing nano bio-fertilizers, chitosan functionalized photo-catalysts, and chitosan-infused amino acids in modern agricultural practices represents a profound leap towards sustainable and resource-efficient farming. This tripartite approach, encompassing enhanced nutrient management, environmentally friendly pest control, and augmented plant growth, holds immense potential to address pressing agricultural challenges while fostering a balanced coexistence with nature. The synergy of these innovative solutions could potentially revolutionize agricultural paradigms while promoting environmental management.

List of Abbreviations

Abbreviation	Meaning
PGPRs	Plant Growth Promoting Rhizobacteria
NPK	Nitrogen- Phosphorous- Potassium
ACC	1-Amino Cyclopropane-1- Carboxylic acid
Auxin	Indoleacetic Acid
P. Fluorescence	Pseudomonas Fluorescence
IG	Inotropic Gelation
PEC	Polyelectrolyte Complexation
ROS	Reactive Oxygen Species
CNDs	Carbon Nano Dots
CQDs	Carbon Quantum Dots
IAA	Indole Acetic Acid
Ch.ZnO	Chitosan. ZnO
Ch. CNDs	Chitosan.CNDs
Ch. Hybrid	Chitosan. Hybrid
MIC	Minimum Inhibitory Concentration
CFU	Colonies Forming Unit Reduction
Ch. Alg. NPK.PGPRs	Chitosan. Alginate.NPK.PGPRs Nano capsules
Ch. Alg. HA. NPK.PGPRs	Chitosan. Alginate. Humic Acid. NPK. PGPRs
Val.Ch.	L- Valine. Chitosan
Tryp.Ch.	L-Tryptophan. Chitosan
Val. Ch.Lys.	L- Valine. Chitosan. L- lysine
Tryp.Ch.Lys.	L- Tryptophan.Chitosan. L-lysine
PAM	Pulse Amplitude Modulated

References

- Maluin, F.N. and M.Z. Hussein, *Chitosan-based agronanochemicals as a sustainable alternative in crop protection*. *Molecules*, 2020. 25(7): p. 1611.
- Law, Q.D., et al., *Greenhouse gas fluxes from turfgrass systems: Species, growth rate, clipping management, and environmental effects*. 2021, Wiley Online Library.
- Kumar, R., R. Kumar, and O. Prakash, *Chapter-5 the impact of chemical fertilizers on our environment and ecosystem*. Chief Ed, 2019. 35: p. 69.
- Wan, L.-J., et al., *Effects of chemical fertilizer combined with organic fertilizer application on soil properties, citrus growth physiology, and yield*. *Agriculture*, 2021. 11(12): p. 1207.
- Khan, H.A., et al., *A performance evaluation study of nano-biochar as a potential slow-release nano-fertilizer from wheat straw residue for sustainable agriculture*. *Chemosphere*, 2021. 285: p. 131382.
- El-Saadony, M.T., et al., *Vital roles of sustainable nano-fertilizers in improving plant quality and quantity-an updated review*. *Saudi journal of biological sciences*, 2021. 28(12): p. 7349-7359.
- Sharma, B., et al., *Nano-biofertilizers as bio-emerging strategies for sustainable agriculture development: Potentiality and their limitations*. *Science of The Total Environment*, 2023. 860: p. 160476.
- Kumar, Y., et al., *Nanofertilizers and their role in sustainable agriculture*. *Annals of Plant and Soil Research*, 2021. 23(3): p. 238-255.
- Chaudhary, A., *Nano-Fertilizers and Nano-pesticides: Benevolence for Sustainable Agriculture*. *Nanochemistry Research*, 2023. 8(2): p. 152-163.
- Jha, A., et al., *Panorama of biogenic nano-fertilizers: A road to sustainable agriculture*. *Environmental Research*, 2023: p. 116456.
- Goyal, S., R. Kumar, and V. Beniwal, *Biogenic Synthesis of Nanoparticles for Sustainable Crop Production: A Review*. 2022, Nanobioletters.

- Mujtaba, M., et al., *Chitosan-based delivery systems for plants: A brief overview of recent advances and future directions*. International journal of biological macromolecules, 2020. 154: p. 683-697.
- Shafiei-Masouleh, S.-S., *Use of magnetic nano-chitosan as bio-fertilizer to reduce production period in three cyclamen cultivars*. Journal of Soil Science and Plant Nutrition, 2022. 22(1): p. 281-293.
- Riseh, R.S., et al., *Chitosan as potential natural compound to manage plant diseases*. International Journal of Biological Macromolecules, 2022.
- Liu, S., et al., *Green and recyclable graphitic carbon nitride/chitosan/polyvinyl alcohol photocatalytic films with efficient antibacterial activity for fruit packaging*. International Journal of Biological Macromolecules, 2023. 236: p. 123974.
- Chadha, U., et al., *Advances in chitosan biopolymer composite materials: from bioengineering, wastewater treatment to agricultural applications*. Materials Research Express, 2022. 9(5): p. Article number: 052002.
- Santiago-Aliste, A., et al., *Multifunctional Nanocarriers Based on Chitosan Oligomers and Graphitic Carbon Nitride Assembly*. Materials, 2022. 15(24): p. 8981.
- Cohen, E. and E.J.C.A.E.J. Poverenov, *Hydrophilic Chitosan Derivatives: Synthesis and Applications*. 2022: p. e202202156.
- Cho, M., H. No, and W.J.J.o.f.s. Prinyawiwatkul, *Chitosan treatments affect growth and selected quality of sunflower sprouts*. 2008. 73(1): p. S70-S77.
- Hidangmayum, A., et al., *Application of chitosan on plant responses with special reference to abiotic stress*. 2019. 25(2): p. 313-326.
- Cohen, E. and E. Poverenov, *Hydrophilic Chitosan Derivatives: Synthesis and Applications*. Chemistry—A European Journal, 2022. 28(67): p. e202202156.
- Singh, A., et al., *Enhancing plant growth promoting rhizobacterial activities through consortium exposure: A review*. Frontiers in Bioengineering and Biotechnology, 2023. 11: p. 1099999.
- Jakhar, A.M., et al., *Nano-fertilizers: A sustainable technology for improving crop nutrition and food security*. NanoImpact, 2022: p. 100411.

- Kour, H., et al., *Nanotechnologies for microbial inoculants as biofertilizers in the horticulture*, in *Sustainable Horticulture*. 2022, Elsevier. p. 201-261.
- Gangwar, J., et al., *Nano-technological interventions in crop production—a review*. *Physiology and Molecular Biology of Plants*, 2023: p. 1-15.
- Singh, G. and B. Singh, *Nanotechnology in Agriculture*.
- Ayoub, H.A., et al., *New Avenue for Sustainable Agriculture: A Short*. *Journal of Chemical Reviews*, 2022. 4(2).
- Zhao, M., et al., *pH/redox dual responsive from natural polymer-based nanoparticles for on-demand delivery of pesticides*. *Chemical Engineering Journal*, 2022. 435: p. 134861.
- Sobel, R., C.-P. Su, and T. Xu, *Novel concepts and challenges of flavor microencapsulation*. *Microencapsulation in the Food Industry*, 2023: p. 427-450.
- Risch, S.J. and G. Reineccius. *Encapsulation and controlled release of food ingredients*. in *ACS symposium series (USA)*. 1995. American Chemical Society.
- Mourya, V. and N.N. Inamdar, *Chitosan-modifications and applications: Opportunities galore*. *Reactive and Functional polymers*, 2008. 68(6): p. 1013-1051.
- Huang, Y., et al., *Recent advances in chitosan-based nano particulate pulmonary drug delivery*. *Carbohydr. Polym*, 2016. 138: p. 114-122.
- Agnihotri, S.A., N.N. Mallikarjuna, and T.M. Aminabhavi, *Recent advances on chitosan-based micro-and nanoparticles in drug delivery*. *Journal of controlled release*, 2004. 100(1): p. 5-28.
- Azmana, M., et al., *A review on chitosan and chitosan-based bionanocomposites: Promising material for combatting global issues and its applications*. *International journal of biological macromolecules*, 2021. 185: p. 832-848.
- Yang, J.-S., Y.-J. Xie, and W. He, *Research progress on chemical modification of alginate: A review*. *Carbohydrate polymers*, 2011. 84(1): p. 33-39.
- Steelink, C., *What is humic acid?* 1963, ACS Publications.

- Ekin, Z., *Integrated use of humic acid and plant growth promoting rhizobacteria to ensure higher potato productivity in sustainable agriculture*. Sustainability, 2019. 11(12): p. 3417.
- Mehmood, U., et al., *A brief review on plant growth promoting rhizobacteria (PGPR): a key role in plant growth promotion*. Plant protection, 2018. 2(2): p. 77-82.
- Vejan, P., et al., *Encapsulation of plant growth promoting Rhizobacteria—prospects and potential in agricultural sector: a review*. Journal of Plant Nutrition, 2019. 42(19): p. 2600-2623.
- Saberi Riseh, R., et al., *Salinity stress: Toward sustainable plant strategies and using plant growth-promoting rhizobacteria encapsulation for reducing it*. Sustainability, 2021. 13(22): p. 12758.
- Patil, P., D. Chavanke, and M. Wagh, *A review on ionotropic gelation method: novel approach for controlled gastroretentive gelspheres*. Int J Pharm Pharm Sci, 2012. 4(4): p. 27-32.
- Patel, M.A., et al., *The effect of ionotropic gelation residence time on alginate cross-linking and properties*. Carbohydrate polymers, 2017. 155: p. 362-371.
- Simsek-Ege, F.A., G.M. Bond, and J. Stringer, *Polyelectrolyte complex formation between alginate and chitosan as a function of pH*. Journal of Applied Polymer Science, 2003. 88(2): p. 346-351.
- Paques, J.P., et al., *Preparation methods of alginate nanoparticles*. Advances in colloid and interface science, 2014. 209: p. 163-171.
- Ford, J., J. Woolfe, and A. Florence, *Nanospheres of cyclosporin A: poor oral absorption in dogs*. International journal of pharmaceutics, 1999. 183(1): p. 3-6.
- Li, P., et al., *Chitosan-alginate nanoparticles as a novel drug delivery system for nifedipine*. International journal of biomedical science: IJBS, 2008. 4(3): p. 221.
- Ahmed, S., M. Ahmad, and S. Ikram, *Chitosan: a natural antimicrobial agent-a review*. Journal of Applicable Chemistry, 2014. 3(2): p. 493-503.
- Muraleedaran, K. and V.A. Mujeeb, *Applications of chitosan powder with in situ synthesized nano ZnO particles as an antimicrobial agent*. International journal of biological macromolecules, 2015. 77: p. 266-272.

- Mohd Yusof, H., et al., *Microbial synthesis of zinc oxide nanoparticles and their potential application as an antimicrobial agent and a feed supplement in animal industry: a review*. Journal of animal science and biotechnology, 2019. 10: p. 1-22.
- Fatoni, A., et al., *Synthesis and characterization Chitosan-ZnO nanoparticle and its application as antibacterial Agent of Staphylococcus aureus ATCC 25923*. Science and Technology Indonesia, 2020. 5(1): p. 1-5.
- Li, H., et al., *Carbon nanodots: synthesis, properties and applications*. Journal of materials chemistry, 2012. 22(46): p. 24230-24253.
- Dhamodharan, D., et al., *Carbon nanodots: synthesis, mechanisms for bio-electrical applications*. Journal of Industrial and Engineering Chemistry, 2022. 110: p. 68-83.
- Hamed, R., et al., *Visible light-driven ZnO nanoparticles/carbon nanodots hybrid for broad-spectrum antimicrobial activity*. Surfaces and Interfaces, 2023. 38: p. 102760.
- Xu, Y., et al., *A magnetic/fluorometric bimodal sensor based on a carbon dots–MnO₂ platform for glutathione detection*. Nanoscale, 2016. 8(27): p. 13414-13421.
- Wang, X., et al., *Highly selective and sensitive electrochemical sensor for L-cysteine detection based on graphene oxide/multiwalled carbon nanotube/manganese dioxide/gold nanoparticles composite*. Journal of Electroanalytical Chemistry, 2015. 757: p. 100-106.
- Jha, C.K., et al., *Microbial enzyme, 1-aminocyclopropane-1-carboxylic acid (ACC) deaminase: an elixir for plant under stress*. Physiological and Molecular Plant Pathology, 2021. 115: p. 101664.
- Liao, X., et al., *A 1-aminocyclopropane-1-carboxylate deaminase MrACCD from Metarhizium robertsii is associated with plant growth promotion for Metarhizium spp*. Journal of Invertebrate Pathology, 2023. 198: p. 107928.
- Yuan, Y., et al., *Isolation and Screening of 1-aminocyclopropane-1-carboxylic acid (ACC) deaminase producing PGPR from Paeonia lactiflora rhizosphere and enhancement of plant growth*. Scientia Horticulturae, 2022. 297: p. 110956.

- Xiao, Y., et al., *Amino acid permease RcAAP1 increases the uptake and phloem translocation of an L-valine-phenazine-1-carboxylic acid conjugate*. *Frontiers in Plant Science*, 2023. 14: p. 1191250.
- HOMMA, Y., T. SHIDA, and T. MISATO, *Studies on the control of plant diseases by amino acid derivatives (1) Effect of N-lauroyl-L-valine on rice blast*. *Japanese Journal of Phytopathology*, 1973. 39(2): p. 90-98.
- Kurnianingsih, N., et al. *Variability of amino acids profiles in Indonesian rice varieties. in AIP Conference Proceedings*. 2023. AIP Publishing.
- Salsabilla, A., L.A. Yusfi, and J. Jamsari. *Determination of the optimum duration for IAA [Indole-3-Acetic Acid] production in Serratia plymuthica UBCF_13. in AIP Conference Proceedings*. 2023. AIP Publishing.
- Huang, W., et al., *Identification of the lysine and histidine transporter family in Camellia sinensis and the characterizations in nitrogen utilization*. *Horticultural Plant Journal*, 2023.
- Dhiman, A., A.K. Sharma, and G. Agrawal, *Polymer based engineered materials for sustainable agriculture*. *ACS Agricultural Science & Technology*, 2022. 2(4): p. 693-711.
- Mesias, V.S.D., et al., *Coated NPK fertilizer based on citric acid-crosslinked chitosan/alginate encapsulant*. *Journal of Ecological Engineering*, 2019. 20(11): p. 1-12.
- Ali, M., et al., *Application of polysaccharides for the encapsulation of beneficial microorganisms for agricultural purposes: A review*. *International Journal of Biological Macromolecules*, 2023: p. 125366.
- D. Gao, P.Z., B. Lyu, Y. Li, Y. Hou, J. Ma, , *Carbon quantum dots decorated on ZnO nanoparticles: An efficient visible-light responsive antibacterial agents*. *Applied Organometallic Chemistry* 2020. 34(8).
- Jing, H.H., et al., *Green carbon dots: Synthesis, characterization, properties and biomedical applications*. *Journal of Functional Biomaterials*, 2023. 14(1): p. 27.

- Khan, A., et al., *Synthesis and antibacterial activity of nanoenhanced conjugate of Ag-doped ZnO nanorods with graphene oxide*. Spectrochimica Acta Part A: Molecular and Biomolecular Spectroscopy, 2023. 290: p. 122296.
- Younis, A.B., et al., *Titanium dioxide nanoparticles: Recent progress in antimicrobial applications*. Wiley Interdisciplinary Reviews: Nanomedicine and Nanobiotechnology, 2023. 15(3): p. e1860.
- Dediu, V., et al., *Trends in Photothermal Nanostructures for Antimicrobial Applications*. International Journal of Molecular Sciences, 2023. 24(11): p. 9375.
- Alharbi, R.A., et al., *Design, synthesis, and characterization of novel bis-uracil chitosan hydrogels modified with zinc oxide nanoparticles for boosting their antimicrobial activity*. Polymers, 2023. 15(4): p. 980.
- Yu, M., et al., *Antibacterial and antibiofilm mechanisms of carbon dots: a review*. Journal of Materials Chemistry B, 2023.
- Hedayati Tabari, F., et al., *Synthesis and Characterization of Chitosan/Poly (Vinyl Alcohol) Polymer Nanofibers Containing Chicory Extract by Electrospun Method and Evaluation of Its Antibacterial Properties*. Journal of Advanced Materials and Technologies, 2023. 11(4): p. 31-44.
- Liu, C. and H. Baumann, *Exclusive and complete introduction of amino groups and their N-sulfo and N-carboxymethyl groups into the 6-position of cellulose without the use of protecting groups*. Carbohydrate research, 2002. 337(14): p. 1297-1307.
- Matsui, Y., et al., *Facile synthesis of 6-amino-6-deoxycellulose*. Carbohydrate research, 2005. 340(7): p. 1403-1406.
- Oh, S.-H., *Stimulation of γ -aminobutyric acid synthesis activity in brown rice by a chitosan/glutamic acid germination solution and calcium/calmodulin*. BMB Reports, 2003. 36(3): p. 319-325.
- Sun, M., et al., *Effects of Valine and Urea on Carbon and Nitrogen Accumulation and Lignin Content in Peach Trees*. Plants, 2023. 12(8): p. 1596.

- Rafiee, H., et al., *Application of plant biostimulants as new approach to improve the biological responses of medicinal plants-A critical review*. Journal of Medicinal Plants, 2016. 15(59): p. 6-39.
- Cho, M., H. No, and W. Prinyawiwatkul, *Chitosan treatments affect growth and selected quality of sunflower sprouts*. Journal of food science, 2008. 73(1): p. S70-S77.
- Saito, B. and M.M. Seckler, *Alkaline extraction of humic substances from peat applied to organic-mineral fertilizer production*. Brazilian Journal of Chemical Engineering, 2014. 31: p. 675-682.
- Bashan, Y. and L.E. González, *Long-term survival of the plant-growth-promoting bacteria Azospirillum brasilense and Pseudomonas fluorescens in dry alginate inoculant*. Applied Microbiology and Biotechnology, 1999. 51: p. 262-266.
- Bettini, S., et al., *SiO₂-Coated ZnO Nanoflakes Decorated with Ag Nanoparticles for Photocatalytic Water Oxidation*. Chemistry—A European Journal, 2019. 25(62): p. 14123-14132.
- Sawalha, S., et al., *Optical properties and photoactivity of carbon nanodots synthesized from olive solid wastes at different carbonization temperatures*. RSC advances, 2022. 12(8): p. 4490-4500.
- Chen, P., et al., *Facile in-situ fabrication of ZnO₂/CQD composites with promoted visible-light photocatalytic activities for organic degradation and bacterial inactivation*. Applied Surface Science, 2022. 604: p. 154629.
- Sawalha, S., et al., *Broad-spectrum antibacterial activity of synthesized carbon nanodots from d-glucose*. ACS Applied Bio Materials, 2022. 5(10): p. 4860-4872.
- Zainin, N., et al., *Antibacterial activity of Boesenbergia rotunda (L.) Mansf. A. extract against Escherichia coli*. International Food Research Journal, 2013. 20(6): p. 3319.
- Zhu, X. and P. Gan, *A Novel Synthesis of 1-Aminocyclopropane-1-Carboxylic Acid (ACC)*. Synthetic communications, 1998. 28(17): p. 3159-3162.

- Kurita, K., et al., *N-phthaloylated chitosan as an essential precursor for controlled chemical modifications of chitosan: Synthesis and evaluation*. Polymer Journal, 2007. 39(9): p. 945-952.
- Li, S., et al., *Application of chitosan/alginate nanoparticle in oral drug delivery systems: Prospects and challenges*. Drug Delivery, 2022. 29(1): p. 1142-1149.
- Ha, N.M.C., et al., *Preparation of NPK nanofertilizer based on chitosan nanoparticles and its effect on biophysical characteristics and growth of coffee in green house*. Research on Chemical Intermediates, 2019. 45: p. 51-63.
- Zohri, M., et al., *Characterization of chitosan/alginate self-assembled nanoparticles as a protein carrier*. Journal of dispersion science and technology, 2011. 32(4): p. 576-582.
- Xing, J., L. Deng, and A. Dong, *Chitosan/alginate nanoparticles stabilized by poloxamer for the controlled release of 5-fluorouracil*. Journal of Applied Polymer Science, 2010. 117(4): p. 2354-2359.
- Trenkel, M.E. *Controlled-release and stabilized fertilizers in agriculture: improving fertilizer use efficiency*. 1997. IFA.
- Ganbold, S., *Pokročilé obaly pro potravinářské a farmaceutické aplikace na bázi vodorozpustného polymeru*. 2010.
- Ritger, P.L. and N.A. Peppas, *A simple equation for description of solute release I. Fickian and non-fickian release from non-swellable devices in the form of slabs, spheres, cylinders or discs*. Journal of controlled release, 1987. 5(1): p. 23-36.
- Shariff, A., et al., *Entrapment of andrographolide in cross-linked alginate pellets: I. Formulation and evaluation of associated release kinetics*. Pakistan Journal of Pharmaceutical Sciences, 2007. 20(1): p. 1-9.
- Huang, X., et al., *Single crystalline wurtzite ZnO/zinc blende ZnS coaxial heterojunctions and hollow zinc blende ZnS nanotubes: synthesis, structural characterization and optical properties*. Nanoscale, 2014. 6(15): p. 8787-8795.
- Kavitha, T., et al., *Glucose sensing, photocatalytic and antibacterial properties of graphene–ZnO nanoparticle hybrids*. Carbon, 2012. 50(8): p. 2994-3000.

- Liu, K.-K., et al., *Carbon-ZnO alternating quantum dot chains: electrostatic adsorption assembly and white light-emitting device application*. *Nanoscale*, 2018. 10(15): p. 7155-7162.
- Zhang, Q., L. Gao, and J. Guo, *Effects of calcination on the photocatalytic properties of nanosized TiO₂ powders prepared by TiCl₄ hydrolysis*. *Applied Catalysis B: Environmental*, 2000. 26(3): p. 207-215.
- Song, S., et al., *Multi-shelled ZnO decorated with nitrogen and phosphorus co-doped carbon quantum dots: synthesis and enhanced photodegradation activity of methylene blue in aqueous solutions*. *RSC advances*, 2019. 9(13): p. 7362-7374.
- Toma, E., et al., *ZnO/CQDs Nanocomposites for Visible Light Photodegradation of Organic Pollutants*. *Catalysts* 2022, 12, 952. *Contemporary Solutions for Advanced Catalytic Materials with a High Impact on Society*, 2022: p. 61.
- Pandiyarajan, T. and B. Karthikeyan, *Cr doping induced structural, phonon and excitonic properties of ZnO nanoparticles*. *Journal of Nanoparticle Research*, 2012. 14: p. 1-9.
- Safardoust-Hojaghan, H., et al., *Green synthesis, characterization and antimicrobial activity of carbon quantum dots-decorated ZnO nanoparticles*. *Ceramics International*, 2021. 47(4): p. 5187-5197.
- Sawalha, S., et al., *Tailoring the sensing abilities of carbon nanodots obtained from olive solid wastes*. *Carbon*, 2020. 167: p. 696-708.
- Molaei, M.J., *Carbon quantum dots and their biomedical and therapeutic applications: a review*. *RSC advances*, 2019. 9(12): p. 6460-6481.
- Kim, K.W., et al., *Antimicrobial Effect of Carbon Nanodots–ZnO Nanocomposite Synthesized Using Sargassum horneri*. *Journal of Marine Science and Engineering*, 2022. 10(10): p. 1546.
- Kavitha, T. and S. Kumar, *Multifunctionalities enabled by the synergistic effects of mesoporous carbon dots and ZnO nanorods*. *Materials Research Express*, 2021. 8(11): p. 115504.
- Koralewski, M., K.H. Bodek, and K. Marczewska, *Optical properties of chitosan in aqueous solution*. *Polish Chitin Society, Monograph XI*, 2006: p. 29-39.

- Anandhavelu, S. and S. Thambidurai, *Effect of annealing temperature on optical and electrochemical properties of chitosan–ZnO nanostructure*. Ionics, 2013. 19: p. 903-909.
- Mohammadi, S., et al., *Carbon dots hybrid for dual fluorescent detection of microRNA-21 integrated bioimaging of MCF-7 using a microfluidic platform*. Journal of nanobiotechnology, 2022. 20(1): p. 1-15.
- Raveendran, V., A.R.S. Babu, and N.K. Renuka, *Mint leaf derived carbon dots for dual analyte detection of Fe (iii) and ascorbic acid*. RSC advances, 2019. 9(21): p. 12070-12077.
- Hasan, M.R., et al., *Formation of carbon quantum dots via hydrothermal carbonization: Investigate the effect of precursors*. Energies, 2021. 14(4): p. 986.
- Mathew, S.A., et al., *Luminescent chitosan/carbon dots as an effective nano-drug carrier for neurodegenerative diseases*. RSC advances, 2020. 10(41): p. 24386-24396.
- Efa, M.T. and T. Imae, *Hybridization of carbon-dots with ZnO nanoparticles of different sizes*. Journal of the Taiwan Institute of Chemical Engineers, 2018. 92: p. 112-117.
- Makula, P., M. Pacia, and W. Macyk, *How to correctly determine the band gap energy of modified semiconductor photocatalysts based on UV–Vis spectra*. 2018, ACS Publications. p. 6814-6817.
- Chang, Q.-Q., et al., *C-doped ZnO decorated with Au nanoparticles constructed from the metal–organic framework ZIF-8 for photodegradation of organic dyes*. RSC advances, 2019. 9(22): p. 12689-12695.
- Je, J.-Y. and S.-K. Kim, *Reactive oxygen species scavenging activity of aminoderivatized chitosan with different degree of deacetylation*. Bioorganic & medicinal chemistry, 2006. 14(17): p. 5989-5994.
- He, W., et al., *Production of reactive oxygen species and electrons from photoexcited ZnO and ZnS nanoparticles: a comparative study for unraveling their distinct photocatalytic activities*. The Journal of Physical Chemistry C, 2016. 120(6): p. 3187-3195.

- Folawewo, A.D. and M.D. Bala, *Nanocomposite Zinc oxide-based photocatalysts: recent developments in Their use for the treatment of dye-polluted wastewater*. Water, 2022. 14(23): p. 3899.
- Guo, Y., et al., *Photocatalytic activity enhanced via surface hybridization*. Carbon Energy, 2020. 2(3): p. 308-349.
- Ming, H., et al., *Large scale electrochemical synthesis of high quality carbon nanodots and their photocatalytic property*. Dalton transactions, 2012. 41(31): p. 9526-9531.
- Wang, W., C. Xue, and X. Mao, *Chitosan: Structural modification, biological activity and application*. International Journal of Biological Macromolecules, 2020. 164: p. 4532-4546.
- Madera-Santana, T.J., C.H. Herrera-Méndez, and J.R. Rodríguez-Núñez, *An overview of the chemical modifications of chitosan and their advantages*. Green Materials, 2018. 6(4): p. 131-142.
- Bell, E.A., *Nonprotein amino acids of plants: significance in medicine, nutrition, and agriculture*. Journal of agricultural and food chemistry, 2003. 51(10): p. 2854-2865.
- Coleman, M.G. and A.O. Hudson, *Isolation, total synthesis, and biological activities of 1-aminocyclopropane-1-carboxylic acid (ACC) containing natural compounds*. Studies in Natural Products Chemistry, 2016. 47: p. 405-430.
- Viswanadham, B., et al., *Efficient and expeditious chemoselective BOC protection of amines in catalyst and solvent-free media*. Research on Chemical Intermediates, 2017. 43: p. 1355-1363.
- Mařík, J., A. Song, and K.S. Lam, *Detection of primary aromatic amines on solid phase*. Tetrahedron Letters, 2003. 44(23): p. 4319-4320.
- Diaz, Y.J., et al., *A versatile and highly selective colorimetric sensor for the detection of amines*. Chemistry—A European Journal, 2017. 23(15): p. 3562-3566.
- Cassan, F., et al., *Cadaverine production by Azospirillum brasilense and its possible role in plant growth promotion and osmotic stress mitigation*. european journal of soil biology, 2009. 45(1): p. 12-19.

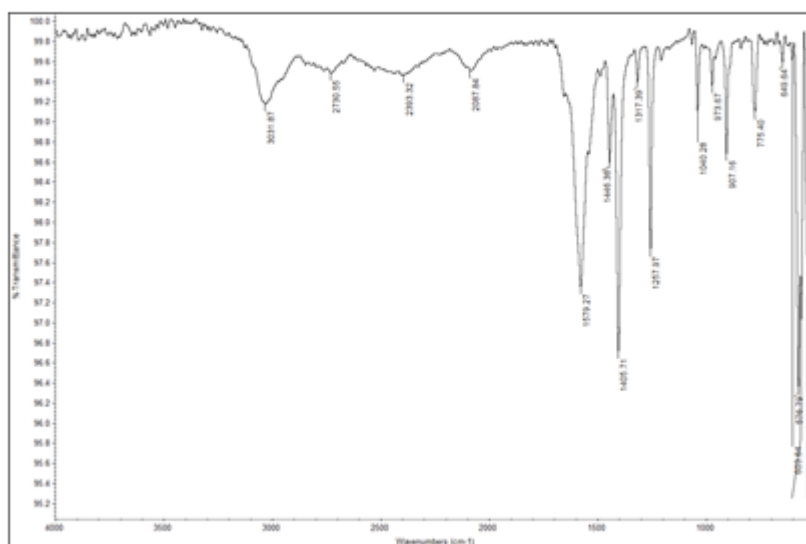
- Bottini, R., F. Cassán, and P. Piccoli, *Gibberellin production by bacteria and its involvement in plant growth promotion and yield increase*. Applied microbiology and biotechnology, 2004. 65: p. 497-503.
- Perrig, D., et al., *Plant-growth-promoting compounds produced by two agronomically important strains of Azospirillum brasilense, and implications for inoculant formulation*. Applied microbiology and biotechnology, 2007. 75: p. 1143-1150.
- Mustafa, A., et al., *Perspectives of using l-tryptophan for improving productivity of agricultural crops: A review*. Pedosphere, 2018. 28(1): p. 16-34.
- Mohite, B., *Isolation and characterization of indole acetic acid (IAA) producing bacteria from rhizospheric soil and its effect on plant growth*. Journal of soil science and plant nutrition, 2013. 13(3): p. 638-649.
- NISHIYAMA, I. and F. MOTOYOSHI, *Cytogenetic studies in Avena, XVI. Chlorophyll formation in albino sand oats under certain culture conditions*. The Japanese Journal of Genetics, 1966. 41(5): p. 403-411.
- Lanfermeijer, F.C., J.W. Koerselman-Kooij, and A.C. Borstlap, *Changing kinetics of L-valine uptake by immature pea cotyledons during development: an unsaturated pathway is supplemented by a saturable system*. Planta, 1990. 181: p. 576-582.
- Li, S., et al., *Mechanisms of high concentration valine-mediated inhibition of peach tree shoot growth*. Frontiers in Plant Science, 2020. 11: p. 603067.
- Zhang, M., et al., *Application of chitosan and its derivative polymers in clinical medicine and agriculture*. Polymers, 2022. 14(5): p. 958.
- Su, S., et al., *Salicylaldehyde and D-(+)-galactose functionalized chitosan oligosaccharide nanoparticles as carriers for sustained release of pesticide with enhanced UV stability*. Colloids and Surfaces A: Physicochemical and Engineering Aspects, 2023. 656: p. 130437.
- Kumaraswamy, R., et al., *Engineered chitosan based nanomaterials: Bioactivities, mechanisms and perspectives in plant protection and growth*. International Journal of Biological Macromolecules, 2018. 113: p. 494-506.

Appendices

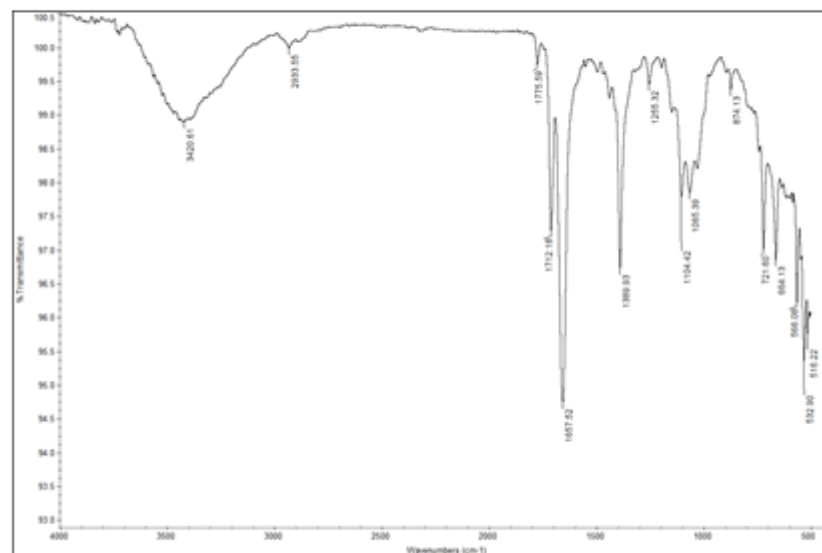
Appendix A

FT-IR of synthesized Ch- Amino acids compounds

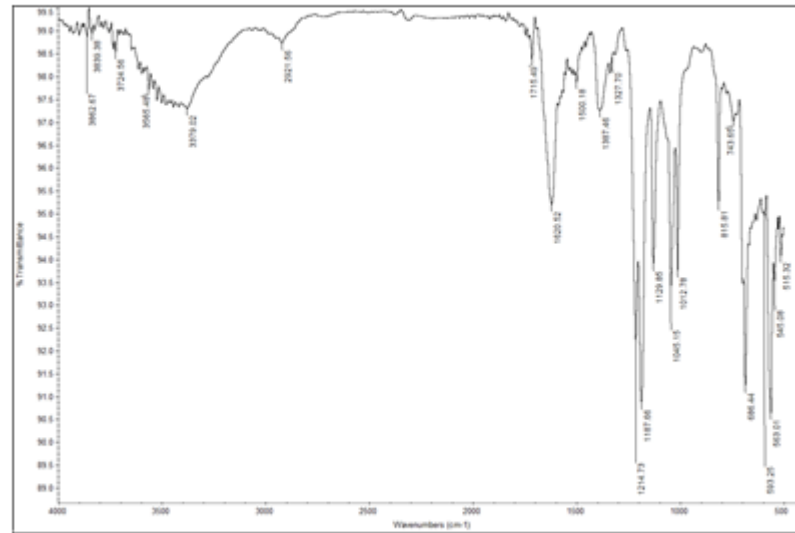
1- amino cyclopropane-1- carboxylic acid (ACC)



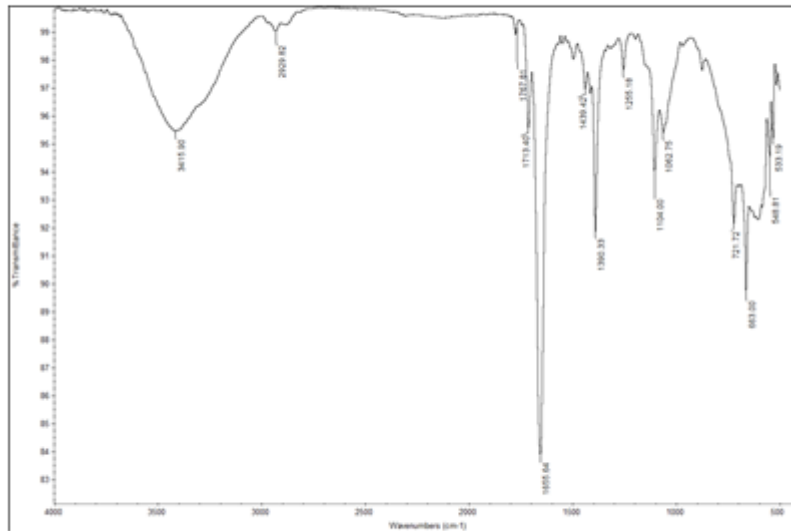
N Phthaloyl chitosan



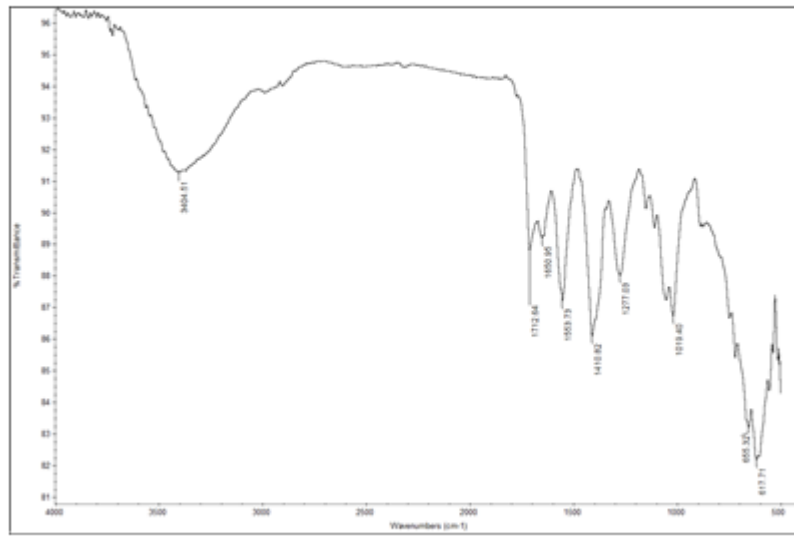
6-O-tosyl-N-phthaloyl-chitosan



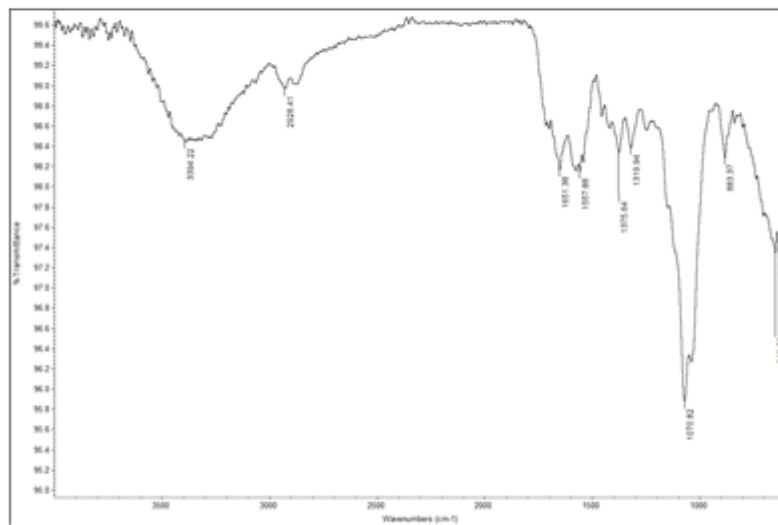
N-phthaloyl-chitosan-ACC



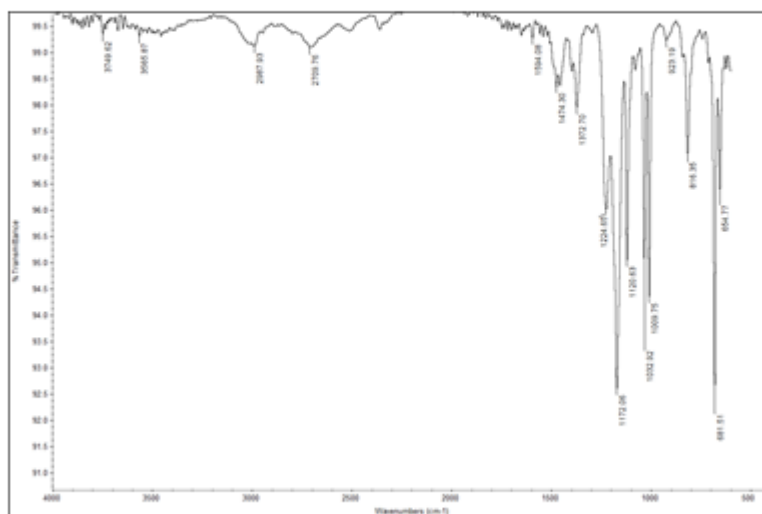
Chitosan ACC



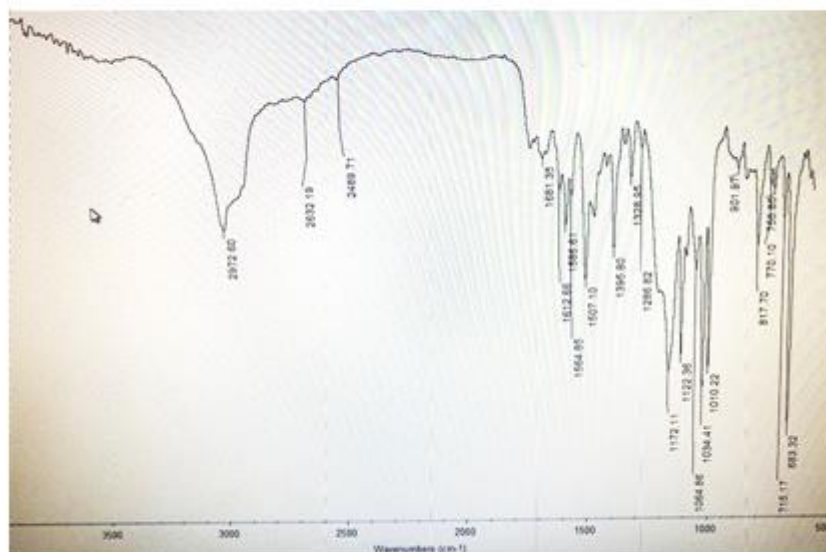
NBOC Chitosan



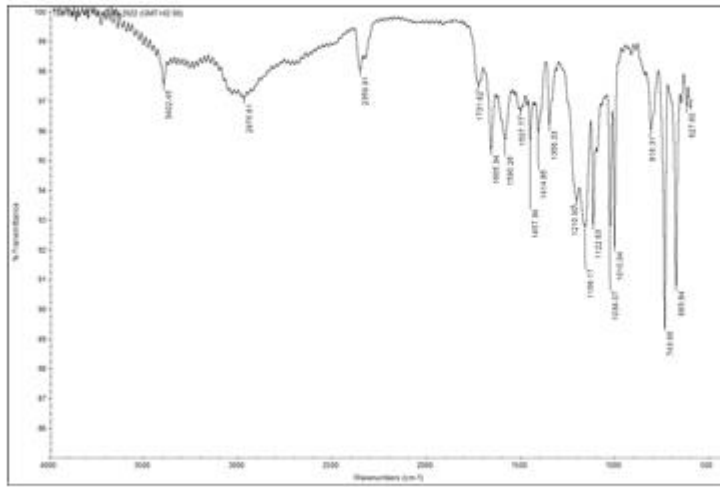
6-O-Tosyl-N-Boc-chitosan



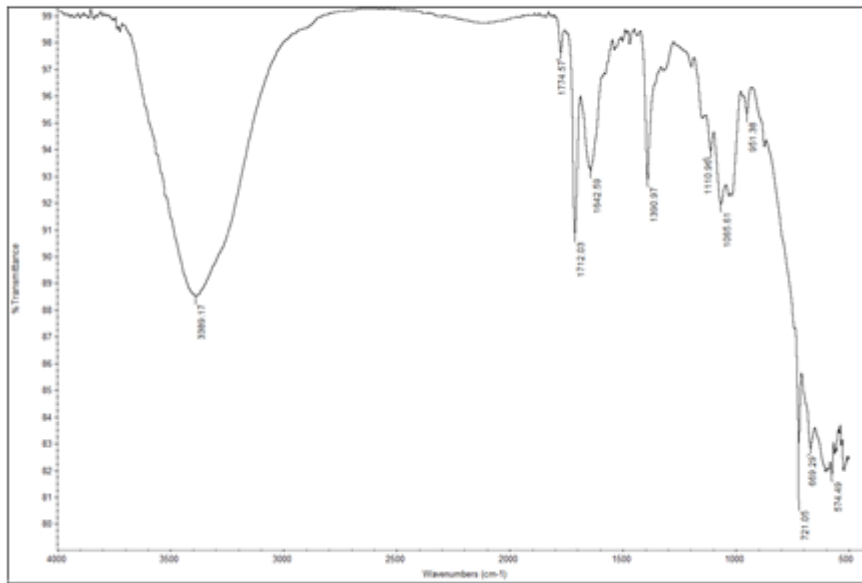
6-O-Valine-N-Boc-chitosan



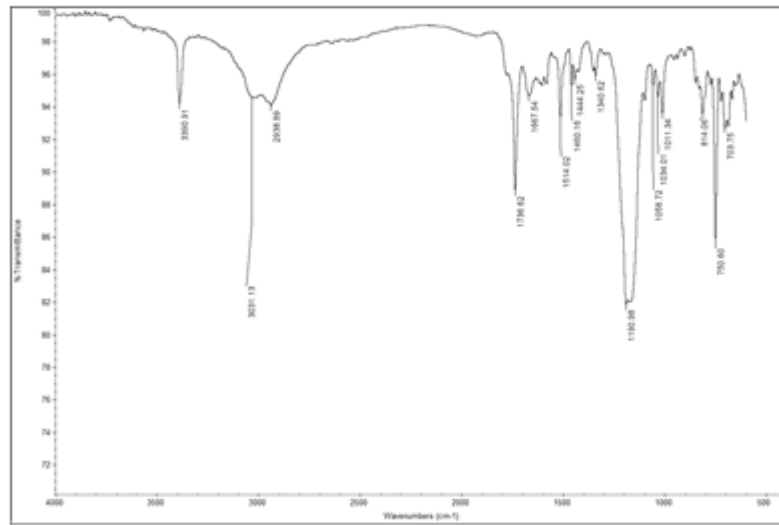
6-O-Tryp-N-Boc-chitosan



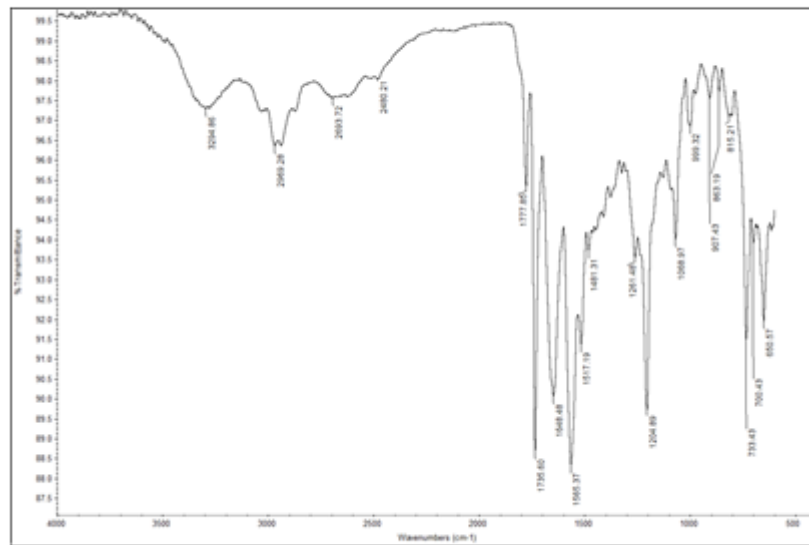
6-O-Val-chitosan



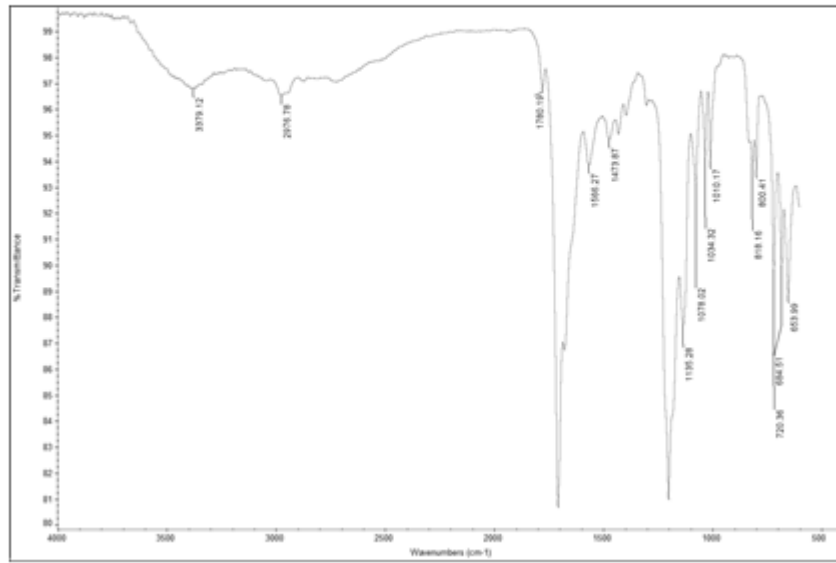
6-O-Tryp chitosan



6-O-Tryp chitosan N-lysine



6-O Val chitosan N-lysine



Appendix B

Nano Biofertilizer

Figure S.1

The appearance of prepared nanocapsules solutions

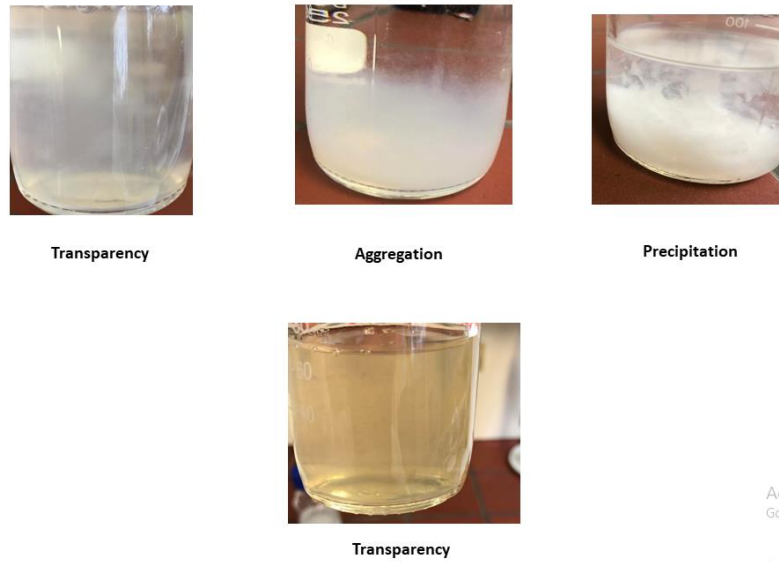
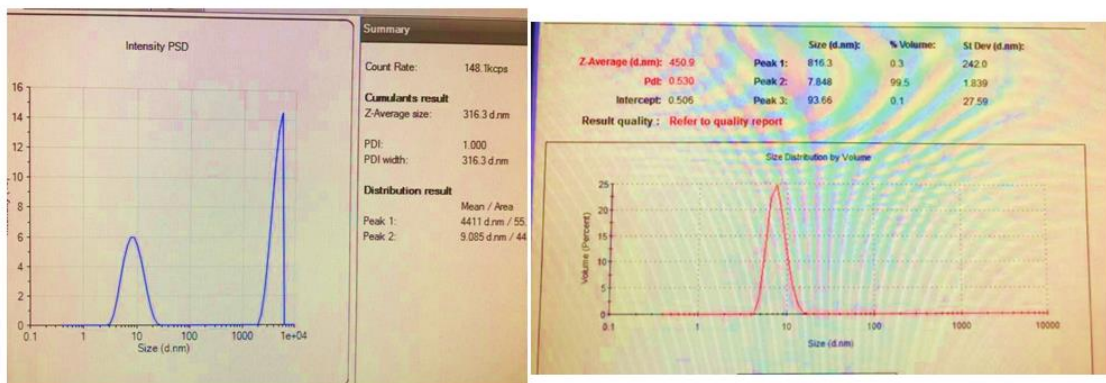


Figure S.2

The DLS (particle size) measurements of synthesized Nano capsules

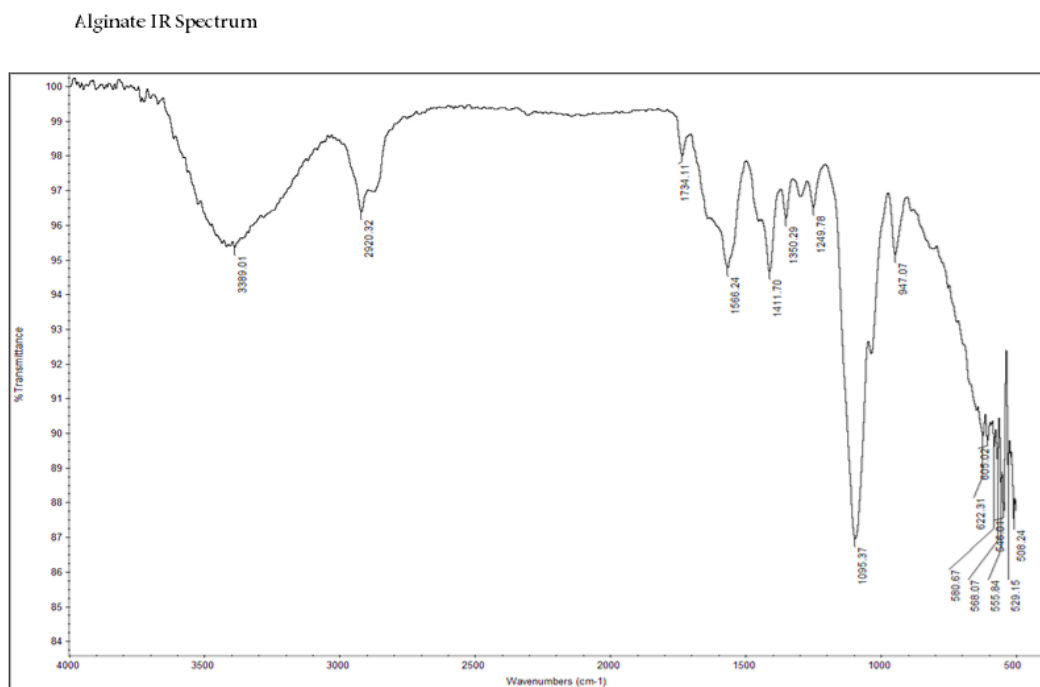
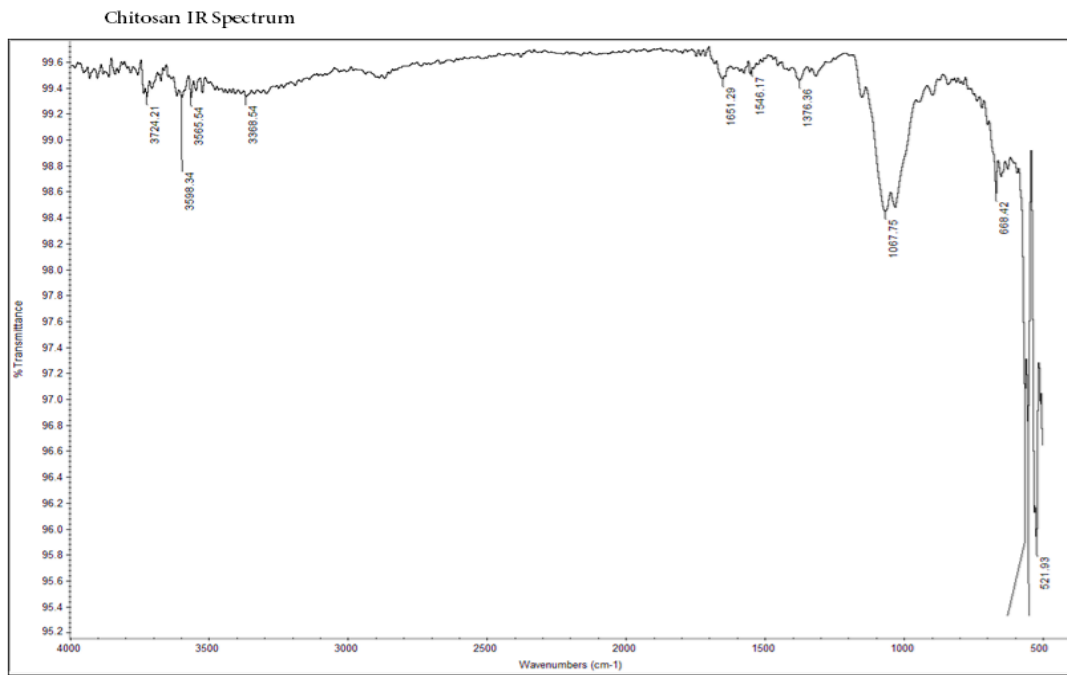


(a) Particle size of (Ch.Alg. NPK) Nano capsules

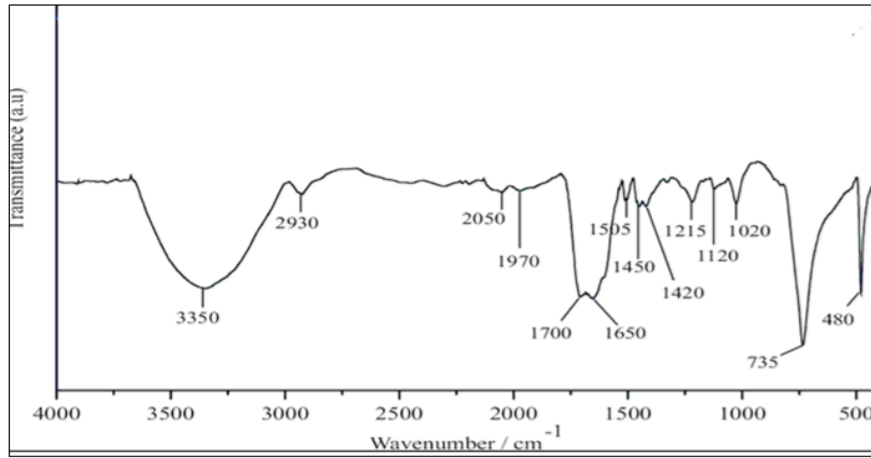
(b) Particle size of (Ch.Alg. HA. NPK) Nano capsules

Figure S.3

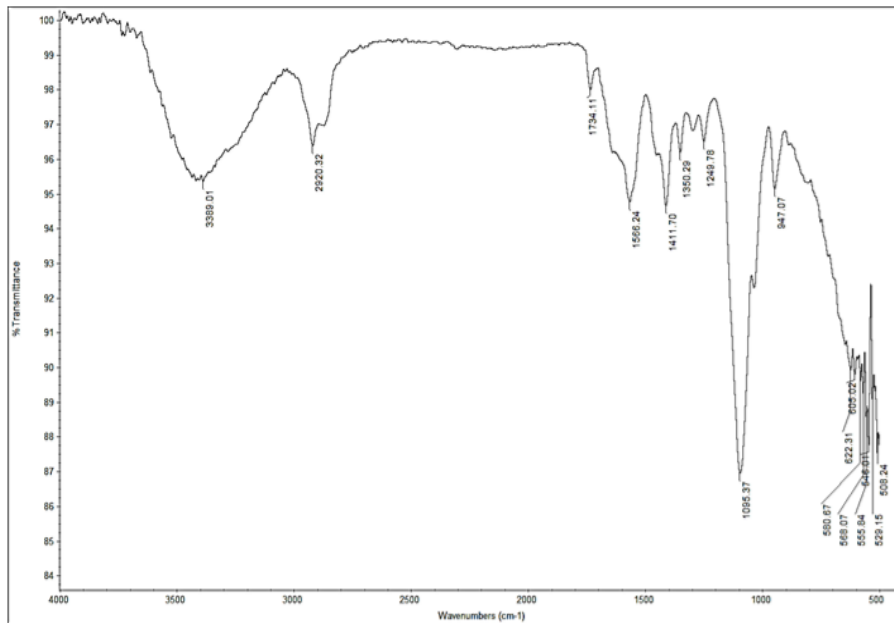
FT_IR of Chitosan ,Alginate, Humic acid, (Ch.Alg.NPK), (Ch.Alg.HA. NPK)



Humic Acid IR Spectrum



(Ch.Alg.NPK) Nano capsule IR Spectrum



(Ch.Alg.HA.NPK) Nano capsule IR Spectrum

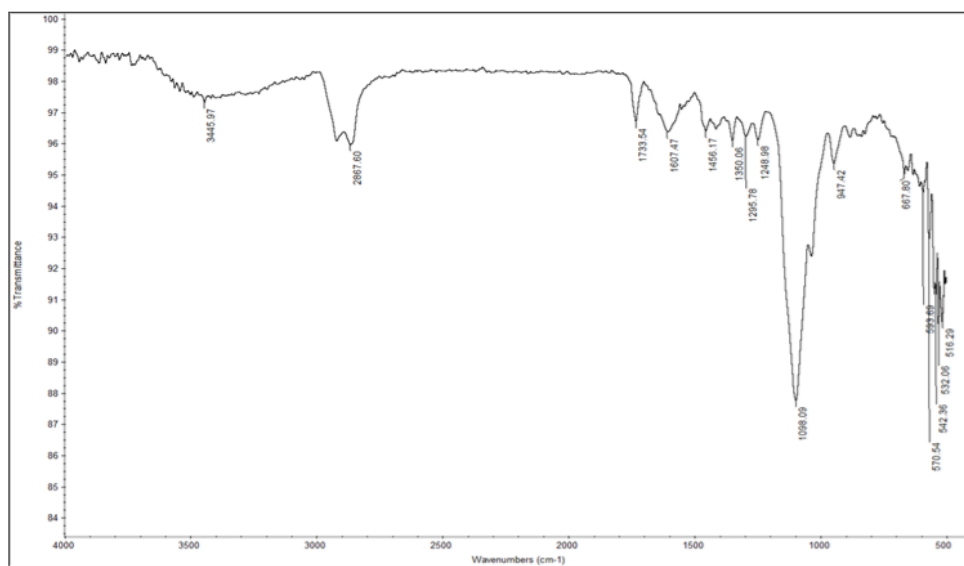


Table S.1

Water retention percentage for (Ch.Alg.NPK) and (Ch. Alg. HA. NPK) Nanocapsules

Time	Control		Ch.Alg.		Ch.Alg.HA		Weight (ref)
Days	Weight(Wt)	Percentage	Weight(Wt)	Percentage	Weight(Wt)	Percentage	
0	160	100	160	100	160	100	150
5	152.739	54.62	156.4	77.5	157.648	85.3	144
10	141.218	30.95	149.39	61	154.723	80.6	132.8
15	124.816	13.34	142.26	55.9	150.175	75.8	119.4
20	114.136	6.4	134.128	47.2	142.556	64.4	111
25	106.155	2.1	126.78	39.6	132.72	50.2	105
30	100	0	118.84	31.4	126.52	44.2	100

Table S.2

Release behavior of active nutrient Nitrogen for (Ch.Alg.NPK) and (Ch. Alg. HA. NPK) Nanocapsules

Time	Log Time	(Ch.Alg.HA) (mg/ml)	% cumulative Release	Log (Mt/Mo)	(Ch.Alg.) (mg/ml)	% cumulative release	Log (Mt/Mo)
0	0	0	0	0	0	0	0
1	0	0.028	6.6	0.8195	0.069	15.18	1.181
5	0.7	0.079	17.94	1.253	0.131	30.2	1.480
10	1	0.084	20.06	1.302	0.153	36.28	1.559
15	1.2	0.110	25.88	1.412	0.157	37.7	1.576
20	1.3	0.122	29.04	1.463	0.162	38.78	1.588
25	1.4	0.131	31.26	1.494	0.163	39.1	1.59
30	1.5	0.139	33.2	1.521	0.169	40.44	1.606

Table S.3

Release behavior of active nutrient Phosphorous for (Ch.Alg.NPK) and (Ch. Alg. HA. NPK) Nanocapsules

Time	Log Time	(Ch.Alg.HA) mg/ml	% cumulative release	Log (Mt/Mo)	(Ch.Alg.) mg/ml	% cumulative release	Log (Mt/Mo)
0	0	0	0	0	0	0	0
1	0	0.070	15.4	1.187	0.061	13.42	1.1277
5	0.7	0.141	32.42	1.510	0.089	20.8	1.318
10	1	0.149	35.6	1.551	0.159	36.76	1.565
15	1.2	0.150	35.98	1.5558	0.170	40.58	1.608
20	1.3	0.160	38.2	1.582	0.179	42.78	1.631
25	1.4	0.163	39.06	1.591	0.190	45.38	1.656
30	1.5	0.170	40.66	1.609	0.200	47.8	1.679

Table S.4

Release behavior of active nutrient Potassium for (Ch.Alg.NPK) and (Ch. Alg. HA. NPK) Nanocapsules

Time	Log Time	(Ch.Alg.HA) mg/ml	% cumulative release	Log (M _t /M ₀)	(Ch.Alg.) mg/ml	% cumulative release	Log (M _t /M ₀)
0	0	0	0	0	0	0	0
1	0	0.073	15.46	1.189	0.087	17.74	1.248
5	0.7	0.090	21.26	1.327	0.141	32.76	1.51
10	1	0.213	48.66	1.687	0.187	45.96	1.66
15	1.2	0.222	53.1	1.725	0.200	47.74	1.678
20	1.3	0.261	61.86	1.791	0.259	60.98	1.78
25	1.4	0.280	66.82	1.824	0.270	64.58	1.81
30	1.5	0.285	68.3	1.834	0.278	66.56	1.823

Figure S.4

Nitrogen Kinetic release of (Ch.Alg.HA. NPK) and (Ch.Alg.NPK) Nanocapsules

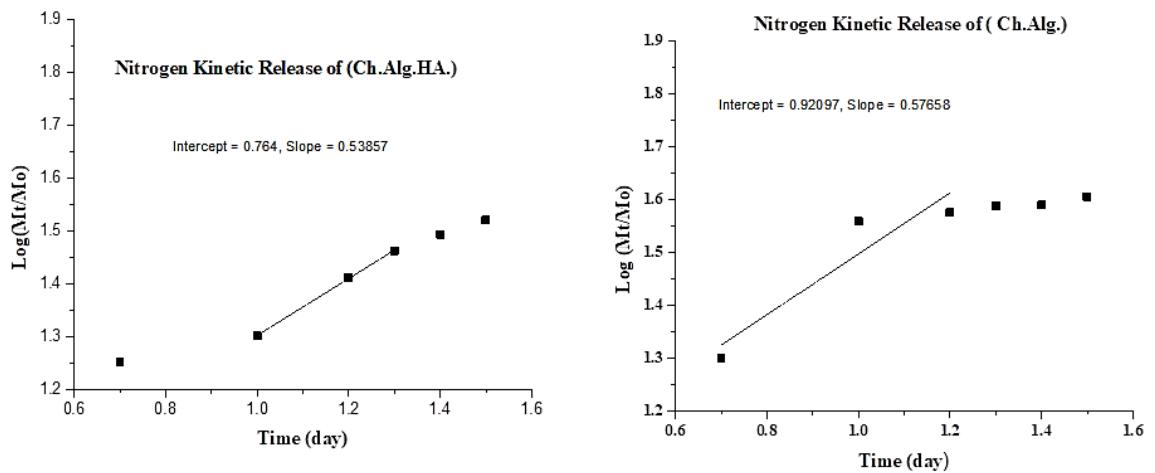


Figure S.5

Phosphorous Kinetic release of (Ch.Alg.HA. NPK) and (Ch.Alg.NPK) Nanocapsules

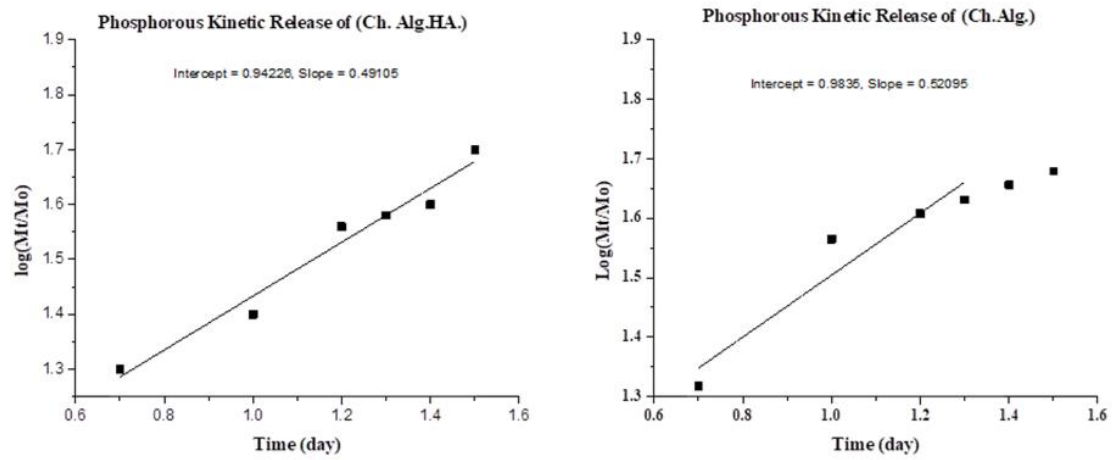
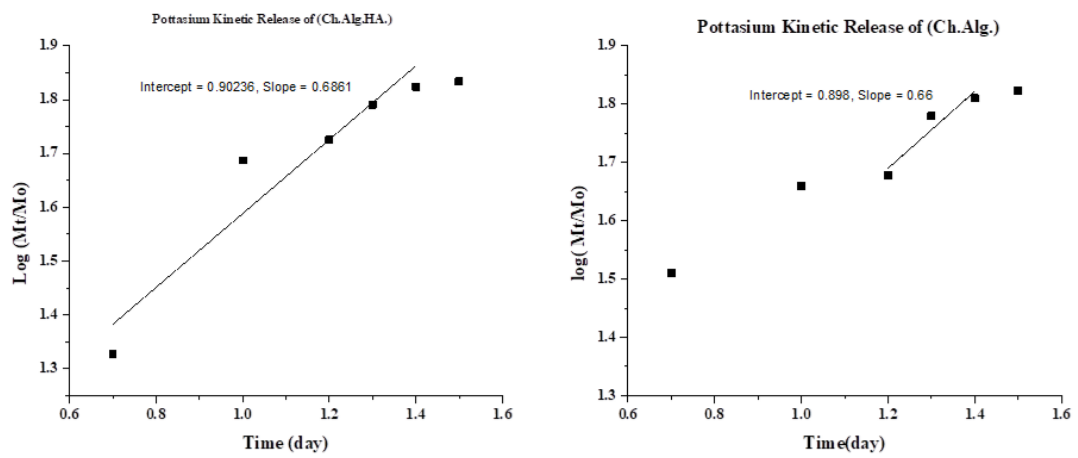


Figure S.6

Potassium Kinetic release of (Ch.Alg.HA. NPK) and (Ch.Alg.NPK) Nanocapsules



Appendix C

Chitosan-based photocatalyst

Figure S.1.a

(a) AFM image of CNDs particles, (b) CNDs size distribution histogram (c) AFM image of ZnO nanoparticles, (d) ZnO size distribution histogram, (e) AFM image of ZnO-CNDs hybrid, (f) Hybrid size distribution histogram

Figure S.1

XRD patterns for CNDs, ZnO, and Hybrid (ZnO/CNDs)

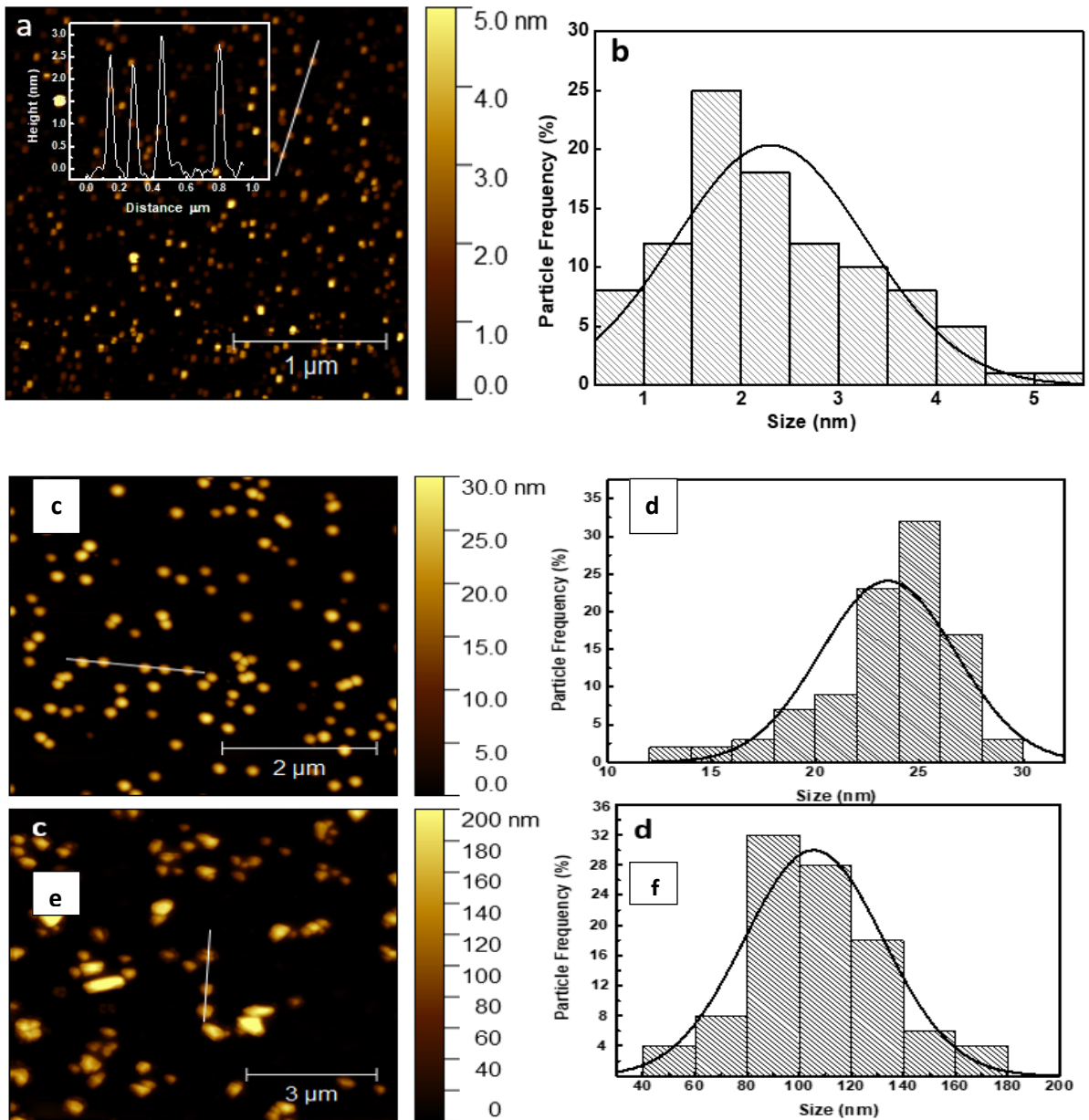


Figure S.2

(a) AFM image of Ch.ZnO, (b) AFM image of Ch.CNDs, (c) AFM image of Ch.Hybrid (ZnO-CNDs)

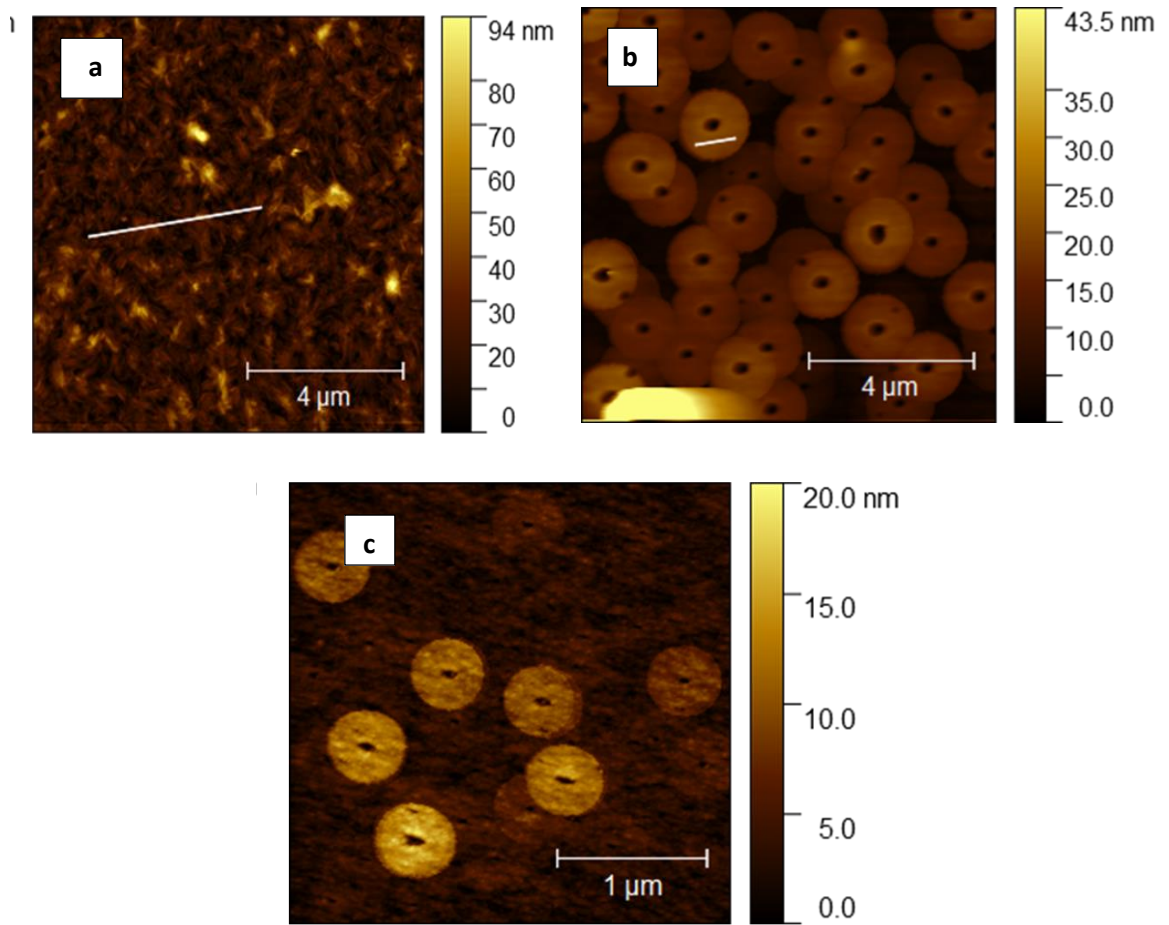


Figure S.3

X-Ray Diffraction of ZnO, CNDs, Hybrid (ZnO/CNDs)

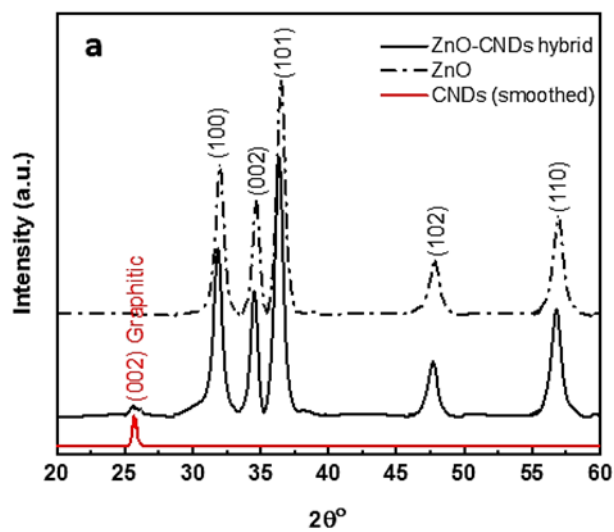


Figure S.4

FT-IR spectra of Chitosan, ZnO, CNDs, Ch.Hybrid (ZnO/CNDs)

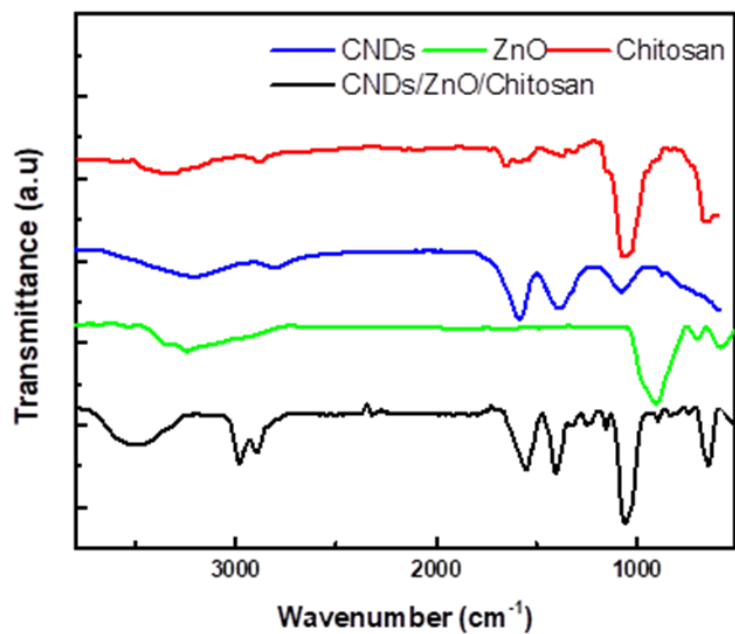
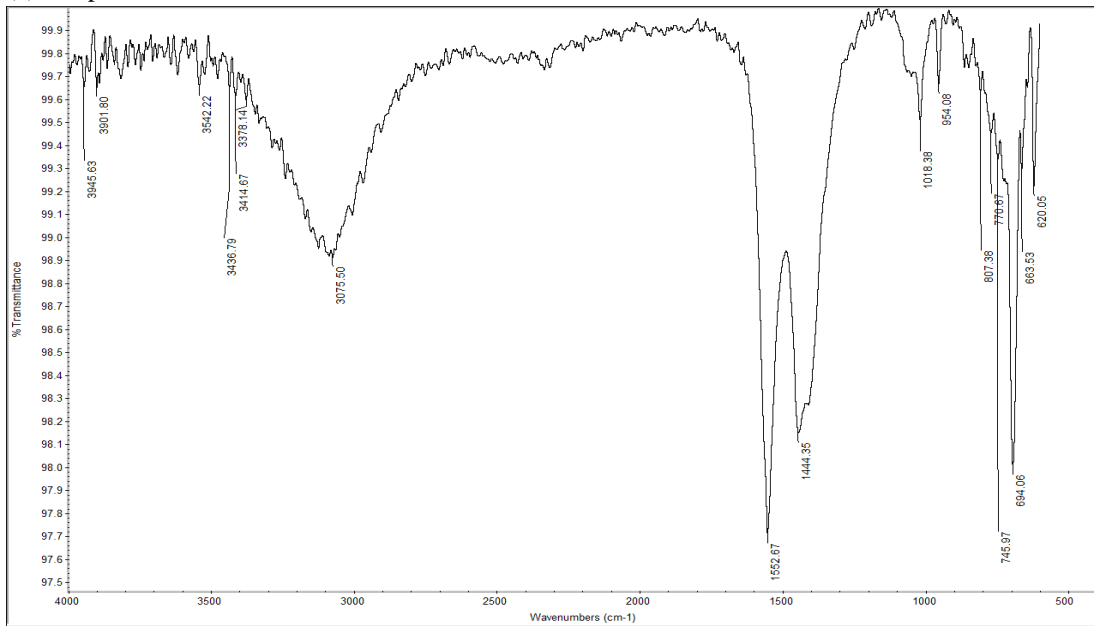


Figure S.5

FT_IR of Ch.ZnO, Ch.CNDs

(a) IR spectrum of Ch.ZnO



(b) IR spectrum for Ch. CNDs

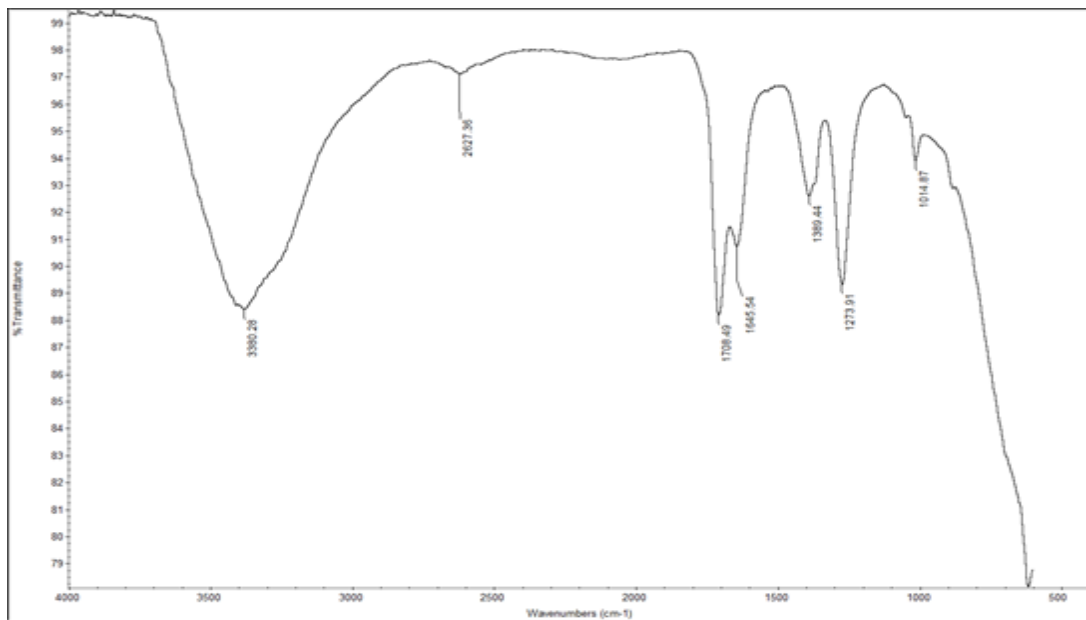


Figure S.6

Raman Spectra of CNDs and Hybrid (CNDs/ZnO)

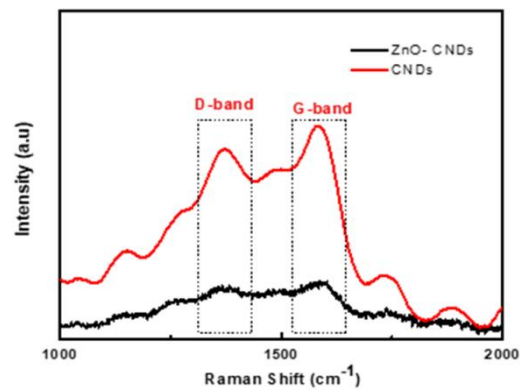


Figure S.7

(a) UV-Vis absorption spectra of CNDs, ZnO, and Hybrid (ZnO/CNDs), (b) Band gaps of ZnO and Hybrid (ZnO/CNDs), (c) UV Vis absorption of Ch.CNDs, Ch.ZnO, and Ch. Hybrid

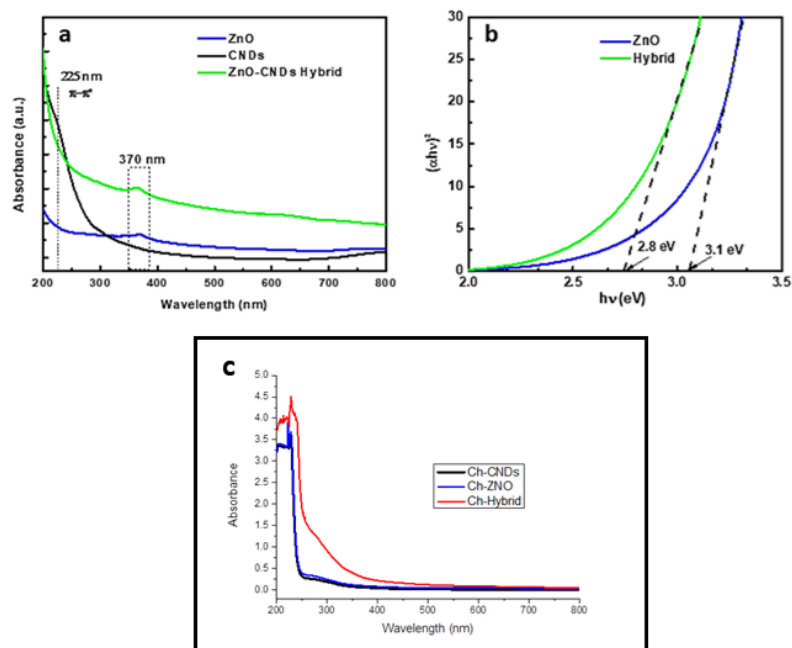


Figure S.8

Loss of Glutathione (%) for synthesized samples in dark mode

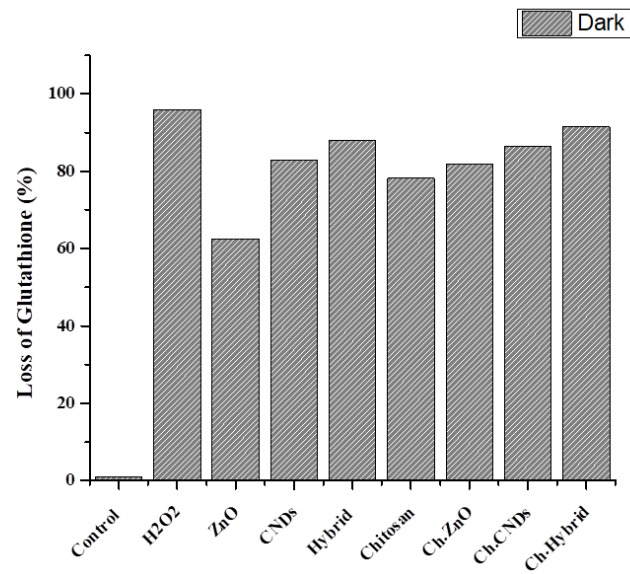


Figure S.9

Loss of Glutathione (%) for synthesized samples in sunlight mode

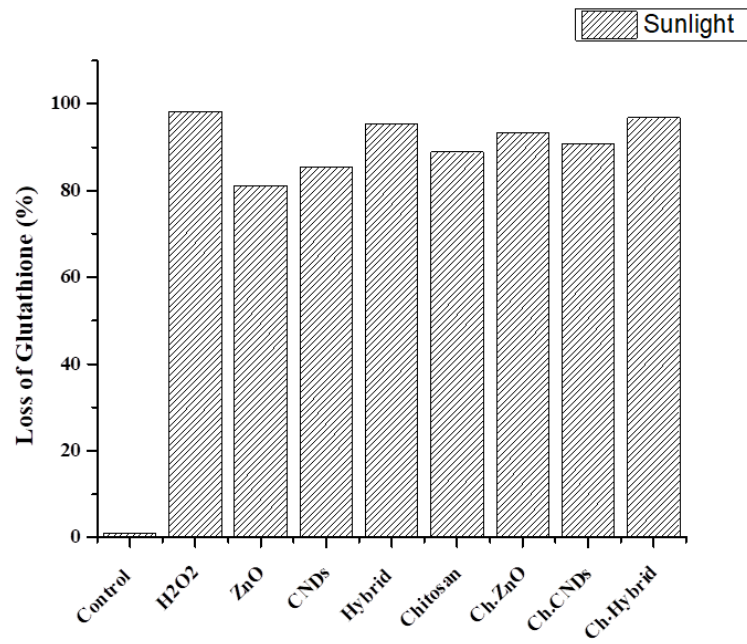


Table S.2

Number of CFU reductions for ZnO, CNDs, and Hybrid for different bacterial and fungal strains under sunlight and dark modes before and after treatment

Initial colonies amount = 250						
Microbial strains	ZnO		CNDs		Hybrid	
	Number of colonies after treatment					
	Dark	Sunlight	Dark	Sunlight	Dark	Sunlight
<i>E. coli</i>	230	160	240	210	3	≈ 0
<i>S. aureus</i>	185	100	200	100	1	≈ 0
<i>K. pneumonia</i>	210	150	210	140	7	1
<i>MRSA</i>	200	100	235	170	7	3
<i>P. aeruginosa</i>	180	80	190	100	3	3
<i>Mold</i>	200	80	240	180	1	≈ 0
<i>Saccharomyces cerevisiae</i>	200	80	240	170	1	≈ 0
<i>Aspergillus fumigatus</i>	230	55	240	190	1	≈ 0

Table S.3

Number of CFU reductions for Chitosan, Chitosan/ZnO, Chitosan/CNDs, and Chitosan/Hybrid for different bacterial and fungal strains under sunlight and dark modes before and after treatment

Initial colonies amount = 250									
Microbial Strains	Gram Type	Chitosan		Chitosan/ZnO		Chitosan/CNDs		Chitosan/Hybrid	
		Number of colonies after treatment							
		Dark	Sunlight	Dark	Sunlight	Dark	Sunlight	Dark	Sunlight
<i>E.coli</i>	-ve	190	110	90	30	125	55	5	1
<i>S. aureus</i>	+ve	80	65	20	12	55	30	1	≈ 0
<i>K.pneumonia</i>	-ve	100	80	60	25	80	40	1	≈ 0
<i>MRSA</i>	+ve	200	190	120	90	160	100	7	3
<i>P.aeruginosa</i>	-ve	230	190	160	100	125	90	10	7
<i>Mold</i>	-	130	20	10	1	15	5	≈ 0	≈ 0
<i>S. cerevisiae</i>	-	90	20	20	2	35	15	≈ 0	≈ 0
<i>A. funigatus</i>	-	80	30	15	3	40	10	≈ 0	≈ 0

Table S.4

Percentage of CFU reduction for ZnO, CNDs, and Hybrid for different bacterial and fungal strains under sunlight and dark modes

Microbial strains	Gram Type	CFU Reduction Percent %					
		ZnO		CNDs		Hybrid	
		Dark	Sunlight	Dark	Sunlight	Dark	Sunlight
<i>E. coli</i>	-ve	8	36	4	16	99	99.99
<i>S. aureus</i>	+ve	26	60	20	60	99.6	99.99
<i>K. pneumonia</i>	-ve	16	40	16	44	97.2	99.6
<i>MRSA</i>	+ve	20	60	6	32	97.2	99
<i>P. aeruginosa</i>	-ve	28	60	24	60	99	99
<i>Mold</i>	-	20	68	4	28	99.6	99.99
<i>Saccharomyces cerevisiae</i>	-	20	68	4	32	99.6	99.99
<i>Aspergillus fumigatus</i>	-	8	78	4	24	99.6	99.99

Table S.5

Percentage of CFU reduction for Chitosan, Chitosan/ZnO, Chitosan/CNDs, and Chitosan/Hybrid for different bacterial and fungal strains under sunlight and dark modes

Microbial Strains	Gram Type	CFU Reduction Percent %							
		Chitosan		Chitosan/ZnO		Chitosan/CNDs		Chitosan/Hybrid	
		Dark	Sunlight	Dark	Sunlight	Dark	Sunlight	Dark	Sunlight
<i>E.coli</i>	-ve	24	44	64	88	50	78	98	99.6
<i>S. aureus</i>	+ve	68	74	92	95.2	78	88	99.6	99.99
<i>K.pneumonia</i>	-ve	60	68	76	90	68	84	99.6	99.99
<i>MRSA</i>	+ve	20	24	52	64	36	60	97.2	98.8
<i>P.aeruginosa</i>	-ve	8	24	36	60	50	64	99.6	97.2
<i>Mold</i>	-	48	92	96	99.6	94	98	99.99	99.99
<i>S. cerevisiae</i>	-	64	92	92	99.2	86	94	99.99	99.99
<i>A. funigatus</i>	-	68	88	94	98.8	84	96	99.99	99.99

Table S.6*Log of CFU reduction for ZnO, CNDs, and Hybrid for different bacterial and fungal strains under sunlight and dark modes*

Microbial strains	Log of CFU Reduction (Mean \pm SD)					
	ZnO		CNDs		Hybrid	
	Dark	Sunlight	Dark	Sunlight	Dark	Sunlight
<i>E.coli</i>	0.03621 \pm 0.154	0.19382 \pm 0.051	0.01773 \pm 0.069	0.07572 \pm 0.013	2.097 \pm 0.001	4.398 \pm 0.101
<i>S. aureus</i>	0.13077 \pm 0.005	0.39794 \pm 0.154	0.09691 \pm 0.016	0.39794 \pm 0.012	2.495 \pm 0.013	4.398 \pm 0.013
<i>K.pnemounia</i>	0.07572 \pm 0.101	0.22185 \pm 0.065	0.07572 \pm 0.005	0.2518 \pm 0.016	1.5528 \pm 0.154	2.495 \pm 0.016
<i>MRSA</i>	0.09691 \pm 0.117	0.13077 \pm 0.012	0.02687 \pm 0.154	0.1675 \pm 0.051	1.5528 \pm 0.005	2.097 \pm 0.065
<i>P. aeruginosa</i>	0.14262 \pm 0.065	0.4685 \pm 0.005	0.11919 \pm 0.065	0.39794 \pm 0.005	2.097 \pm 0.065	2.097 \pm 0.008
<i>Mold</i>	0.09691 \pm 0.051	0.49485 \pm 0.117	0.1773 \pm 0.051	0.14267 \pm 0.051	2.495 \pm 0.012	4.398 \pm 0.051
<i>Saccharomyces cerevisiae</i>	0.09691 \pm 0.101	0.49485 \pm 0.021	0.1773 \pm 0.031	0.1075 \pm 0.045	2.495 \pm 0.101	4.398 \pm 0.058
<i>Aspergillus fumigatus</i>	0.03621 \pm 0.016	0.6576 \pm 0.101	0.01773 \pm 0.117	0.11919 \pm 0.067	2.495 \pm 0.012	4.398 \pm 0.001

Table S.7

Log of CFU reduction for Chitosan, Chitosan/ZnO, Chitosan/CNDs, and Chitosan/Hybrid for different bacterial and fungal strains under sunlight and dark modes

Microbial Strains	Gram Type	Log of CFU reduction (Mean \pm SD)							
		Chitosan		Chitosan/ZnO		Chitosan/CNDs		Chitosan/Hybrid	
		Dark	Sunlight	Dark	Sunlight	Dark	Sunlight	Dark	Sunlight
<i>E.coli</i>	-ve	0.1191 \pm 0.005	0.2518 \pm 0.009	0.4437 \pm 0.011	0.9208 \pm 0.039	0.301 \pm 0.023	0.6576 \pm 0.008	1.699 \pm 0.097	2.398 \pm 0.025
<i>S. aureus</i>	+ve	0.4948 \pm 0.019	0.5850 \pm 0.010	1.097 \pm 0.047	1.3188 \pm 0.032	0.658 \pm 0.079	0.9208 \pm 0.057	2.398 \pm 0.039	4.398 \pm 0.008
<i>K.pneumonia</i>	-ve	0.3979 \pm 0.012	0.4948 \pm 0.002	0.6198 \pm 0.052	1 \pm 0.044	0.4948 \pm 0.042	0.7959 \pm 0.018	2.398 \pm 0.014	4.398 \pm 0.049
<i>MRSA</i>	+ve	0.0969 \pm 0.008	0.1192 \pm 0.083	0.3187 \pm 0.053	0.4437 \pm 0.063	0.1938 \pm 0.077	0.3979 \pm 0.055	1.5528 \pm 0.073	1.921 \pm 0.002
<i>P.aeruginosa</i>	-ve	0.03621 \pm 0.003	0.1192 \pm 0.065	0.1938 \pm 0.096	0.3979 \pm 0.090	0.301 \pm 0.090	0.4437 \pm 0.019	1.398 \pm 0.081	1.5528 \pm 0.001
<i>Mold</i>	-	0.2840 \pm 0.020	1.097 \pm 0.027	1.398 \pm 0.017	2.398 \pm 0.028	1.222 \pm 0.058	1.699 \pm 0.064	4.398 \pm 0.059	4.398 \pm 0.081
<i>S. cerevisiae</i>	-	0.4437 \pm 0.017	1.097 \pm 0.011	1.097 \pm 0.099	2.097 \pm 0.073	0.854 \pm 0.014	1.2218 \pm 0.095	4.398 \pm 0.088	4.398 \pm 0.035
<i>A. funigatus</i>	-	0.4948 \pm 0.031	0.9208 \pm 0.003	1.222 \pm 0.053	1.921 \pm 0.022	0.796 \pm 0.089	1.3980 \pm 0.042	4.398 \pm 0.012	4.398 \pm 0.006

Appendix D

Chitosan based Amino Acid as PGPRs and Plant biostimulants

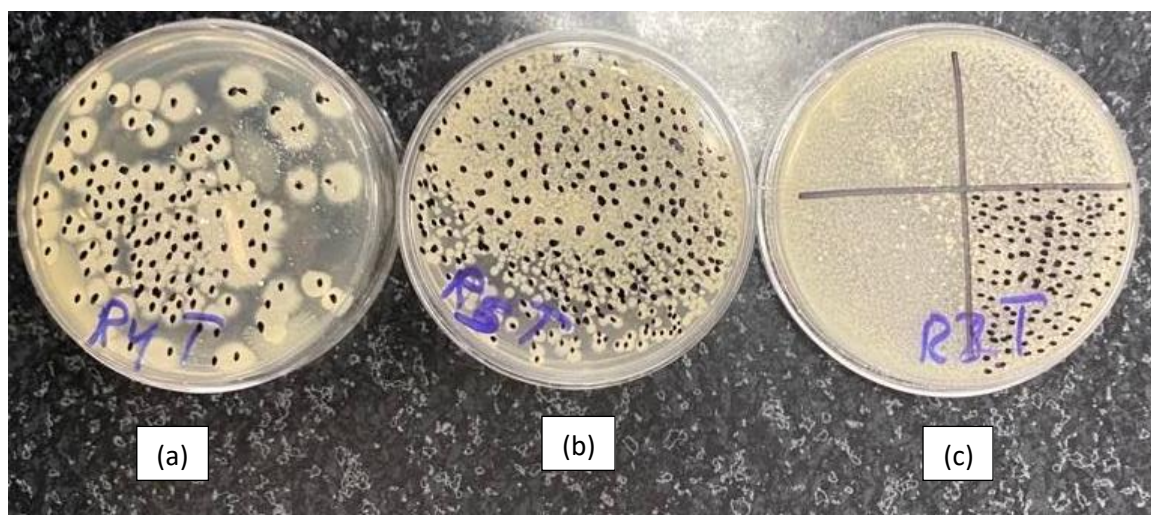
Table S1

Calculated amine groups obtained from Kaiser test for N-protected compound using two N-protection approaches

Kaiser Test	Chitosan	N-Phthaloyl chitosan	N- Boc chitosan
N- protection	0.9146×10^7 Micromol/g	0.2677×10^{10} Micromol/g	0.0501×10^{10} Micromol/g
De- protection	1×10^7 Micromol/g	0.769×10^{10} Micromol/g	0.896×10^{10} Micromol/g

Figure S1

In vitro test of Petri-plate of testing of bacterial growth of (a)chitosan, (b)ACC, (c) chitosan-ACC



Appendix E

**Certificate of acceptance of the research extracted from the dissertation Research
title: Visible light-driven ZnO nanoparticles/carbon nanodots hybrid for
broad-spectrum antimicrobial activity**





جامعة النجاح الوطنية
كلية الدراسات العليا

توليف التشيتوسان كأداة متعددة الإستخدامات في الزراعة المستدامة

إعداد

ريناد جلال يحيي حامد

إشراف

أ. د. شحدة جودة

قدمت هذه الأطروحة استكمالاً لمتطلبات الحصول على درجة دكتوراه في الكيمياء، من كلية الدراسات العليا، في
جامعة النجاح الوطنية، نابلس - فلسطين.

2023

ب

توليف التشيتوسان كأداة متعددة الإستخدامات في الزراعة المستدامة

إعداد

رناد جلال يحيي حامد

إشراف

أ. د. شحدة جودة

الملخص

تعتبر المبيدات والأسمدة الكيميائية كملوثات رئيسية للبيئة والزراعة، وقد لفتت البوليمرات المشتقة من التشيتوسان اهتماماً كبيراً في التطبيقات الزراعية وعلوم النبات، ولذلك، في هذا البحث تم اجراء مساهمات علمية لتحسين تركيب ووظائف التشيتوسان كأداة متعددة الإستخدامات في الزراعة المستدامة.

يرتكز هذا البحث على عدة بنود مهمة ألا وهي: عملية استخدام التشيتوسان في تصنيع كبسولات ناوية مبتكرة للأسمدة الحيوية، بهدف توصيل العناصر الزراعية الفعالة الأساسية، ألا وهي أيونات النيتروجين والفسفور والبوتاسيوم، بالإضافة إلى الميكروبات الجذرية المفيدة في تعزيز نمو النباتات ضمن آلية ذكية تعتمد على إحتياج النبات لتلك العناصر.

حيث تعتمد تقنية تغليف هذه المكونات الزراعية والحيوية الرئيسية على تقنية مبتكرة قائمة على التقاط الأيونات والترابط بين التشيتوسان والأجينات مع حمض الهيوميك من خلال التجمع الأيوني والتجمع البولي. كما تم التحقق من خصائصها المورفولوجية والهيكلية لتلك الكبسولات النانوية بإستخدام تقنية الليزر الديناميكي، والأشعة تحت الحمراء، والمجهر الإلكتروني الماسح، وتحليل الإنحراف الحراري، وكما تم تحديد قدرة التغليف للمواد المحاصرة، وسلوك الاحتفاظ المائي، وحركية التحرر للمواد المحاصرة.

عكست النتائج بدور حمض الهيوميك في عمل تشبيك متين لأيونات التشيتوسان والألجينات أثناء تكون الكبسولات وفي زيادة فعالية الكبسولات في تحرير المواد المغلفة وتوصيلها ضمن كفاءة عالية وضمن إطار زمني أطول، مما يمكن أن يسهم في زيادة الإنتاجية الزراعية واستدامتها.

ومن ناحية أخرى، تناول البحث بالبند الثاني عملية توظيف التشيتوسان المدمج مع مواد المحفزات الضوئية كطريقة واعدة لتطوير المبيدات الحيوية كبديل للمبيدات التقليدية، حيث ارتكز على توظيف التشيتوسان مع ثلاثة مواد محفزة ضوئية، ألا وهي: أكسيد الزنك، جسيمات الكربون النانوية، والهجينات المدمجة (أكسيد الزنك/ الجسيمات الكربون النانوية)، ودورها المحتمل كمضادات للميكروبات النشطة ضد عدد من السلالات البكتيرية والفطرية تحت ظرفي أشعة الشمس والعتمة.

وتم عمل فحوصات الخصائص المورفولوجية والهيكلية والبصرية لتلك المواد المحفزة المصنعة باستخدام أجهزة فحصية مختلفة وعكست النتائج نجاح تصنيع تلك المركبات وفعاليتها على استخدام هذه المركبات كمبيدات حيوية لأغراض الزراعة.

أخيراً، في البند الثالث تناول البحث إمكانية توظيف التشيتوسان المدمج مع الاحماض الأمينية لتصبح محفزات حيوية لنمو النباتات والبكتيريا الجذرية النافعة. حيث تم تحضير مركبات التشيتوسان مع مركب حمض 1- أمينو سيكلوبروبان-1- كربوكسيليك أسيد كمحفز لنمو البكتيريا الجذرية النافعة. ومن ناحية أخرى، تم تحضير مركبات من التشيتوسان معززة بأحماض أمينية مختلفة مثل حمض الفالين، حمض التريبتوفان، حمض اليسين باستخدام سلسلة تفاعل كيميائية خضراء حديثة.

وكما تم تحديد الخصائص المورفولوجية والهيكلية لتلك المركبات وإضافة لذلك تم تطبيق تلك المركبات في الإطار المخبري على نبات الشعير والبكتيريا الخضراء وتم فحص المعايير الزراعية والفسولوجية لمعالجات النباتات المختلفة وعكست النتائج رؤى واضحة في عملية توظيف تلك المركبات كمحفزات حيوية لنمو النباتات والبكتيريا الجذرية النافعة.

الكلمات المفتاحية: السماد الحيوي النانوي، الكبسولات النانوية الحجم، الربط المتشابك، مركب محفز

ضوئي غير متجانس التركيب، محفزات حيوية للمحاصيل.